# ANALYTICAL MODELING FOR LOAD DISTRIBUTION OF FOUR-POINT CONTACT SLEWING BEARINGS

A THESIS SUBMITTED TO
THE GRADUATE SCHOOL OF NATURAL AND APPLIED SCIENCES
OF
MIDDLE EAST TECHNICAL UNIVERSITY

BY

GÜNEŞ ECE MÜFTÜOĞLU

IN PARTIAL FULFILLMENT OF THE REQUIREMENTS
FOR
THE DEGREE OF MASTER OF SCIENCE
IN
MECHANICAL ENGINEERING

SEPTEMBER 2014

Approval of the thesis:

**ANALYTICAL MODELING FOR LOAD DISTRIBUTION OF FOUR-POINT CONTACT SLEWING BEARINGS**

submitted by **GÜNEŞ ECE MÜFTÜOĞLU** in partial fulfillment of the requirements for the degree of **Master of Science in Mechanical Engineering Department, Middle East Technical University** by,

Prof. Dr. Canan Özgen
Dean, Graduate School of **Natural and Applied Sciences** _____

Prof. Dr. Süha Oral
Head of Department, **Mechanical Engineering** _____

Prof. Dr. Metin Akkök
Supervisor, **Mechanical Engineering Dept., METU** _____

**Examining Committee Members**

Prof. Dr. Orhan Yıldırım
Mechanical Engineering Dept., METU _____

Prof. Dr. Metin Akkök
Mechanical Engineering Dept., METU _____

Prof. Dr. Suat Kadıoğlu
Mechanical Engineering Dept., METU _____

Assoc. Prof. Dr. Ender Ciğeroğlu
Mechanical Engineering Dept., METU _____

Bülent Acar, M.Sc.
Manager Engineer, ROKETSAN _____

**Date: 01.09.2014**

**I hereby declare that all information in this document has been obtained and presented in accordance with academic rules and ethical conduct. I also declare that, as required by these rules and conduct, I have fully cited and referenced all material and results that are not original to this work.**

Name, Last name : Güneş Ece Müftüoğlu

Signature :

## ABSTRACT

ANALYTICAL MODELING FOR LOAD DISTRIBUTION OF FOUR-POINT CONTACT SLEWING BEARINGS

Müftüoğlu, Güneş Ece

M. S., Department of Mechanical Engineering

Supervisor: Prof. Dr. Metin Akkök

September 2014, 110 pages

In this thesis, different loading cases of four-point contact slewing bearings and load distribution on the balls are investigated. The purpose is to determine that analytical modeling of load and deflections which give more effective results as compared to numerical solutions. In order to have numerical solutions, complex finite element models are needed to be prepared with many assumptions. With analytical method, the solutions can be done with fewer simplifications as compared to FEA models. In order to be able to use analytical model for four-point contact bearings the results of finite element modeling and analytical method for load distribution on the balls are compared with each other for simplified models. Analytical based MATLAB code is generated for analytical calculation and an appropriate finite element analysis model is prepared using the parametric design language (APDL) of a commercial program (ANSYS). At the end, the results of the FEAs are compared with the analytical method for calculating the deflections and load on each ball. It is observed that the results of the FEA model and the MATLAB code are confirmed each other. Therefore it is decided that in the further studies for different slewing bearings,

MATLAB model can be used for investigation of load distribution and deflection in bearings. With the result of analytical code, more complex studies are done. Since modeling clearance in FEA is not a practical method because of the convergence issues, the effect of clearance is studied in the analytical model. The change of contact angles due to clearance is also studied with the analytical model. With the created MATLAB model dimensional changes in the bearings are also studied and the effects of different load cases are combined in one solution.

**Keywords:** Slewing bearings, four-point contact bearings, MATLAB algorithms, load distribution, finite element analysis, ANSYS, APDL, MATLAB

# ÖZ

DÖRT NOKTA TEMASLI DÖNER TABLA RULMANLARININ ANALİTİK OLARAK MODELLENEREK YÜK DAĞILIMININ ELDE EDİLMESİ

Müftüoğlu, Güneş Ece

Yüksek Lisans, Makine Mühendisliği Bölümü

Tez Yöneticisi: Prof. Dr. Metin Akkök

Eylül 2014, 110 sayfa

Bu tezde dört nokta temaslı rulmanlardaki yükleme koşullarına göre bilyalardaki yük dağılımları incelenmiştir. Amaç yük dağılımı için literatürdeki olan analitik metodun kullanılabilirliğini doğrulamak ve ilerideki çalışmalarda bu yöntemin kullanılmasıyla bu tip rulman tasarımlarını hızlandırmak ve kolaylaştırmaktır. Sonlu elemanlar metodu kullanılarak yapılan çalışmalarda çok sayıda basitleştirmeye ihtiyaç duyulmakta ve çözümü uzun zaman alan kompleks modellerin çözümünün hazırlanması gerekmektedir. Sonlu elemanlar metodu ile yapılan çalışmalarda çözüme ulaşabilmek için boşlukların modellenmediği basitleştirilmiş modellere gidilmektedir. Bu durumda önemli bir değişken ihmal edilmiş olmaktadır. Bunun yerine daha az ihmal kullanılan analitik çözümü kullanmak daha uygun olacaktır. Sonlu elemanlar yöntemi ile ihmal edilen değişkenleri de değerlendirebilmek için literatürdeki analitik hesaplama metoduna uygun analitik kod (MATLAB) oluşturulmuş ve uygun sonlu elemanlar modeli (ANSYS) hazırlanmıştır. Analitik çözümün kullanılabilirliğini doğrulamak için analitik temelli MATLAB moelinin sonuçları sonlu elemanlar analizinin sonuçları ile karşılaştırılmıştır. Karşılaştırılan

sonuçların birbirini doğrular nitelikte olduğu gözlenmiştir. Bu durumda, sonlu elemanlar yöntemi ile değerlendirilmesi uzun ve zahmetli olan rulman boşluklarına bağlı olarak yük, deplasman ve kontak açısı değişimleri MATLAB modeli ile göz önünde bulundurulabilecektir. Böylece daha gerçekçi sonuçlar elde edilebilecektir. Bunun yanı sıra farklı dört nokta temaslı rulmanlar için farklı sonlu elemanlar modeli hazırlamak yerine hızlıca analitik modelin çıktıları kullanılabilecektir. Bu sayede tasarım süreçleri hızlandırılabilecektir.

**Anahtar Kelimeler:** Döner tabla rulmanı, dört nokta temaslı rulman, MATLAB algoritma, yük dağılımı, sonlu elemanlar metodu, ANSYS, APDL, MATLAB

**ACKNOWLEDGEMENTS**

First of all I would like to express my sincere appreciation to my thesis supervisor Prof. Dr. Metin AKKÖK for his guidance throughout my thesis study.

I am in debt of gratitude to Bülent ACAR in ROKETSAN Inc. for his friendly support with the finite element analysis method and his patience.

I wish to express my gratitude to Caner GENÇOĞLU for his guidance throughout my thesis study.

I also owe thanks to my colleagues in my unit in ROKETSAN Inc. who helped me in every subject throughout the years of my study.

Finally I wish to express my sincere thanks to my father Ahmet MÜFTÜOĞLU, my mother Mukadder MÜFTÜOĞLU and my fiance Mehmet Tuğcan GÜNAY for their endless support.

**TABLE OF CONTENTS**

ABSTRACT ..... v

ÖZ ..... vii

ACKNOWLEDGEMENTS ..... ix

TABLE OF CONTENTS ..... x

LIST OF TABLES ..... xiii

LIST OF FIGURES ..... xiv

LIST OF SYMBOLS ..... xx

LIST OF ABBREVIATIONS ..... xxv

CHAPTERS ..... 1

1. INTRODUCTION ..... 1

1.1 Literature Survey ..... 1

1.2 Objective and Scope of Thesis ..... 11

1.3 Thesis Outline ..... 12

2. ANALYTICAL MODELING OF SLEWING BEARING LOAD DISTRIBUTION ..... 15

2.1 Analytical Solution Methodology of Slewing Bearings' Load Distribution 15

2.2 Load Distribution Calculation Procedure ..... 23

2.2.1 When the Contact is Between Cii and Ces; ..... 27

2.2.2 When the Contact is Between Cis and Cei; ..... 30
2.3 MATLAB Modeling and Samples for Analytical Based MATLAB Model30
2.3.1 Verification of Axial Loading Condition for MATLAB Model..... 31
2.3.2 Verification of Radial Loading Condition for MATLAB Model ..... 33
2.3.3 Verification of Moment Loading Condition for MATLAB Model ..... 36
3. VERIFICATIONS OF ANALYTICAL STUDIES WITH BENCHMARK FORMULAE AND NUMERICAL FEA MODELS ..... 39
3.1 Verifications of Analytical Studies with Benchmark Models..... 39
3.1.1 Verification of Coefficient K with Benchmark Model ..... 39
3.1.2 Verification of MATLAB Results with Benchmark Models..... 41
3.2 Verifications of Analytical Studies with Numerical FEA Models..... 43
3.2.1 Raceway Modeling of the Slewing Bearing in FEA Model ..... 44
3.2.2 Spring Modeling of the Balls of the Slewing Bearing in FEA Model . 45
3.2.3 System Modeling of Raceways and Balls in FEA Model..... 46
3.2.4 FEM Results of Pure Moment Loading ..... 47
3.2.5 FEM Results of Pure Axial Displacement ..... 49
3.2.6 FEM Results of Pure Radial Loading ..... 52
4. ANALYTICAL STUDIES FOR FURTHER CASES IN MATLAB..... 57
4.1 Effect of Clearance (Endplay) on Displacement, Contact Angle and Load Distribution..... 57
4.1.1 Effect of Clearance (Endplay) of 0.05 mm for Pure Moment Loading Condition ..... 58
4.1.2 Effect of Clearance (Endplay) of 0.1 mm for Pure Moment Loading Condition ..... 62
4.1.3 Effect of Clearance of 0.05 mm for Pure Axial Loading Condition.... 65
4.1.4 Effect of Clearance of 0.1 mm for Pure Axial Loading Condition..... 66

4.1.5 Effect of Clearance of 0.05 mm for Pure Radial Loading Condition .. 68

4.1.6 Effect of Clearance of 0.1 mm for Pure Radial Loading Condition .... 69

4.2 Effect of Different Ball Diameter and Radius of Curvature of Raceways on Displacement, Contact Angle and Load Distribution ..... 72

4.2.1 Effect of Increasing Raceway Diameter with Zero-Clearance ..... 73

4.2.2 Effect of Increasing Raceway Diameter with Clearance of 0.05 mm .. 75

4.2.3 Effect of Increasing Raceway Diameter with Clearance of 0.1 mm .... 76

4.2.4 Effect of Different Ball Diameter ..... 80

4.3 Effect of Combined Load Case and Clearance on Displacement, Contact Angle and Load Distribution ..... 83

5. DISCUSSION OF THE RESULTS AND CONCLUSIONS ..... 89

5.1 Discussion of the Results ..... 89

5.2 Conclusions ..... 92

REFERENCES ..... 95

APPENDICES ..... 99

A.SOLUTION PROCEDURE OF MATLAB CODES ..... 99

B.MATLAB ANALYTICAL CALCULATION CODES ..... 101

C.BACKGROUND OF IMPORTANT MATLAB CODES ..... 105

D.APDL CODE PREPARED FOR FINITE ELEMENT MODEL ..... 107

E.IMPORTANT CODES AND ELEMENT PROPERTIES USED IN ANSYS APDL CODE ..... 109

## LIST OF TABLES

TABLES

Table 1 - Comparison of FEM & MATLAB deformation versus force data..... 22

Table 2 - Comparison of K coefficients found by theoretical formulae and numerical FEA method ..... 40

Table 3 - Verification of analytical based MATLAB model results with the results of the benchmark formulation ..... 43

Table 4 - Comparison of analytical based MATLAB and numerical FEM solution . 55

Table 5 - Comparison of the results for deflection angle and maximum load with different clearance values due to pure moment loading condition ..... 64

Table 6 - Comparison of deflection angle “θ” and maximum load “Qmax” values for different clearance conditions for different loading types ..... 71

Table 7 - Effect of clearance and effect of change in the radius of curvature of the raceways on Qmax and θ ..... 78

Table 8 - Sample data region for contribution of balls to load distribution for different $r_c$ values ..... 79

Table 9 - Effect of the change in the ball diameter ..... 82

## LIST OF FIGURES

FIGURES

Figure 1 - Slewing bearing in a weapon system [1] ..... 2

Figure 2 - Offshore and marine applications of slewing bearings [2] ..... 2

Figure 3 - Offshore and marine applications of slewing bearings [2] ..... 3

Figure 4 - Heavy construction equipment application of slewing bearings [3] ..... 3

Figure 5 - Topology of a four contact point slewing bearing [4] ..... 4

Figure 6 - External loads on a large roller slewing bearing assembly (a), components of a large three-row roller slewing bearing (b) [5]. ..... 5

Figure 7 - ½ Symmetry FEM-model of a three-row roller slewing bearing: external loads, support and couplings (a), detail of the bearing FEM-model with visible mesh and 1D connectors (b) [5] ..... 5

Figure 8 - Graph of axial (left) and radial (right) components [6] ..... 6

Figure 9 - The influence of different clearances on the distribution of the contact forces for axial load and moment [11] ..... 7

Figure 10 - Flow chart of calculating distribution of contact forces in [12] ..... 8

Figure 11 - Two-node truss element (a) and nonlinear elastic material model (b) [13]9

Figure 12 - Numerical modeling of ball contact [14] ..... 9

Figure 13 - Finite element model of deep groove ball bearing [15] ..... 10

Figure 14 - Position angle vs. normal force under different radial deformations while axial deformation is 0.01 mm [16] ..... 10

Figure 15 - Radial load vs. radial deformation under different axial loads [16] ..... 11

Figure 16 - a) Deep groove ball bearing b) 4-Point contact ball bearing [6] ..... 12

Figure 17 - Loading directions and coordinate system [6] ..... 16

Figure 18 - Degrees of freedom of a bearing ..... 16

Figure 19 - Centers of curvatures of the raceways [6] ..... 17

Figure 20 - Center of curvature locations in contact [6] ..... 18

Figure 21 - Dimensional parameters of the slewing bearing inner geometry ..... 19

Figure 22 - Dimensional parameters of the outer geometry of the slewing bearing .. 19

Figure 23 - Fit for the coefficient K (K=450 $kN/mm^{3/2}$) versus FEA data [20] ..... 20

Figure 24 - Abaqus model for ball deflection model [20] ..... 21

Figure 25 - Dimensional parameters for clearance between the races and ball bearings [6] ..... 25

Figure 26 - Possible contact types [6] ..... 27

Figure 27 - Projection of distances, angles and forces on the XY plane in the contact Cii–Ces. [6] ..... 29

Figure 28 - Basic schematic for calculation methodology ..... 30

Figure 29 - Load Distribution on Balls for Axial Loading Condition ..... 32

Figure 30 - Contact Angle of Balls due to pure axial loading condition (alpha 2) .... 32

Figure 31 - Total load distribution on balls due to pure axial loading condition ..... 33

Figure 32 - Total load distribution on balls due to pure radial loading condition (blue line and red line are coincident) ..... 34

Figure 33 - Load distribution on balls due to radial loading condition ..... 35

Figure 34 - Contact angle of balls due to radial loading condition (alpha2 and alpha1) ..... 35

Figure 35 - $\delta z_2$ due to pure moment loading ..... 37

Figure 36 - Load distribution on the balls due to pure moment loading condition .... 37

Figure 37 - Contact angle of balls due to pure moment loading condition (alpha2 and alpha1) ..... 38

Figure 38 - Total load distribution on balls for moment loading condition ..... 38

Figure 39 - SOLID 185 element of ANSYS [22-23] ..... 44

Figure 40 - Meshing of raceways in FEM ..... 45

Figure 41 - COMBIN 39 element of ANSYS [22-23] ..... 45

Figure 42 - Meshing of raceways and balls with solid and spring elements ..... 47

Figure 43 - Displacement in the z-axis for moment loading condition ..... 48

Figure 44 - Load distribution in Newtons on balls for pure moment loading condition ..... 49

Figure 45 - Displacement [mm] and reaction force [N] the master node in the z-axis for pure axial displacement condition ..... 50

Figure 46 - Load distribution in Newtons on balls for pure axial displacement condition ..... 51

Figure 47 - Load distribution in on balls for pure axial loading of 38.5 kN ..... 52

Figure 48 - Displacement in the y-axis for pure radial loading condition ..... 53

Figure 49 - Load distribution in Newtons on balls for pure radial loading condition 54

Figure 50 - Load distribution for 0.05 mm clearance and pure moment loading of 100 kN.m ..... 59

Figure 51 - Total load distribution on balls for clearance of 0.05 mm due to moment loading of 100 kN.mm ..... 60

Figure 52 - Change in the contact angle alpha for clearance of 0.05 mm due to moment loading of 100 kN.m ..... 61

Figure 53 - Locuses of centers of curvatures ..... 61

Figure 54 - Load distribution for 0.05 mm clearance and moment loading ..... 62

Figure 55 - Total load distribution on balls for clearance of 0.1 mm due to moment loading ..... 63

Figure 56 - Change in the contact angle alpha for clearance of 0.1 mm due to moment loading ..... 64

Figure 57 - Total load distribution on balls for clearance of 0.05 mm due to axial loading of 100 kN ..... 65

Figure 58 - Change in the contact angle alpha for clearance of 0.05 mm due to axial loading of 100 kN ..... 66

Figure 59 - Total load distribution on balls for clearance of 0.05 mm due to axial loading of 100 kN ..... 67

Figure 60 - Change in the contact angle alpha for clearance of 0.05 mm due to axial loading of 100 kN ..... 67

Figure 61 - Total load distribution on balls for clearance of 0.05 mm due to radial loading of 10 kN ..... 68

Figure 62 - Change in the contact angle alpha for clearance of 0.05 mm due to radial loading of 10 kN ..... 69

Figure 63 - Total load distribution on balls for clearance of 0.1 mm due to radial loading of 10 kN ..... 70

Figure 64 - Change in the contact angle alpha for clearance of 0.1 mm due to radial loading of 10 kN ..... 70

Figure 65 - Trend of change in the Qmax with respect to clearance ..... 72

Figure 66 - Load distribution for K= 271.4 kN/mm$^{3/2}$(1. 2 ×$r_c$), zero clearance and pure moment load of 100 kN.m ..... 74

Figure 67 - Contact angle distribution for K= 271.4 kN/mm$^{3/2}$ (1. 2 ×$r_c$) , zero clearance and pure moment load of 100 kN.m ..... 74

Figure 68 - Load distribution for K= 271.4 kN/mm$^{3/2}$ (1. 2 ×$r_c$), 0.05 mm clearance and pure moment load of 100 kN.m ..... 75

Figure 69 - Contact angle distribution for K= 271.4 kN/mm$^{3/2}$ (1. 2 ×$r_c$), 0.05 mm clearance and pure moment load of 100 kN.m ..... 76

Figure 70 - Load distribution for K= 271.4 kN/mm$^{3/2}$ (1. 2 ×$r_c$), 0.1 mm clearance and pure moment load of 100 kN.m ..... 77

Figure 71 -Contact angle distribution for K= 271.4 kN/mm$^{3/2}$ (1. 2 ×$r_c$), 0.1 mm clearance and pure moment load of 100 kN.m ..... 77

Figure 72 - Change of maximum load observed on the balls with respect to radius of curvature for pure moment loading ..... 79

Figure 73 - Change of deflection angle “θ” with respect to radius of curvature for pure moment loading ..... 80

Figure 74 - Load distribution for K= 387.8 kN/mm$^{3/2}$ (0.95×d) 0.05 mm clearance and pure moment load of 100 kN.m ..... 81

Figure 75 - Load distribution for K= 387.8 kN/mm$^{3/2}$ (0.95×d) 0.1 mm clearance and pure moment load of 100 kN.m ..... 81

Figure 76 - Contact angle distribution for K= 387.8 kN/mm$^{3/2}$ (0.95×d) 0.1 mm clearance and pure moment load of 100 kN.m..... 82

Figure 77 - Load distribution for combined axial and moment loading for a) 0 mm clearance, b) 0.1 mm clearance ..... 84

Figure 78 - Load distribution for combined moment load of 100 kN.m and axial load of 100 kN for clearance of 0 mm ..... 85

Figure 79 - Load distribution for combined moment load of 100 kN.m and axial load of 100 kN for clearance of 0.1 mm ..... 85

Figure 80 - Contact angle distribution for combined moment load of 100 kN.m and axial load of 100 kN for clearance of 0 mm..... 86

Figure 81 - Contact angle distribution for combined moment load of 100 kN.m and axial load of 100 kN for clearance of 0.1 mm..... 87

Figure 82 - Working procedure of MATLAB codes that is prepared for analytical calculations..... 100

## LIST OF SYMBOLS

SYMBOLS

| | |
|---|---|
| *a* | Half distance between radii of curvature of raceways in axial direction |
| *A* | Initial distance between diagonally opposed center of curvatures |
| *A'* | Distance between diagonally opposed center of curvatures when contact occurs |
| *A1* | Final distance between diagonally opposed center of curvatures |
| bcr | Ball center radius |
| bch | Ball center height |
| Cii | The center of curvature of the lower inner raceway |
| Cis | The center of curvature of the upper inner raceway |
| Cei | Center of curvature of the lower outer raceway |
| Ces | Center of curvature of the upper outer raceway |
| *d* | Rolling element diameter |
| *dm* | Mean diameter of bearing |
| *dout* | Maximum diameter of the bearing |
| E | Elastic modulus |
| *Fzt* | Total axial load in z direction |

| | |
|---|---|
| *Frt* | Total radial load in x-y plane |
| *h* | Half distance between radii of curvature of raceways in radial direction |
| *J* | Mechanical gap in z direction |
| K | Coefficient for elastic deformation of the balls |
| *m* | Moment of the reaction |
| *Mt* | Total moment load |
| *n* | Number of balls |
| *Pr* | Existing radial clearance in the bearing |
| *q* | Reaction force on balls |
| *q1* | Reaction force on balls for Cii-Ces contact |
| *q2* | Reaction force on balls for Cis-Cei contact |
| *Q* | The force on each ball |
| *Qmax* | The force on the maximum loaded ball |
| $r_{in}$ | Inner radius of inner ring |
| $r_{out}$ | Inner radius of outer ring |
| $r_c$ *inner* | Groove radius of inner-ring raceway |
| $r_c$ *outer* | Groove radius of outer-ring raceway |
| $r_c$ | Groove radius of outer and inner raceways when $r_c$ inner equals to $r_c$ outer |
| *R* | The vector position of the point of application of the reaction |
| $t_{in}$ | Thickness of inner ring |
| $t_{out}$ | Thickness of outer ring |

| | |
|---|---|
| $z_{out}$ | Outer ring distance from the ground |
| $\alpha$ | Contact angle |
| $\delta z$ | Displacement in the z direction |
| $\delta z2$ | Displacement in the z direction due to pure moment load |
| $\delta r$ | Displacement in the r direction |
| $\theta$ | Rotation about y axis |
| $\kappa$ | Mean curvature ratio |
| $\kappa_j$ | Curvature ratio at the inner ring |
| $\kappa_A$ | Curvature ratio at the outer ring |
| $v$ | Poisson's ratio |
| $\Psi$ | Angle of ball location in x-z plane |
| $\Phi$ | Angle of ball location in x-y plane |
| $\Delta$ | Displacement between *A1* and *A'* |

## LIST OF ABBREVIATIONS

ABBRAVIATIONS

| | |
|---|---|
| APDL | ANSYS Parametric Design Language |
| FEM | Finite element model |
| FEA | Finite element analysis |

# CHAPTER 1

# INTRODUCTION

## 1.1 Literature Survey

Four-point contact slewing bearings are mostly used with internal or external gear system in order to transfer rotational motion. These bearings are mostly used in turn tables in rotational systems like cranes, cradles, tanks, medical equipment like MR machines, offshore and marine applications, wind turbines and military radars. Launcher systems of weapon systems are other important usage areas of slewing bearings. Figure 1 is an example of turntable system in a weapon system. Offshore and marine applications of slewing bearings are given in Figure 2 and Figure 3. Figure 4 is an example for usage of slewing bearings in heavy construction equipment. The most common usage area of slewing bearings is cranes with turn tables. The bearings are dominantly exposed to moment loading in the cranes just like in the weapon systems and other usage areas.


**Figure 1 - Slewing bearing in a weapon system [1]**

**Figure 2 - Offshore and marine applications of slewing bearings [2]**

**Figure 3 - Offshore and marine applications of slewing bearings [2]**

**Figure 4 - Heavy construction equipment application of slewing bearings [3]**

A slewing bearing is the most important component of a turntable. It transfers the rotation into turning parts of the system while holding the fixed body apart from the rotation. Slewing bearings are large sized components with respect to the standard bearings and must be analyzed in a different way than standard bearings. They contain inner and outer ring holes for mounting purposes. The schematic of a slewing bearing with single row is given in Figure 5.

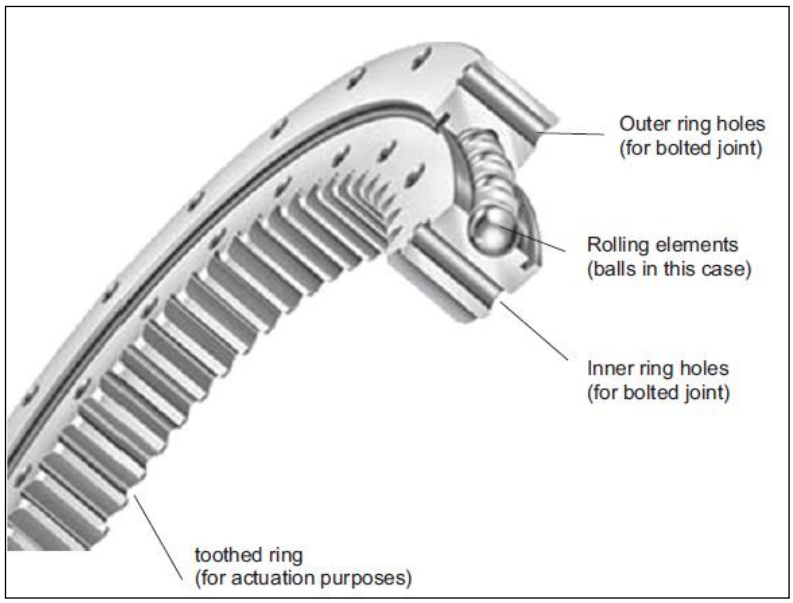


**Figure 5 - Topology of a four contact point slewing bearing [4]**

Finite element method is applied to a sample bearing in this thesis. There are examples of using finite element method for slewing bearings in the literature. In [4] a complex finite element model of a slewing bearing is prepared. In this thesis, FEA model is simplified as much as possible in order to verify analytical calculations in a simplified manner. In [4], springs are connected to rigid raceways while the rest of the inner and outer rings are assumed as elastic. Furthermore, raceways and inner and outer rings in the FEM are both modeled as rigid in order to have same assumptions with the analytical model.

A different example of finite element analysis method of a slewing bearing can be found in [5]. A three-row slewing bearing is investigated with three types of rollers; cylindrical roller (without profile correction), fully crowned roller (logarithmic-profile) and partially crowned roller (ZB-profile) in [5]. Contact stresses are determined numerically and displacement-force characteristic is used in further fatigue analysis in this study. Types of rollers and geometry of the slewing bearing in [5] can be seen on Figure 6.

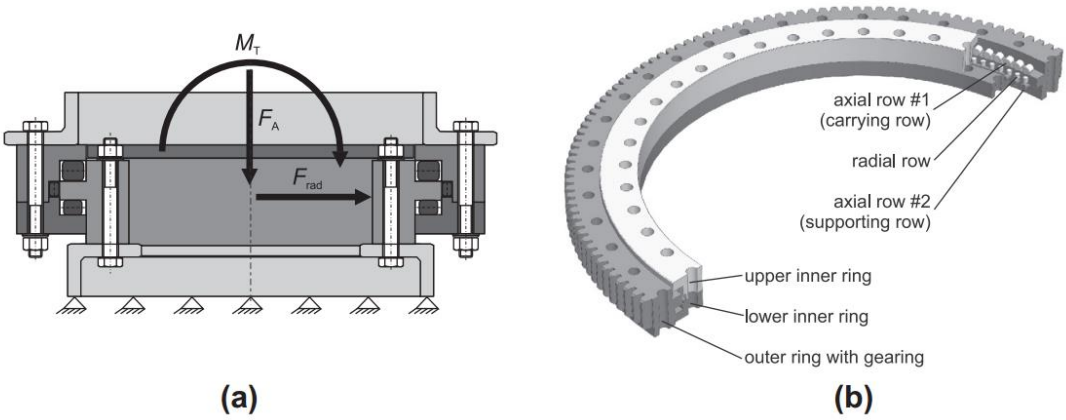


**Figure 6 - External loads on a large roller slewing bearing assembly (a), components of a large three-row roller slewing bearing (b) [5].**

During the modeling of the raceways and balls similar method to this thesis is used in [5]. The balls' being modeled as non-linear connectors in this study can be observed from Figure 7.

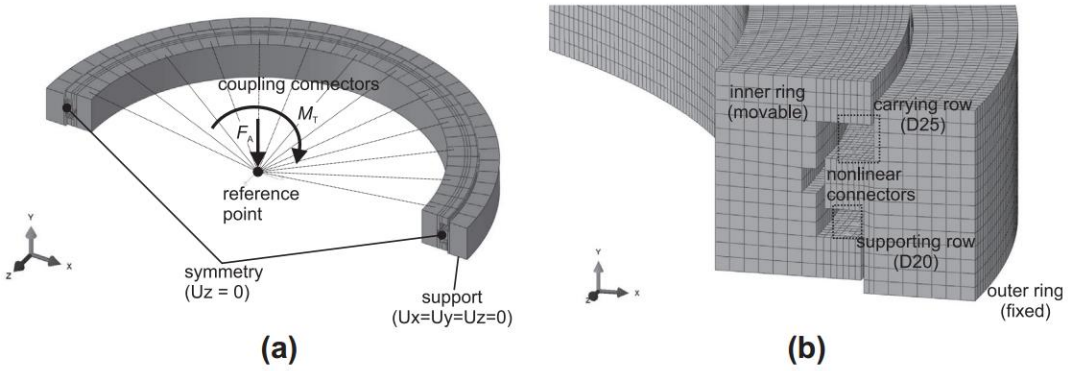


**Figure 7 - ½ Symmetry FEM-model of a three-row roller slewing bearing: external loads, support and couplings (a), detail of the bearing FEM-model with visible mesh and 1D connectors (b) [5].**

In this thesis finite element model is analyzed in order to verify the analytical calculations. Analytical calculations are preferred with respect to complex finite element methods. Analytical calculations in [6] are investigated throughout the analytical modeling part of the thesis.

Load distribution in a slewing bearing can be calculated with analytical method by using the geometrical changes on the balls and raceways. In [6], the load distribution and geometrical changes in a loaded bearing are calculated for a single row slewing bearing. In this thesis the calculation procedure is applied to a sample slewing bearing. Figure 8 shows the sample load distribution due to combined loading found in [6].

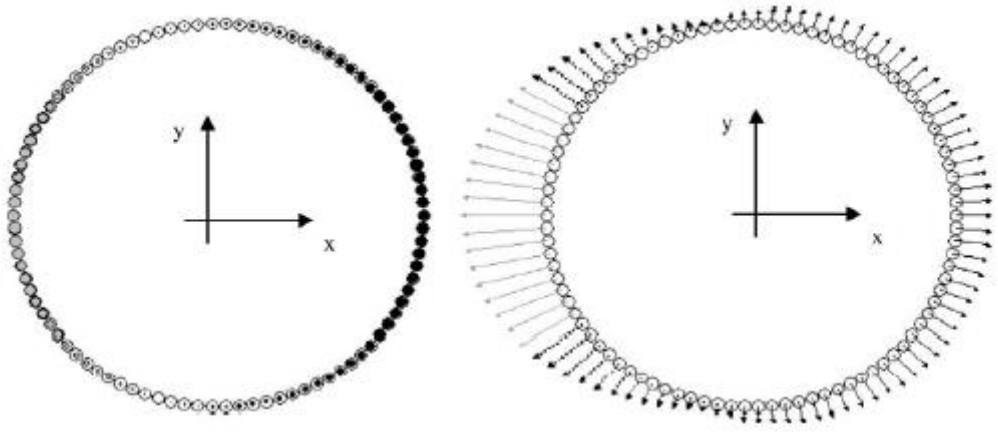


**Figure 8 - Graph of axial (left) and radial (right) components [6]**

In Figure 8, load components are shown in two pictures. "The reaction components for the different contacts are distinguished by colors and line style (Cii–Ces=black ,Cis–Cei= grey , and when the contact is made on the two diagonals line is dashed). On the graph of the axial components, the heavier the load on a ball bearing is, the bolder the fill-in color. The axial component follows a perpendicular direction to the screen. If it is black, it means that its direction is incoming into the screen. If it is grey, it is outgoing from the screen. The radial components of the reactions of the ball bearing are always towards the outside of the bearing" [6] (See p.17 for details).
Similar calculations to this thesis are also made in [7-10]. In accordance with analytical computations in [7-10], load distribution for certain conditions is found in [11]. Examples of load distribution data in [11] are given in Figure 9. Figure 9 also shows the load distribution under axial and moment loadings and effect of the clearance is examined. Clearance is observed as force discontinuities in application of moment.

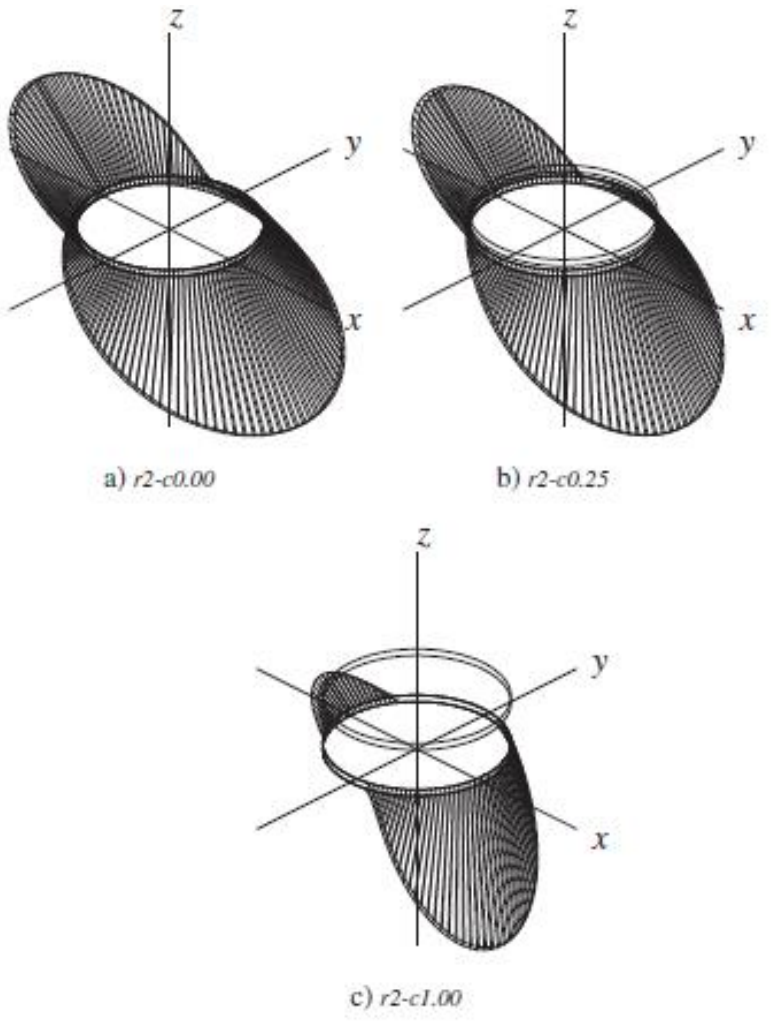


**Figure 9 - The influence of different clearances on the distribution of the contact forces for axial load and moment [11]**

Contact force distribution and static load-carrying capacity of large size double row four-point contact ball bearing are calculated in a similar method in [12]. The analytical calculation procedure is similar in this thesis and flow chart of calculating procedure for distribution of contact forces in [12] is given in Figure 10.

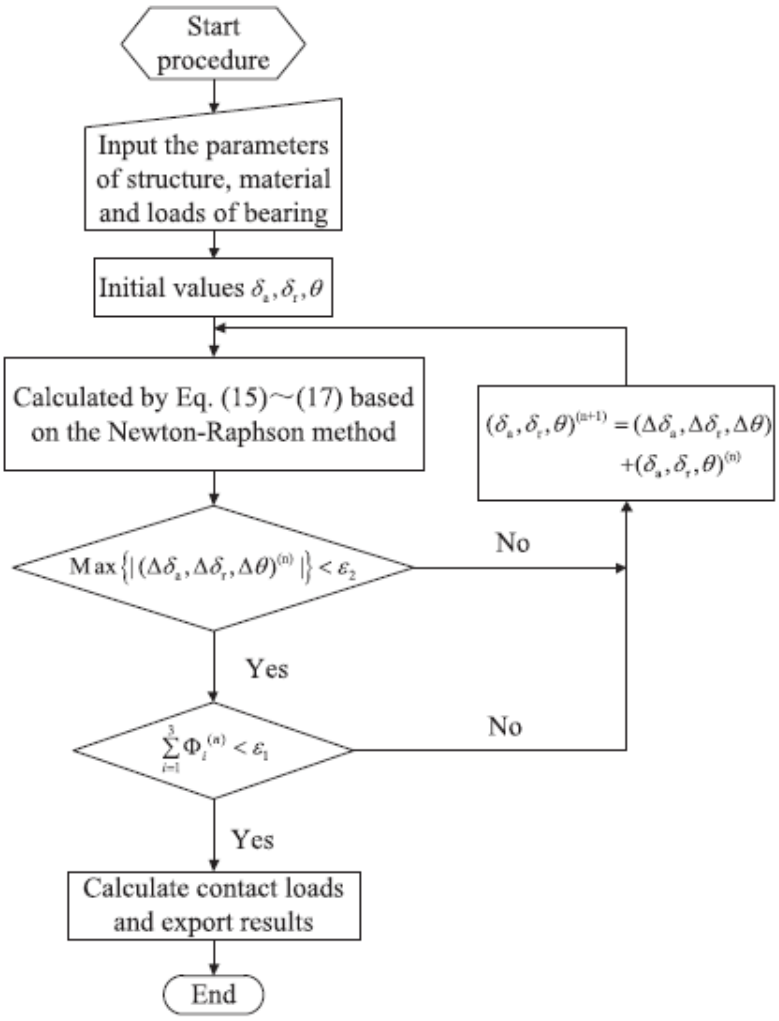


**Figure 10 - Flow chart of calculating distribution of contact forces in [12]**

Finite element analysis of ball bearings requires contact characteristics of balls to be determined before the total analysis. Hertzian contact occurs between the balls and the raceways. This contact requires time-consuming analyses to be done. Since it is not feasible to make this analysis for every single ball of a slewing bearing in the final finite element analysis, ball characteristics can be turned into a stiffness curve with a single ball contact analysis. An example of getting stiffness matrix from single ball analysis is done in the paper "Modeling of rollers in calculation of slewing bearing with the use of finite elements" [13]. Sample stiffness curve and used FEM element is given in Figure 11.

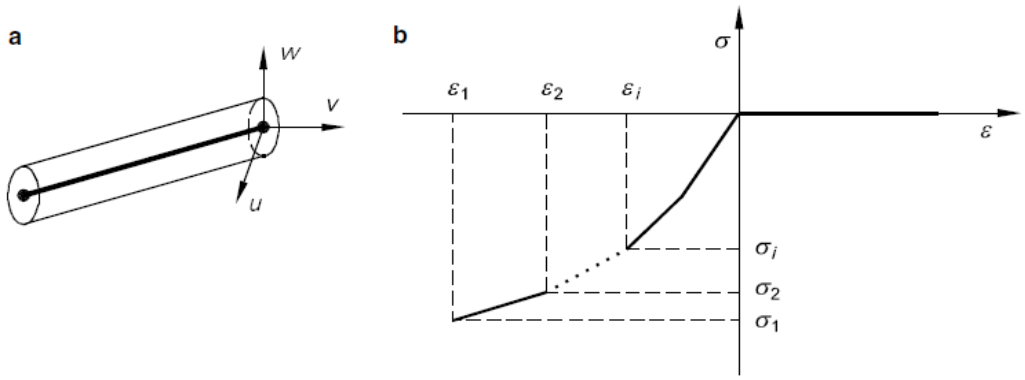


**Figure 11 - Two-node truss element (a) and nonlinear elastic material model (b) [13]**

Modeling ball-raceway contact in FEM requires fine meshing in the contact zone. In Figure 12, sample for meshing in FEM analysis of ball-raceway contact is given.

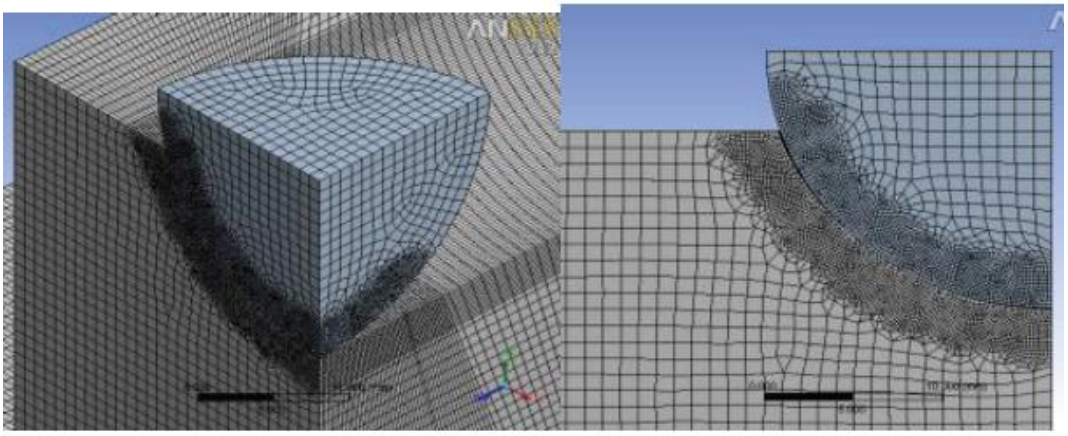

**Figure 12 – Numerical modeling of ball contact [14]**

In literature, it is also seen that bearing analyses are done with complete modeling of bearings. This may be optional for small sized bearings but FEM modeling of relatively large sized bearings with complete meshing would be inappropriate due to solution capabilities of FEM programs. Figure 13 is an example of complete FEM modeling of a small sized bearing.

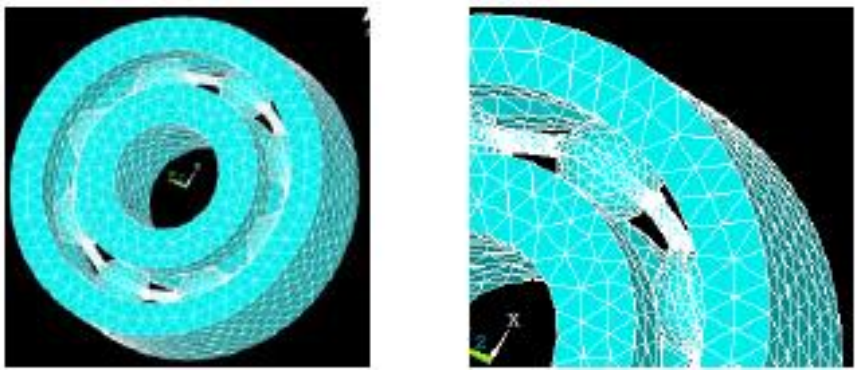

**Figure 13 - Finite element model of deep groove ball bearing [15]**

For angular contact bearings and deep groove ball bearings force distribution is also calculated in literature. Load distribution for ball positions are found for angular contact ball bearings in [16] with analytical calculations similar to this thesis. Figure 14 and Figure 15 show the analytical calculation results of force distribution for different loading conditions in [16].

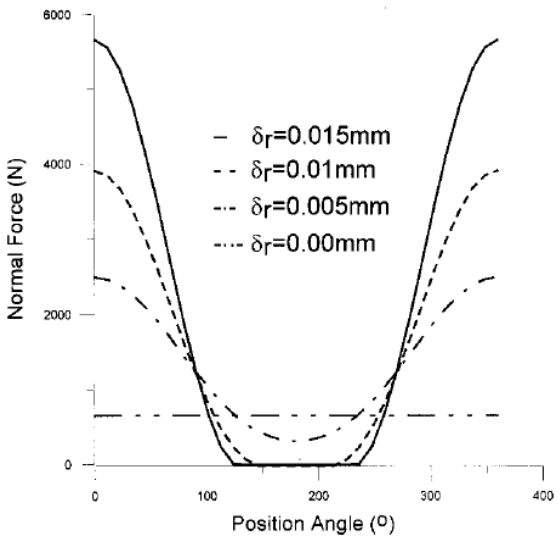


**Figure 14 - Position angle vs. normal force under different radial deformations while axial deformation is 0.01 mm [16]**

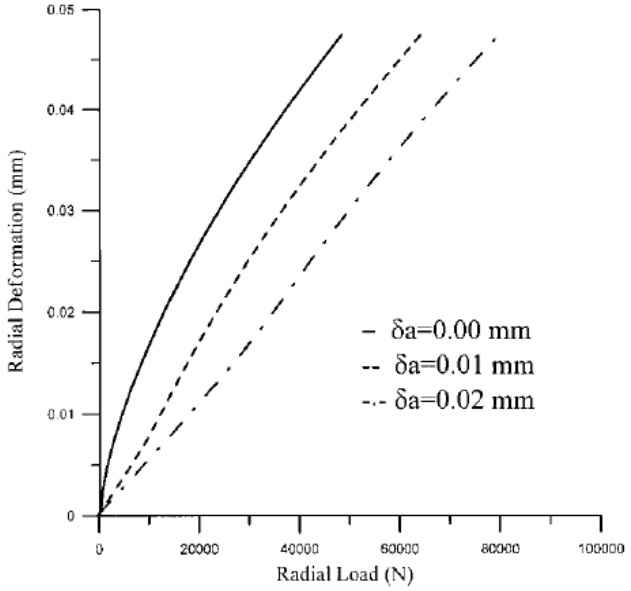


**Figure 15 - Radial load vs. radial deformation under different axial loads [16]**

## 1.2 Objective and Scope of Thesis

The objective of the thesis is to determine whether there is a more effective method then FEA for analyzing a slewing bearing system deformation and load distribution.

In order to have numerical solutions using FEA, complex finite element models need to be prepared with many assumptions. With analytical calculation method, solutions can be done with less simplified models with fewer assumptions as compared to FEA models. In order to make the decision that analytical calculation method is a more effective solution, literature survey has been done for analytical calculations and appropriate calculations are found and proper analytical MATLAB code is generated. Empirical maximum load formulae in the literature are checked and FEA model is prepared for validation of the calculations. In order to prepare FEA model, a simplified method is conducted in accordance with the literature survey. Finite element analysis model is prepared using a parametric design language (APDL) of a commercial program (ANSYS). At the end, results of the finite element analysis are compared with the results of analytical MATLAB model. It is observed that results of the FEA model and the analytical code are good in agreement. Therefore it is

decided that, in the further studies for different slewing bearings, analytical MATLAB model can be used for investigation of load distribution and deflection in bearings, instead of preparing a new and finite element model with many assumption. With the result of analytical code, more complex studies are done. Effect of clearance and different inner geometry are studied and the effect of different contact angle is investigated.

Deep groove ball bearings have one curvature for one raceway but four-point contact bearings have both upper and lower curvatures in one raceway. Balls can contact different raceways for different axial loading conditions. In Figure 16 comparison of deep grove ball bearing and four-point contact ball bearing can be observed.

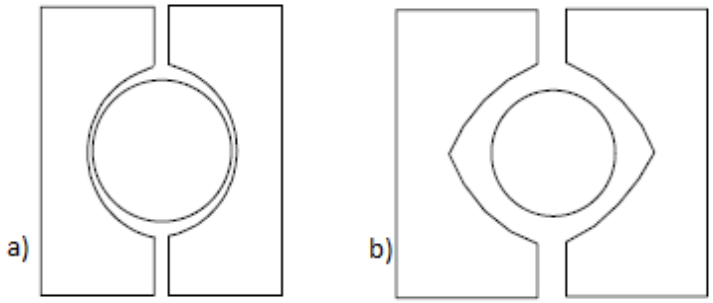


**Figure 16 - a) Deep groove ball bearing b) 4-Point contact ball bearing [6]**

Generally raceways of the bearings are manufactured with high accuracy and the materials of the raceways are reinforced. Since the stiffness of the raceways is very high compared to the balls, raceways are assumed as rigid both in the FEM method and the analytical calculation in MATLAB. It is assumed that there is no geometrical change in the raceways in the calculations.

## 1.3 Thesis Outline

This study is carried out in order to gain more theoretical knowledge on the loaded behavior of slewing bearings. In the first chapter an introduction to four-point contact bearings is made by presenting the examples of slewing bearing solutions applied to engineering structures used in cranes, cradles, tanks, medical equipment like MR

machines, offshore and marine applications, wind turbines and military radars. In addition to slewing bearings load distribution is investigated for standard bearings like deep-groove ball bearings and angular contact ball bearings. Background of the theory of load distribution in slewing bearings is strongly based on the standard bearing load distribution studies.

In the second chapter of the study, analytical calculations are explained in detail. Geometrical designations that are used in analytic calculations are explained clearly and sample solutions are presented. As a theoretical background of the analytical calculations, eighty relations are used in order to solve the deflection and load distributions.

In the third chapter, verifications of the analytical calculation and stiffness calculations are presented. At the first part of third chapter, coefficient "K" that is used in the second chapter is verified with a benchmark formulation in literature. The comparison of the results shows that the FEM is consistent with the formulation with the confidence of 0.5%. At the second part of the third chapter, results of the sample load cases that are studied in analytical code are verified with the approximation formulae in literature. At the third part of second chapter, prepared finite element method is explained. The solutions of finite element method are compared with analytical calculations for proper load case samples. Comparison of analytical and numerical results is given in Table 4. It can be concluded that the analytical calculations are consistent with the numerical solutions. In the light of this observation, analytical solution can be preferred for faster design steps. Convergence problems can be eliminated and fewer assumptions can be considered.

Fourth chapter of the study is dedicated to case studies for effective bearing parameters including clearance, different ball diameter and radius of curvature of raceways. It is impossible to produce a bearing with exactly zero clearance between balls and raceways and it is concluded that the clearance in the bearings is a very important parameter that is needed to be considered. Clearance affects both load distribution and deflection results of the load cases significantly. Without considering clearances, change in the contact angle cannot be observed, either. In FEA models clearances cannot be modeled because of convergence problems. The combination of

the effects of contact angle and clearance determines the deflection characteristics and load distribution of the bearings. With the increased clearance maximum load on balls increases significantly for moment loading and radial loading. During the design steps of the systems with slewing bearings with inner clearance, analytical MATLAB model should be preferred instead of finite element models.

In the second part of fourth chapter, increasing radius of curvature of the raceways is studied. Insignificant decrease in maximum load can be observed in the bearings with clearance, while the deflection angle $\theta$ increases. An optimization between deflection angle $\theta$ and maximum load on balls can be done with changing clearance value for optimizing those parameters.

In the last part of fourth chapter, effect of decreasing ball diameter is investigated. Decrease of ball diameter gives the same characteristic properties with increasing radius of curvature of the raceways.

The concluding remarks are presented in Chapter 5 as a conclusion.

# CHAPTER 2

# ANALYTICAL MODELING OF SLEWING BEARING LOAD DISTRIBUTION

## 2.1 Analytical Solution Methodology of Slewing Bearings' Load Distribution

Calculation methodology in "Load Distribution in a Four Contact-Point Slewing Bearing" [6] is used for analytical calculations. Equations (1-54) are obtained from [6]. Displacements of the balls are calculated with respect to geometry of the initial and the final positions of the balls.

It is predicted that three types of loading will be applied to the bearing. These are;

- Axial loading: $F_z$
- Radial loading: $F_r$
- Moment: M

In accordance with these loads, raceways of the bearing have 3 degrees of freedom. These are;

- Axial displacement: $\delta z$
- Radial displacement: $\delta r$

- Rotation: θ

Loads and the displacements are given in Figure 17 and Figure 18. Coordinate axis of the bearing is determined with respect to loads. Angles Φ and ψ is defined in order to define the locations of the bearings. Angle "Φ" represents the location in x-y plane while "ψ" represents the location in x-z plane. Angles that represent ball locations are given in Figure 17.

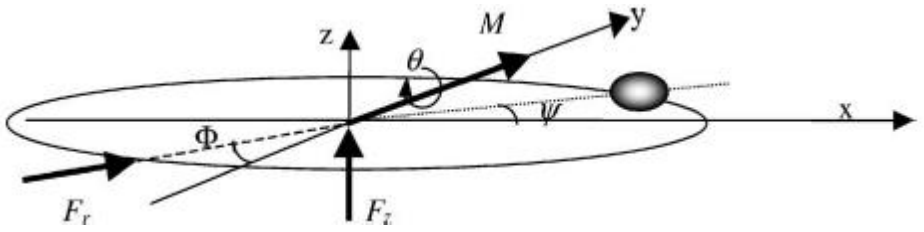


**Figure 17 - Loading directions and coordinate system [6]**

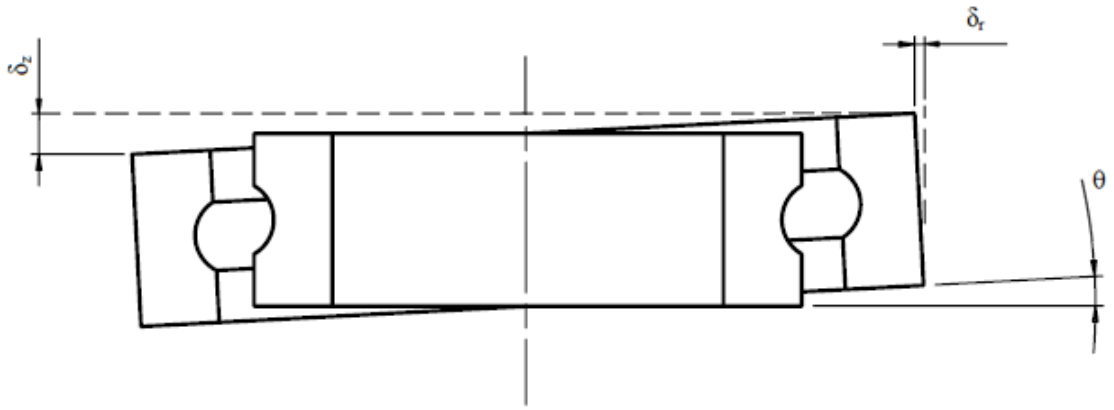


**Figure 18 - Degrees of freedom of a bearing**

In this thesis, inner raceway is stationary and deflections are on the outer raceway. The sample bearing has maximum diameter of about 1.7m and mean diameter (*dm*) of about 1.4 meters, while the diameters of the balls are approximately 25 mm.

Four-point contact bearings have four curvatures and both curvatures have a center of curvature. These center points are defined for geometry of the bearing. Change in the geometry of the bearing is calculated from the change of these center points. Initial coordinates of the center points are defined in Figure 19.

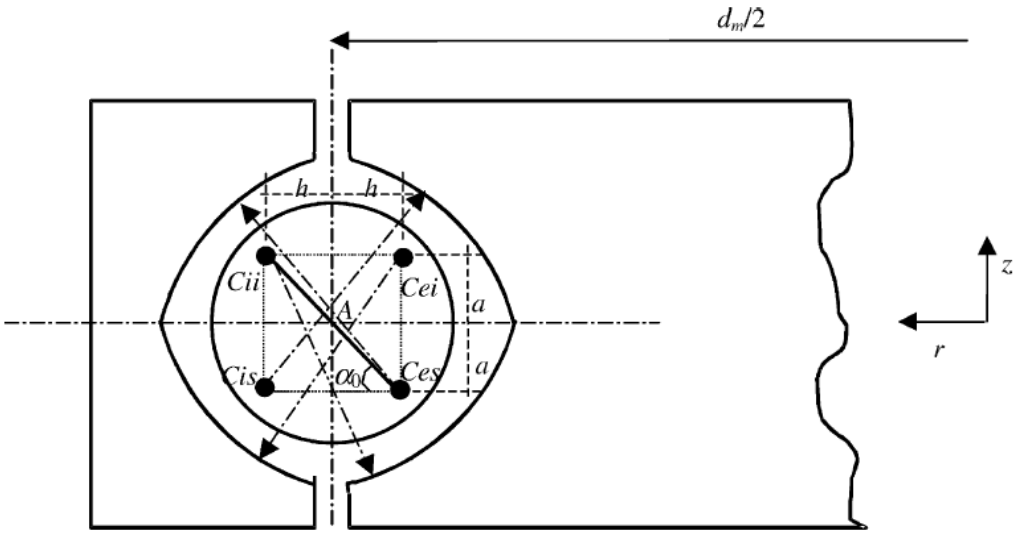


**Figure 19 - Centers of curvatures of the raceways [6]**

Definition of each center of curvature;

"• Cii represents the center of curvature of the lower inner raceway.

• Cis represents the center of curvature of the upper inner raceway.

• Cei represents the center of curvature of the lower outer raceway.

• Ces represents the center of curvature of the upper outer raceway.

• a and h are variables given by the design parameters, such as a0, ball bearing diameter and conformity" [6]

In this study, Cii and Cis are stationary. Displacement in the Cei and Ces is calculated and load magnitude and direction on each ball is determined from this displacement.

Cii, Cis, Cei and Ces represent free conditioned location of the center of curvatures without any contact.

Cii1, Cis1, Cei1 and Ces1 represent the contact obtained location of the center of curvatures without any loading. Contact location is given in Figure 20. In this configuration parameter "j" represents the endplay. That parameter shows us the mechanical gap in the z direction between the inner and outer raceways. That gap is closed with contact of the balls to the raceways before loading.

Cii2, Cis2, Cei2 and Ces2 represent the loaded location of the center of curvatures. Deflections are determined with final and contact obtained locations.

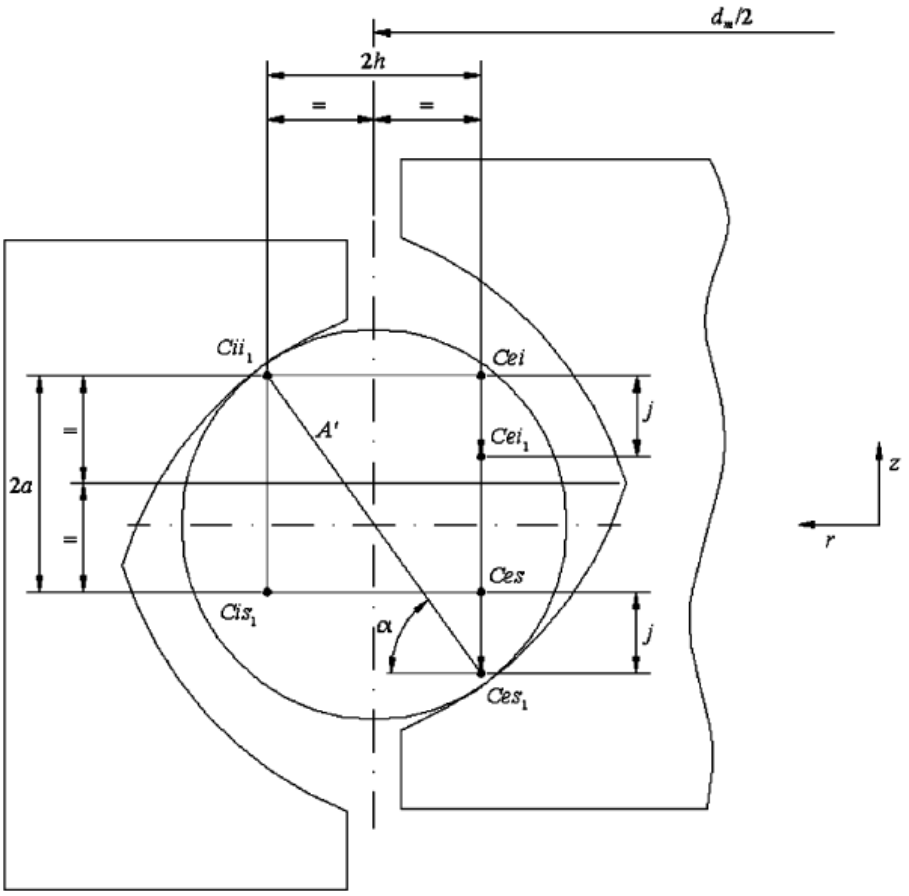


**Figure 20 - Center of curvature locations in contact [6]**

In this thesis sample geometry of a slewing bearing is examined. Dimensional parameters of the inner bearing geometry that will be analyzed are given in Figure 21 while the dimensional parameters of the outer geometry are given in Figure 22.

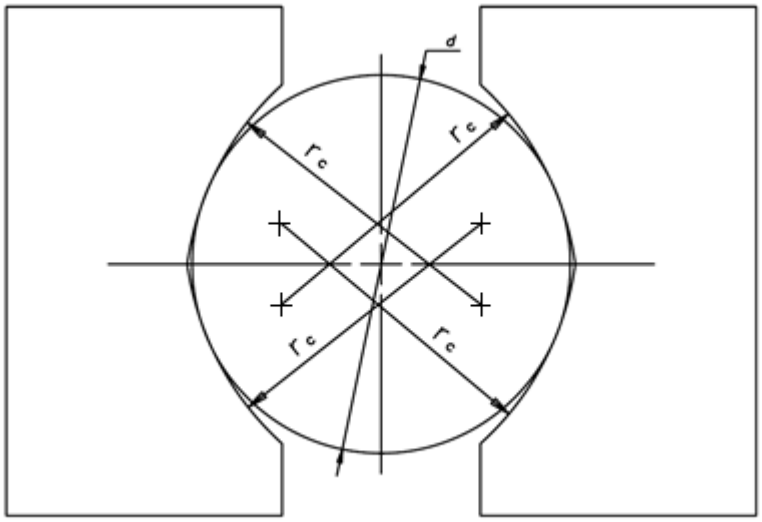


**Figure 21 - Dimensional parameters of the slewing bearing inner geometry**

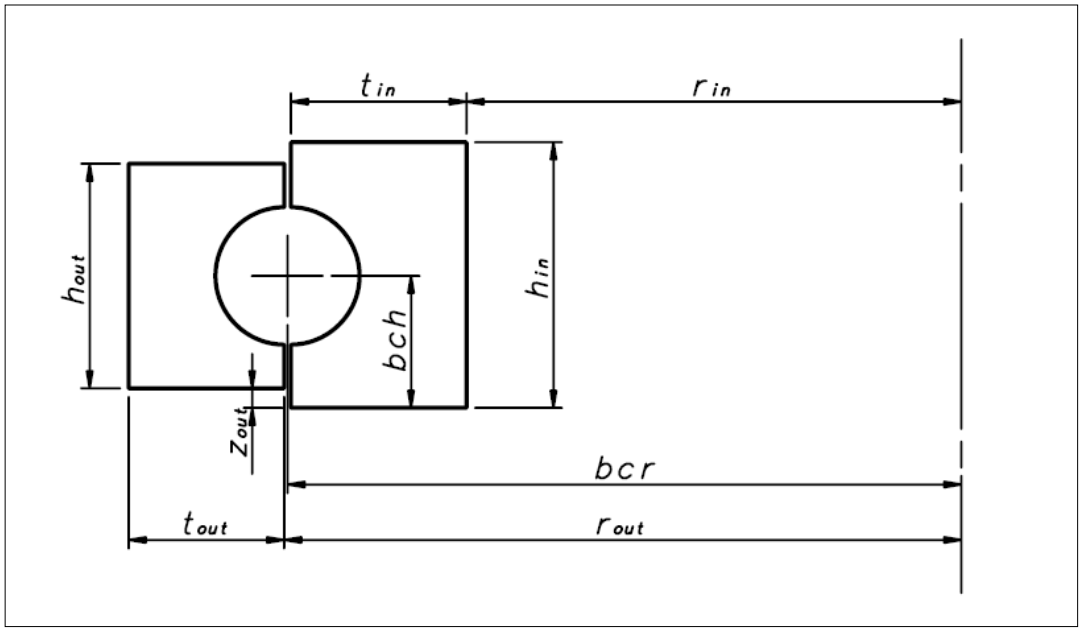


**Figure 22 - Dimensional parameters of the outer geometry of the slewing bearing**

The contact between the balls and the raceways is defined as Hertz contact. The force is proportional to the deflection of the balls after canceling out the endplay. The force is defined with the relation below for $\delta > 0$ [6][17][18][10].

$$Q = K.\delta^{n} \quad (1)$$

Here Q is the force on each ball and K is the coefficient that represents the total elastic deformation of the balls. While δ is the deflection on the ball, parameter n is taken as 1.5 for point contact [6][17][18][10]. The finite element analysis is done for single bearing in ABAQUS. In this model parameter "n" is taken as 1.5 and coefficient "K" is obtained. The deflection is determined from Finite Element Analysis model (Abaqus [19]) and K is determined for analytical study. The K value is also verified with analytical calculations in [18]. Fit line that is obtained with equation (1) is given in Figure 23.

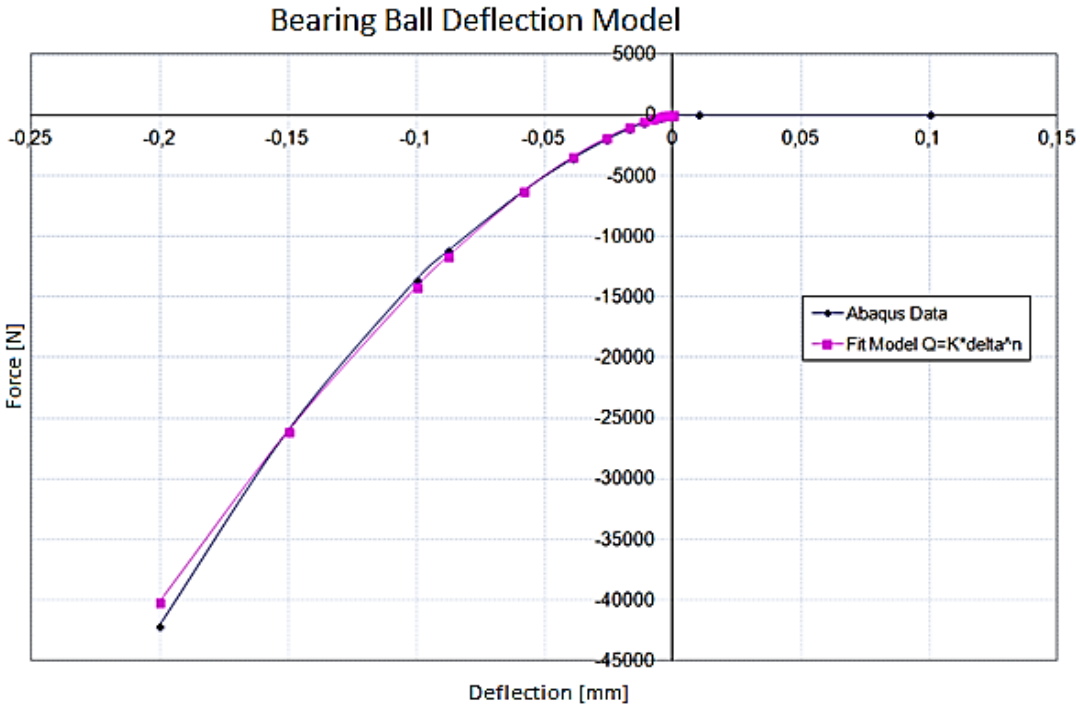


**Figure 23 - Fit for the coefficient K (K=450 kN/mm$^{3/2}$) versus FEA data [20]**

In ABAQUS model raceways are modeled as rigid in order to make same assumptions with analytical model. E=205000 MPa and ν = 0.3 is used as ball material (steel) properties. The mesh is prepared with 120 elements on the perimeter of the ball and 48 elements per the half perimeter of the raceways.

Finite element model ball-deflection solution in ABAQUS is also presented in [20] and the result of the analysis is verified with benchmark formulation in Chapter 2. The finite element model that is prepared to analyze ball deflection parameters is given in Figure 24. It can be observed from Figure 24 that mesh density is increased at the contact areas.

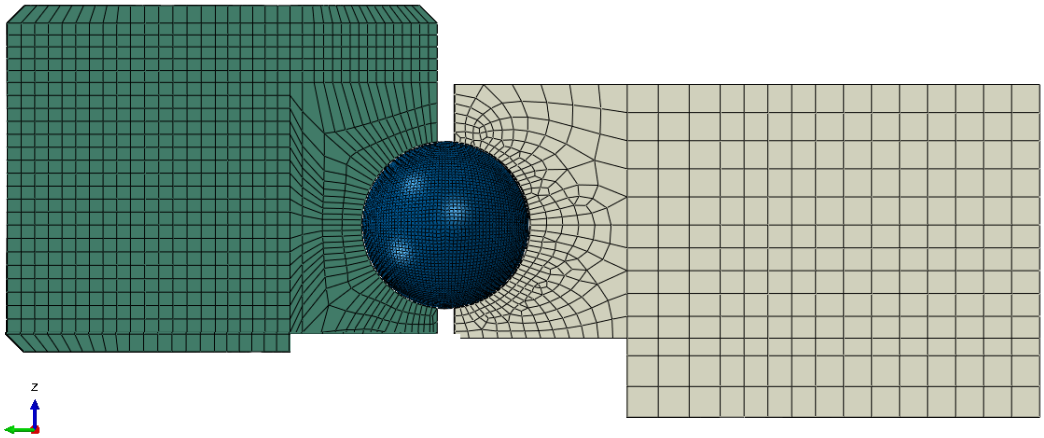


**Figure 24 - ABAQUS model for ball deflection model [20]**

The fit values for coefficient K is obtained in accordance with Figure 23. K is obtained as K = 450 kN/mm$^{3/2}$ in accordance with (1). This coefficient K is used in MATLAB model. Displacements versus force values are given Table 1. In Table 1 finite element results of force and the fit value of formula (1) is compared.

The fit values that are given in Table 1 are also used as real constants in finite element model. Deflection values and the force values for K coefficient of 450 kN/mm$^{3/2}$ are used in the finite element model.

The first three displacement values in Table 1 are given in order to simulate tension of the springs. Infinitesimal force values are defined in order to eliminate convergence problems.

**Table 1 - Comparison of FEM & MATLAB deformation versus force data**

| Displacement: "δ" [μm] | Force ( FEA Output) "F" [N] | $F= K \delta^n$ for ($K=450$ kN/mm$^{3/2}$) Used in MATLAB model "F" [N] |
|---|---|---|
| 100 | 0.000001 | 0.000001 |
| 10 | 0.000001 | 0.000001 |
| 0. 1 | 0.000001 | 0.000001 |
| 0 | 0 | 0 |
| -0. 1 | -0.7763 | -0.45 |
| -0. 2 | -2.319 | -1.273 |
| -0. 4 | -5.043 | -2.947 |
| -0. 6 | -10.40 | -6.205 |
| -0. 9 | -19.99 | -12.40 |
| -1.4 | -36.98 | -24.04 |
| -2.2 | -67.16 | -45.74 |
| -3.3 | -120.1 | -85.97 |
| -5.0 | -207.9 | -160.3 |
| -7.5 | -364.9 | -297.5 |
| -11.4 | -651.02 | -550.1 |
| -17.2 | -1135 | -1015 |
| -25.8 | -2036 | -1870 |
| -38.8 | -3567 | -3442 |
| -58.3 | -6292 | -6332 |
| -87.5 | -11210 | -11643 |
| -100 | -13626 | -14230 |
| -150 | -26107 | -26142 |
| -200 | -42198 | -40249 |

After determining the coefficient K, displacements of the center of curvatures are determined in accordance with the deflection of the balls due to loading conditions. With these deflection values, load on each ball is calculated. With known values of $\delta_z$, $\delta_r$ and $\theta$ the forces $F_z$, $F_r$ and M can be calculated. But in this problem it is needed to obtain $\delta_z$, $\delta_r$ and $\theta$ from $F_z$, $F_r$ and M. Here, three equations with three unknowns are solved. These equations given below [6];

$$Fz - \sum_0^{2\pi} fz(\delta z, \delta r, \theta, \Psi) = 0 \tag{2}$$

$$Fr - \sum_0^{2\pi} fr(\delta z, \delta r, \theta, \Psi) = 0 \tag{3}$$

$$M - \sum_0^{2\pi} m(\delta z, \delta r, \theta, \Psi) = 0 \tag{4}$$

In the equations $f_r, f_z$ and m values of each ball are summed. Initial conditions for $\delta_z$, $\delta_r$ and $\theta$ parameters are input for the analytical code. With an optimization loop on MATLAB model, it is tried to find $F_z$, $F_r$ and M values. After solution of $\delta_z$, $\delta_r$ and $\theta$ values, all the loads on the balls and the directions of the loads are calculated again in order to obtain load distribution and the contact angle graphs. In the FEA model contact angles can be used as input parameters. It can be observed that with internal clearance contact angles change dramatically. In FEA modeling of the balls as springs, springs are attached to the raceways through that contact angles. Changes in the contact angle can be found only with an analytical model, since it is unpractical to model all the balls in the bearing with radial and axial clearances.

## 2.2 Load Distribution Calculation Procedure

The calculation procedure is mainly based on the calculation of the locations of centers of curvatures. The initial locations in with axial clearance in Figure 19 can be calculated as follows [6];

$$XCii = \left(\frac{dm}{2} + h\right) cos\,\psi \tag{5}$$

$$YCii = \left(\frac{dm}{2} + h\right) sin\,\psi \tag{6}$$

$$ZCii = a \tag{7}$$

$$XCis = \left(\frac{dm}{2} + h\right) cos\,\psi \quad (8)$$

$$YCis = \left(\frac{dm}{2} + h\right) sin\,\psi \quad (9)$$

$$ZCis = a \quad (10)$$

$$XCei = \left(\frac{dm}{2} - h\right) cos\,\psi \quad (11)$$

$$YCei = \left(\frac{dm}{2} - h\right) sin\,\psi \quad (12)$$

$$ZCei = a \quad (13)$$

$$XCes = \left(\frac{dm}{2} - h\right) cos\,\psi \quad (14)$$

$$YCes = \left(\frac{dm}{2} - h\right) sin\,\psi \quad (15)$$

$$ZCes = -a \quad (16)$$

Initial distance between diagonally opposed center of curvatures [6];

$$A = 2\sqrt{(a^2 + h^2)} \quad (17)$$

When the axial clearance (endplay) is taken into consideration, some of the coordinates are changed in the Z axis.

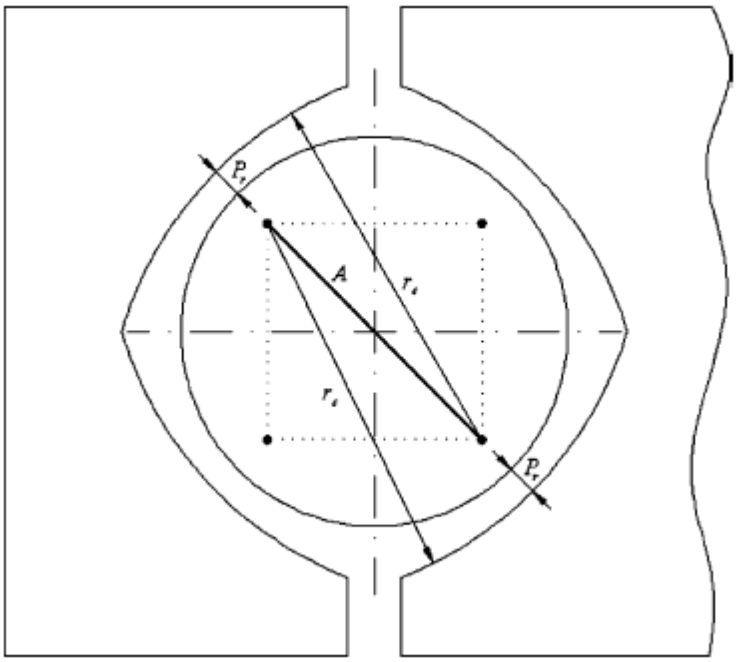


**Figure 25 - Dimensional parameters for clearance between the races and ball bearings [6]**

If $P_r$ is defined as being the existing radial clearance, $r_c$ as the radius of curvature and d as the diameter of the ball bearing, the following relation can be used (Figure 25) [6]:

$$2(r_c - Pr) - A = d \tag{18}$$

Taking the inner ring as a reference, the outer ring will move down by an amount j, equal to the axial clearance, until contact exists between the sphere and the raceways. Figure 19 shows the positions of the centers of curvature in the initial position, taking into account the axial clearance j. The following relationship may be deduced from Figure 20 as stated in [6]:

$$A'^2 = (2h)^2 + (2a + j)^2 \tag{19}$$

From expression (18), as the balls and raceways are in the contact $P_r = 0$, it can be deduced that [6];

$$2\,r_c - A' = d \tag{20}$$

From the expressions (19) and (20) it can be deduced that [6];

$$A' = 2Pr + A \tag{21}$$

Finding j from Eq. (19) and substituting Eq. (21) in this equation, the following equation is obtained for the axial clearance [6];

$$j = \sqrt{(2Pr + A)^2 - (2h)^2} - 2a \tag{22}$$

Thus, taking the axial clearance into account, the initial coordinates on the Z axis of the centers of curvature Cei1 and Ces1 are modified, where [6];

$$ZCei1 = a - j \tag{23}$$

$$ZCes1 = -a - j \tag{24}$$

The rest of the initial coordinates are same with initial coordinates.

After the loads $F_z$, $F_r$ and M are applied, final coordinates of the center of curvatures can be calculated. The directions of the loads are given in Figure 17. So the final coordinates can be calculated as [6];

$$XCii2 = XCii1 \tag{25}$$

$$YCii2 = YCii1 \tag{26}$$

$$ZCii2 = ZCii1 \tag{27}$$

$$XCis2 = XCis1 \tag{28}$$

$$YCis2 = YCis1 \tag{29}$$

$$ZCis2 = ZCii1 \tag{30}$$

$$XCei2 = XCei1 + \delta r \sin\varphi \tag{31}$$

$$YCei2 = YCei1 + \delta r \cos\varphi \tag{32}$$

$$ZCei2 = ZCei1 + \delta z - \theta(\frac{dm}{2} - h)\cos\psi \tag{33}$$

$$XCes2 = XCes1 + \delta r \sin\varphi \tag{34}$$

$$YCes2 = YCes1 + \delta r \cos\varphi \tag{35}$$

$$ZCei2 = ZCei1 + \delta z - \theta(\frac{dm}{2} - h)\cos\psi \quad (36)$$

There are three contact possibilities in four-point contact bearings and these possibilities are shown in Figure 26.

- Cis-Cei contact
- Cii-Ces contact
- Cis-Cei and Cii-Ces contact at the same time

In the calculations these three possibilities are taken into consideration.

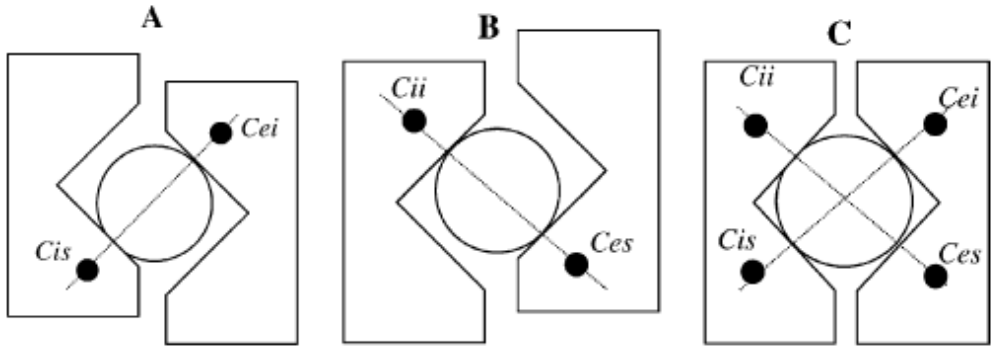


**Figure 26 - Possible contact types [6]**

### 2.2.1 When the Contact is Between Cii and Ces;

The distance between the centers of curvatures is [6];

$$A_1 = \sqrt{(XCii1 - XCes2)^2 + (YCii1 - YCes2)^2 + (ZCii1 - ZCes2)^2} \quad (37)$$

$$\Delta_1 = A_1 - A' \quad (38)$$

The contact angle will be [6];

$$\propto_1 = arcsin\frac{(ZCii1 - ZCes2)}{A_1} \quad (39)$$

The reaction in the ball bearing will be [6];

$$q_1 = \mathrm{K}\,\Delta_1^n \quad (40)$$

$A_1 \cos \propto_1$ is the projection on the x-y plane of the distance between centers of curvature Cii and Ces [6]. The angles $\beta_1$ and $\beta_2$ can be obtained from Figure 27 as below;

$$cos\,\beta_1 = \frac{XCii2 - XCes2}{A_1\, cos \propto_1} \tag{41}$$

$$sin\,\beta_1 = \frac{YCii2 - YCes2}{A_1\, cos \propto_1} \tag{42}$$

The x, y, z components of the reaction will be [6];

$$q1_x = q1\, cos\, \propto_1 cos\,\beta_1 \tag{43}$$

$$q1_y = q1\, cos\, \propto_1 sin\,\beta_1 \tag{44}$$

$$q1_z = q1\, sin\, \propto_1 \tag{45}$$

The vector position of the point of application of the reaction shows the following x; y; z components [6];

$$R1_x = XCii2 + \frac{(d - A_1)}{2} cos\, \propto_1 cos\,\beta_1 \tag{46}$$

$$R1_y = YCii2 + \frac{(d - A_1)}{2} cos\, \propto_1 sin\,\beta_1 \tag{47}$$

$$R1_z = ZCii2 + \frac{(d - A_1)}{2} sin\, \propto_1 \tag{48}$$

Where d is the diameter of the ball bearing.

By substituting (41) in (46) and (42) in (47), the following can be obtained [6];

$$R1_x = XCii2 + \frac{(d - A_1)}{2} \frac{XCii2 - XCes2}{A_1} \tag{49}$$

$$R1_y = YCii2 + \frac{(d - A_1)}{2} \frac{YCii2 - YCes2}{A_1} \tag{50}$$

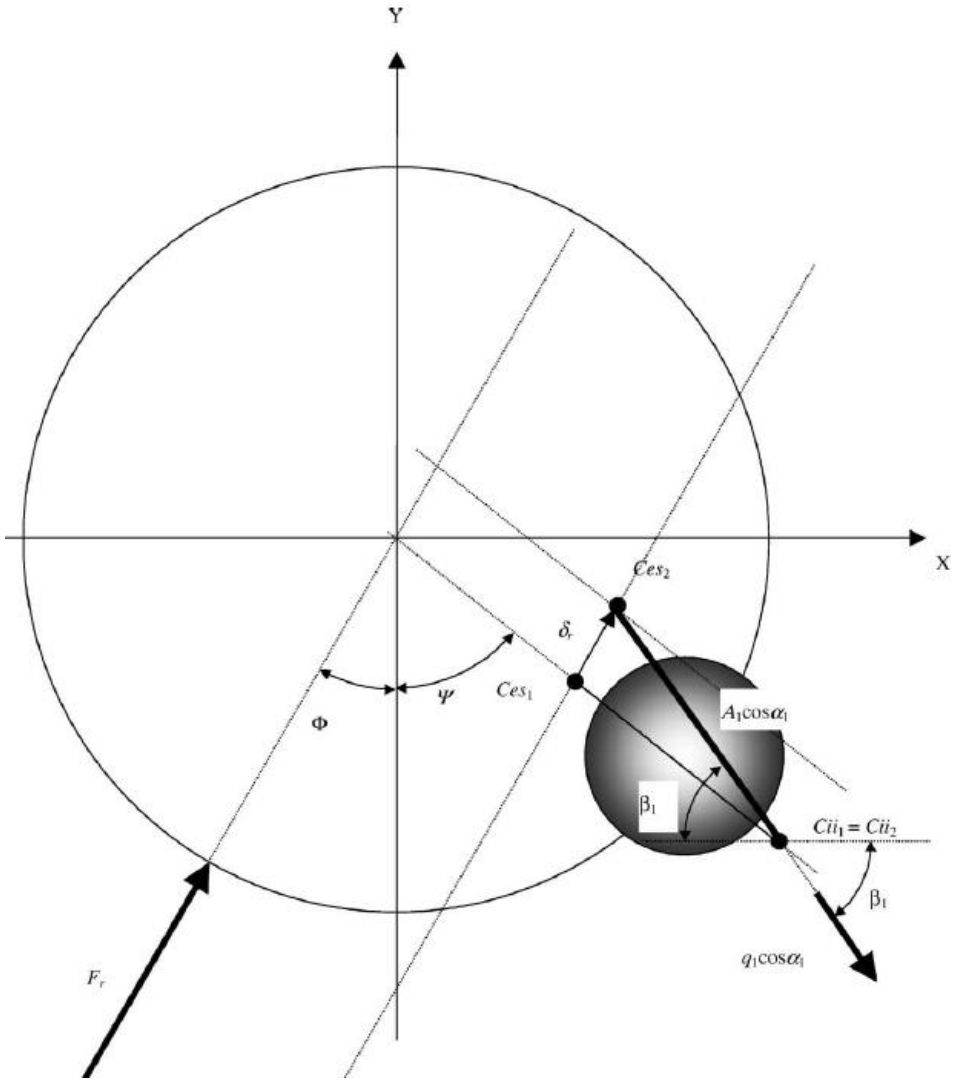


**Figure 27 - Projection of distances, angles and forces on the XY plane in the contact Cii–Ces. [6]**

The moment of the reaction with respect to the point of origin is [6];

$$M1 = q1 \times R1 \tag{51}$$

The components of this moment are [6];

$$m1_x = q1_y R1_z - q1_z R1_y \tag{52}$$

$$m1_y = q1_z R1_x - q1_x R1_z \tag{53}$$

$$m1_z = q1_x R1_y - q1_y R1_x \tag{54}$$

### 2.2.2 When the Contact is Between Cis and Cei;

For contact between Cis-Cei, same geometrical calculation method is used. Detailed calculation procedure for Cis-Cei contact can be found in [6]. For simultaneous contact between Cis-Cei and Cii-Ces, the summation of the loads for two types of contact is used.

## 2.3 MATLAB Modeling and Samples for Analytical Based MATLAB Model

Basic schematic for calculation methodology is given in Figure 28.

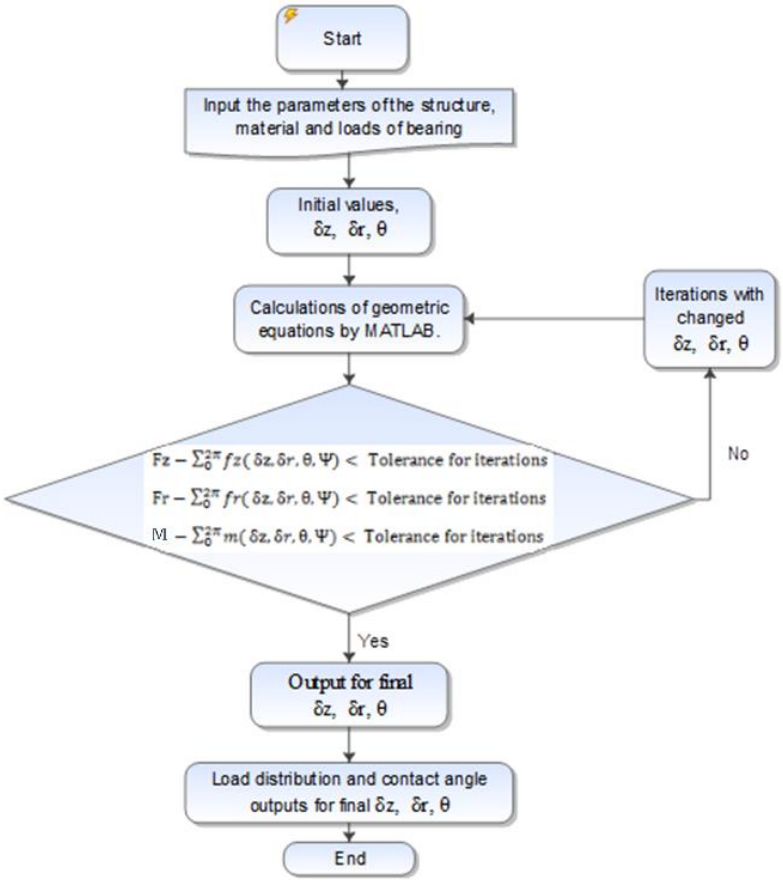


**Figure 28 - Basic schematic for calculation methodology**

In order to justify the study in MATLAB [21], some pure loading conditions are calculated. These conditions are;

- Axial loading
- Radial loading
- Moment loading

### 2.3.1 Verification of Axial Loading Condition for MATLAB Model

The code is firstly confirmed for $F_z$ value of 100 kN axial load condition. This condition simulates a dummy weight of a sample system. $C_{is}$-$C_{ei}$ contact condition is predicted. Load distribution is given in Figure 29. Load vectors in Figure 29 are non-dimensional. The axes of the graph are the coordinates of the balls.

For $P_r$=0 (zero-endplay), analytical calculations are solved with using the MATLAB code. As a solution net total force values are converged to zero as follows;

$$Frt = 0.02\ N$$

$$Fzt = -3.8 \times 10 - 7\ N$$

$$Mt = 0.85\ N.mm$$

As a result of iterative analytical calculations displacements are found as follows;

$$\delta r = 0.000\ mm$$

$$\delta z = 0.024\ mm$$

$$\theta = 0.000\ degrees$$

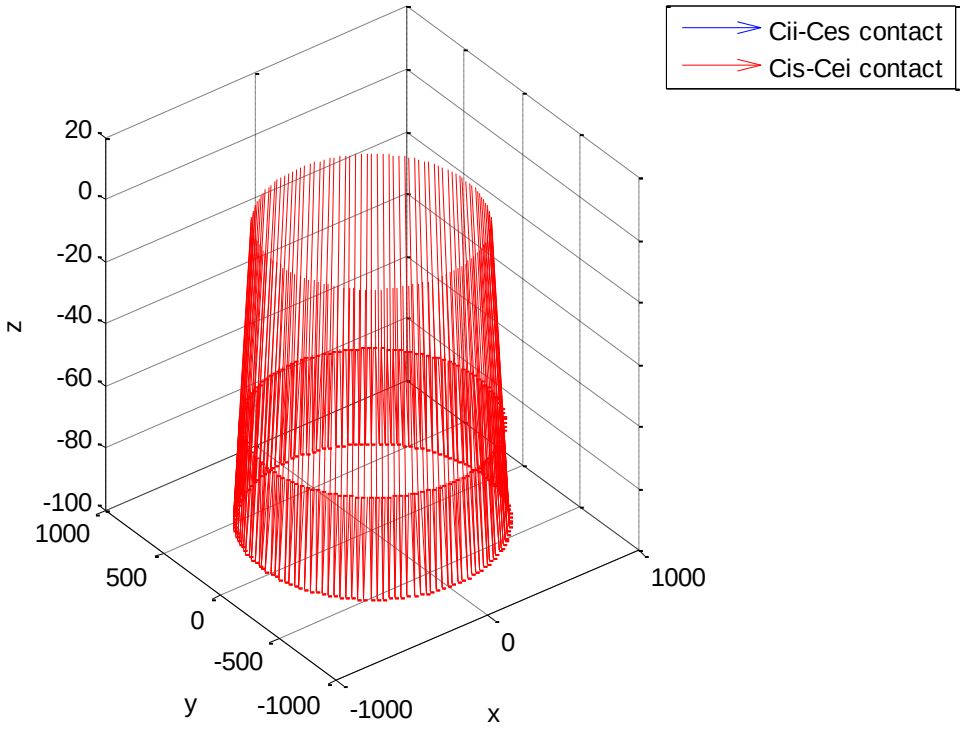


**Figure 29 - Load Distribution on Balls for Axial Loading Condition**

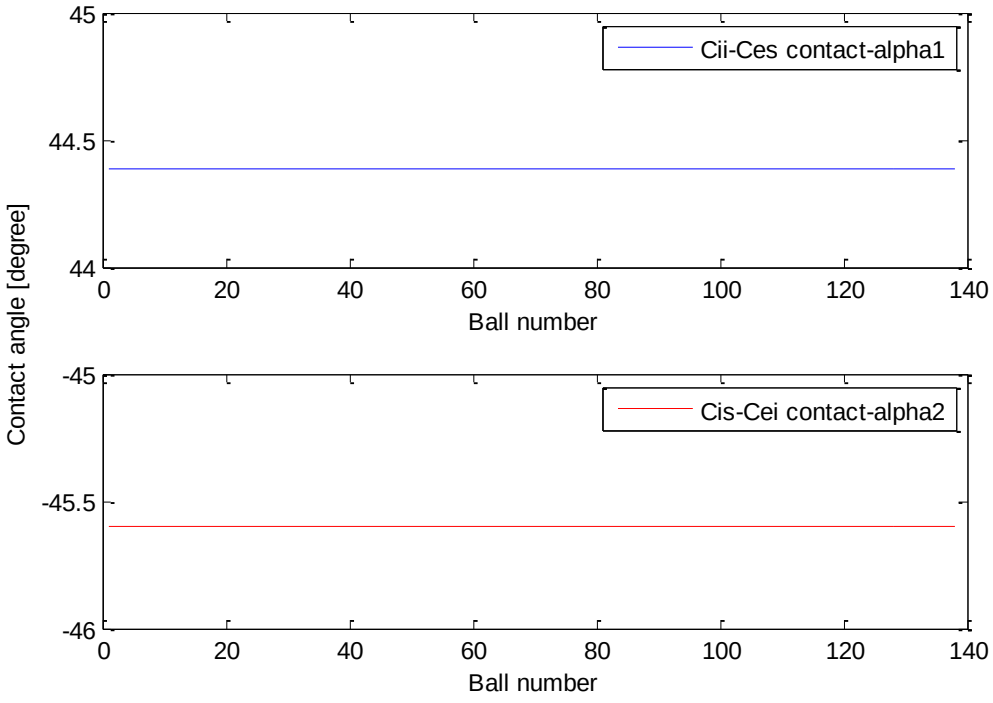


**Figure 30 - Contact Angle of Balls due to pure axial loading condition (alpha 2)**

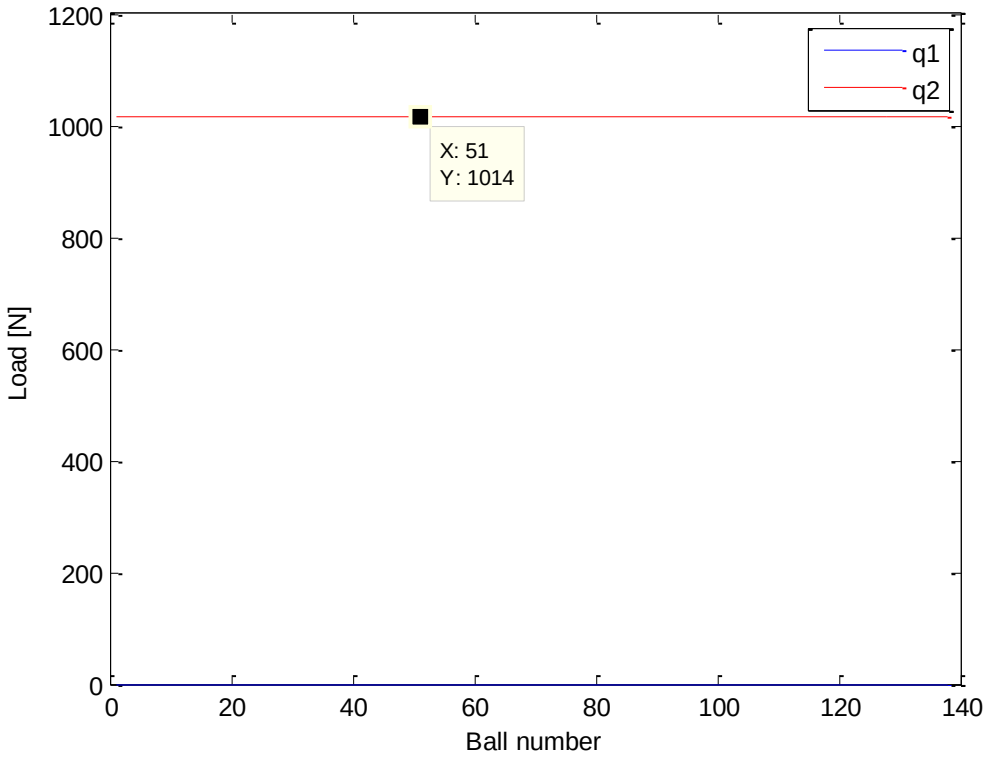


**Figure 31 - Total load distribution on balls due to pure axial loading condition**

Load on each ball is 1014 N for this load condition and contact angle alpha is 45.5˚ for $C_{is}$-$C_{ei}$ contact condition. It can be seen that there is no change in the contact angle for pure axial loading.

Fa (axial total load) can be calculated as follows;

$$Fa = 1014\ x(sin\,\alpha\,) \times n = 97.8\ kN$$

### 2.3.2 Verification of Radial Loading Condition for MATLAB Model

The code is secondly confirmed for $F_r$ value of 10 kN radial loading condition. In this condition outer ring of the bearing is pushed in x-y plane. This load condition is not a critical condition as much as moment loading but the result of the code is also checked for this condition.

In this condition it is predicted that both contact conditions to occur simultaneously. Load distribution is given in Figure 33. Load vectors in Figure 33 are non-dimensional. The axes of the graph are the coordinates of the balls.

For $P_r = 0$ (zero-endplay), analytical calculations are solved with using the MATLAB code. As a solution net total force values are converged to zero.

$Frt = -4.73e-08\ N$

$Fzt = -5.64e-10\ N$

$Mt = 2.55\ e-07\ N.mm$

As a result of iterative analytical calculations displacements are found as follows;

$\delta r = 0.009\ mm$

$\delta z = 0.000\ mm$

$\theta = 0.000\ degrees$

Load distribution is given in Figure 33. As expected, both contact conditions occurred. Contact angle is given in Figure 34. In the balls alpha1 is for contact condition $C_{ii}$-$C_{es}$, alpha2 is for contact condition $C_{is}$-$C_{ei}$. It can be seen that change in the contact angle can be neglected for pure radial loading.

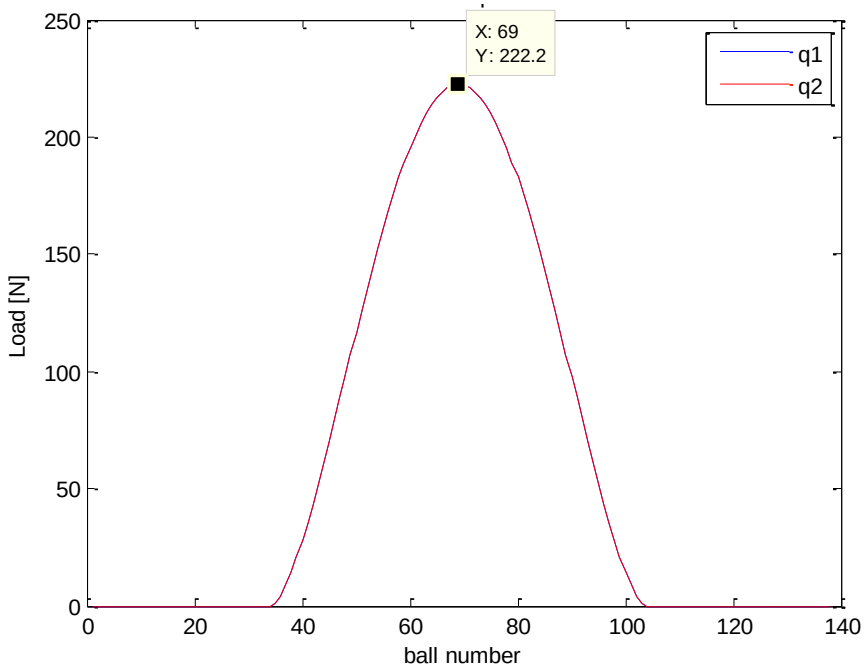


**Figure 32 - Total load distribution on balls due to pure radial loading condition (blue line and red line are coincident)**

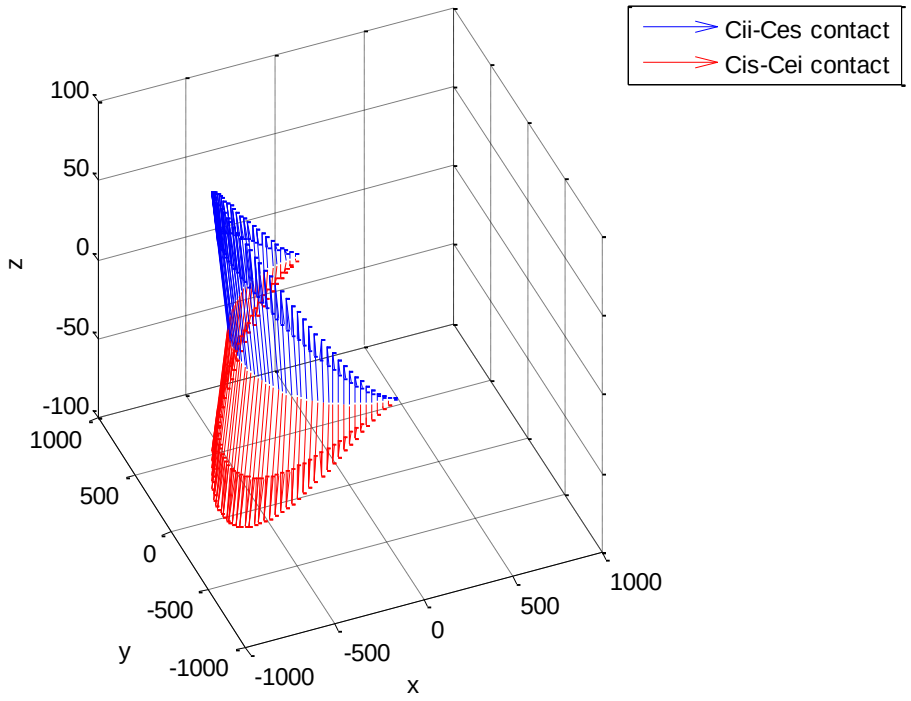


**Figure 33 - Load distribution on balls due to radial loading condition**

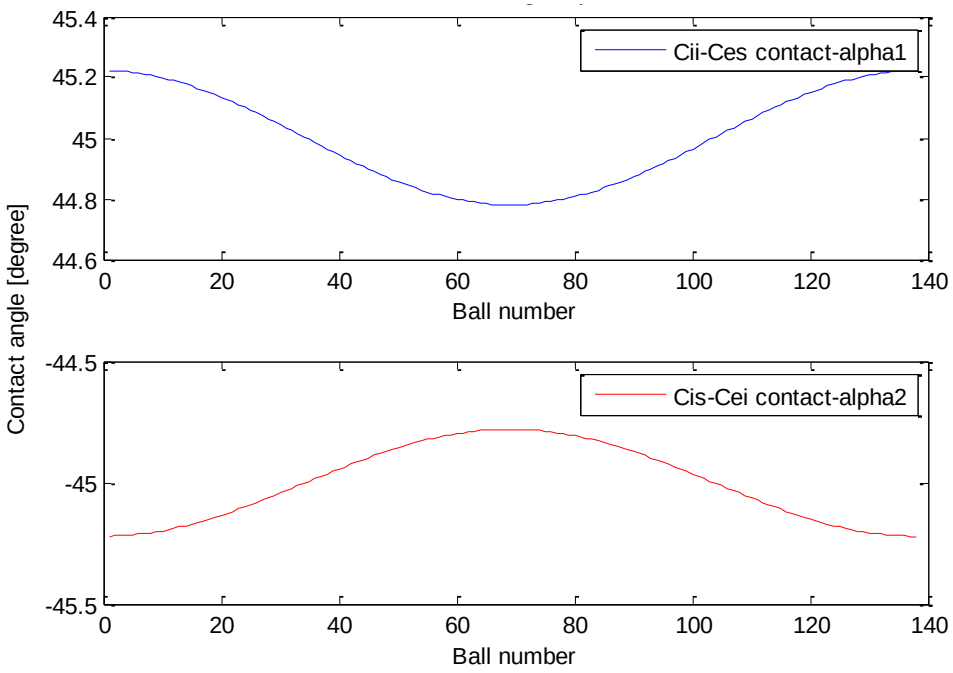


**Figure 34 - Contact angle of balls due to radial loading condition (alpha2 and alpha1)**

### 2.3.3 Verification of Moment Loading Condition for MATLAB Model

The code is confirmed for M value of 100 kN.m moment loading condition. In this condition outer ring is tilted around y axis. Moment load is the most important load type for this study. The load that is applied in this sample simulates the approximate bending moments in this kind of systems. The loading and deflection characteristic in this load type is determinant in the real system.

For this type of loading it is predicted that both contact conditions to occur simultaneously. Load distribution is given in Figure 36.

For $P_r$ = 0 (zero-endplay), analytical calculations are solved using the MATLAB code. As a solution net total force values are converged to zero.

$Frt = 4.44e-04$

$Fzt = -3.57e-09$

$Mt = 7.15e-05$

As a result of iterative analytical calculations displacements are found as follows;

$\delta r = 0.000\ mm$

$\delta z = 0.000\ mm$

$\theta = 0.005\ degrees$

The θ angle can also be seen from Figure 18. Due to moment loading displacement of $\delta_z 2$ occurs from the initial horizontal axis of the bearing and this displacement is represented in Figure 35.

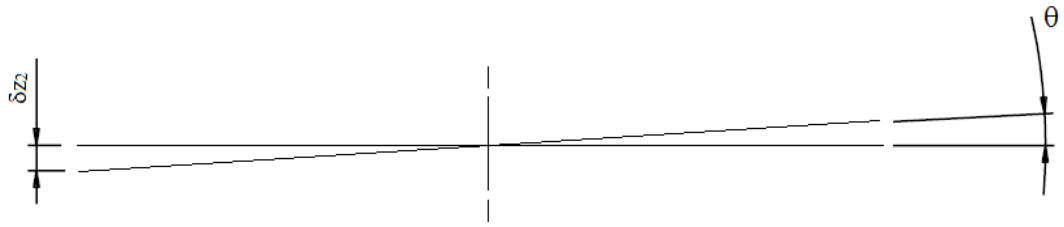


**Figure 35 - $\delta z_2$ due to pure moment loading**

$$\delta z2 = ((rout + tout) \times sin\,\theta)/2 \tag{55}$$

$$\delta z2 = 0.071\ mm$$

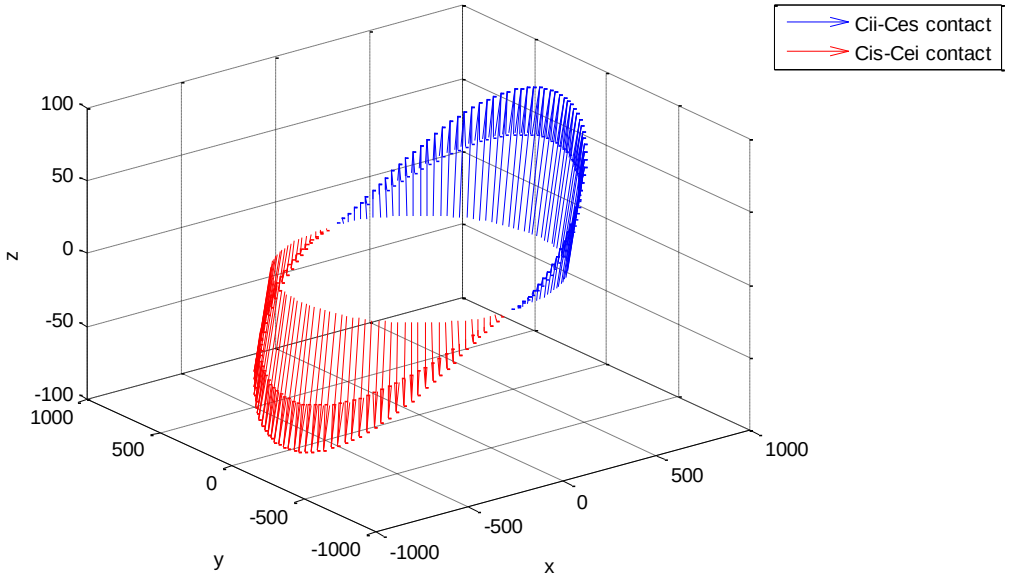


**Figure 36 - Load distribution on the balls due to pure moment loading condition**

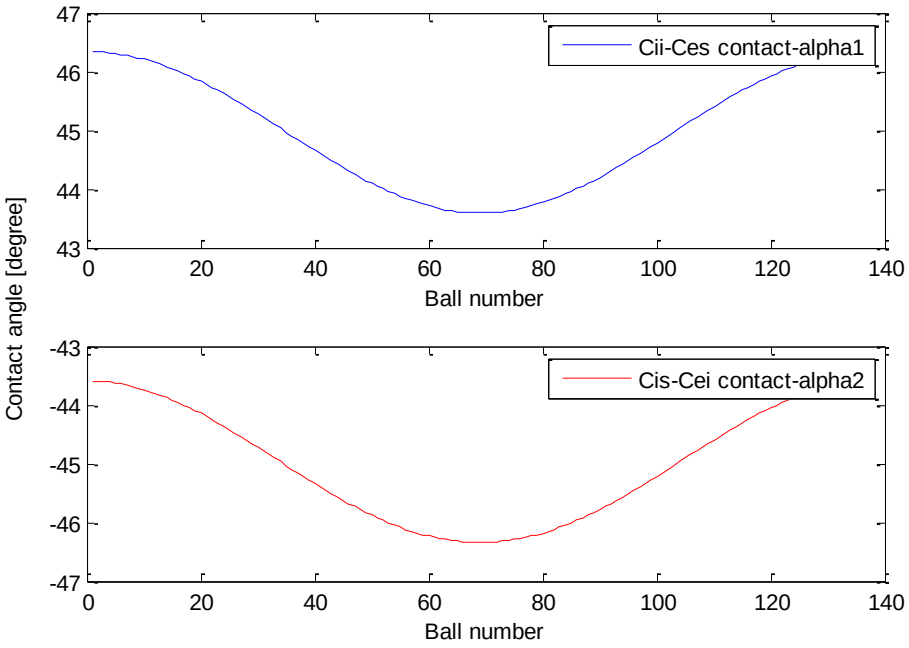


**Figure 37 - Contact angle of balls due to pure moment loading condition (alpha2 and alpha1)**

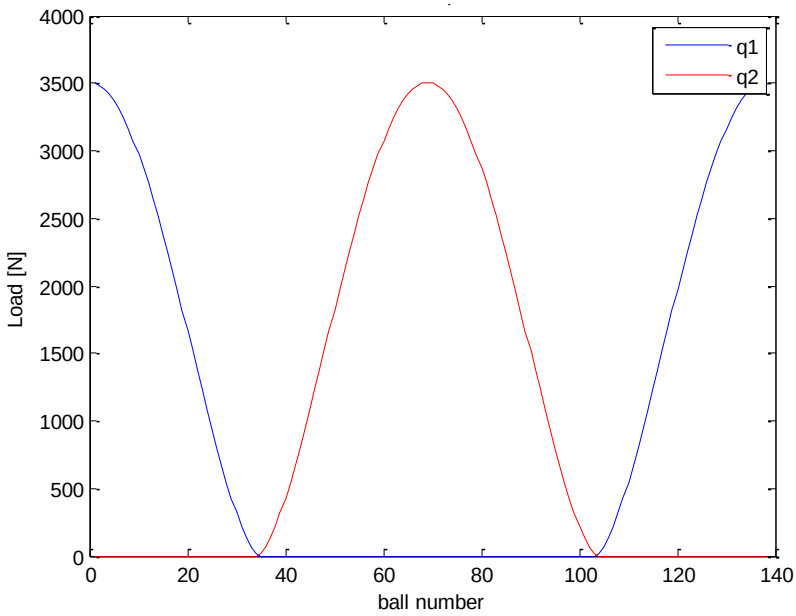


**Figure 38 - Total load distribution on balls for moment loading condition**

The results of the load cases that are carried out through Chapter 2 are verified with benchmark models and numerical FEA models in Chapter 3.

# CHAPTER 3

# VERIFICATIONS OF ANALYTICAL STUDIES WITH BENCHMARK FORMULAE AND NUMERICAL FEA MODELS

The formulation that is explained throughout Chapter 2 needs to be verified in order to be able to use the code in further studies. FEA model of stiffness calculation is verified with theoretical formulae in [18] and Results of the MATLAB is checked with formulation used in [6] and [17]. The MATLAB model is also verified with the finite element analysis method in the verification chapter.

## 3.1 Verifications of Analytical Studies with Benchmark Models

Analytical based MATLAB results are also validated with the benchmark formulation that is obtained from literature. Respectively, the coefficient K and the MATLAB results of the sample loading conditions are compared with benchmark formulation.

### 3.1.1 Verification of Coefficient K with Benchmark Model

The coefficient K that is obtained in Chapter 2 is validated with the formulation represented in [18].

The constant K can also be found by means of the approximation formulae [18];

$$K = 34300 \times d^{1/2}/\kappa^{0.35} \text{ (N/mm}^{3/2}\text{)} \quad (56)$$

$$\kappa = 0.5(\kappa_j + \kappa_A) \quad (57)$$

$$\kappa_j = (2 \times r_c inner - d)/d \quad (58)$$

$$\kappa_A = (2 \times r_c outer - d)/d \quad (59)$$

Where;

$\kappa$: Mean curvature ratio

$\kappa_j$: Curvature ratio at the inner ring

$\kappa_A$: Curvature ratio at the outer ring

d : Rolling element diameter (mm)

$r_c$inner: Groove radius of inner-ring raceway (mm)

$r_c outer$: Groove radius of outer-ring raceway (mm)

When the coefficient K is calculated with the formula (55-58) K can be found as;

$K = 452.4\ kN/mm^{3/2}$

The result of the formulae in literature and the result of the FEA method are highly consistent for coefficient K calculation.

**Table 2 - Comparison of K coefficients found by theoretical formulae and numerical FEA method**

| Theoretical Solution | Numerical Solution (Fit value) | Error % |
|---|---|---|
| 452.4 kN/mm$^{3/2}$ | 450 kN/mm$^{3/2}$ | 0.5% |

It can be concluded that the theoretical formulation (56-59) is sufficient for obtaining coefficient K. For different bearings with different geometries formulation can be preferred with respect to preparing a FEM that requires contact solution.

### 3.1.2 Verification of MATLAB Results with Benchmark Models

In order to validate the calculation procedure used in MATLAB, the solution for sample load cases are need to be checked with the formulae in literature. Three load cases are verified with benchmark models in this part. Comparison of the results with theoretical formulation can be seen in Table 3.

#### 3.1.2.1. Verification of Pure Axial Loading Results with Benchmark Model

In order to validate the calculation procedure in axial loading condition, maximum load that occur on a ball can be checked with the formulation in literature. Maximum load on a ball can be calculated with an equation from [6] [17];

For pure axial loading;

$$Qmax = Fz/(n \times sin(\propto)) \tag{60}$$

$Qmax = 1046.8\ N$ with using (60).

Result is consistent with the output of analytical based MATLAB model;

$Qmax\ (MATLAB) = 1014\ N$

#### 3.1.2.2. Verification of Pure Radial Loading Results with Benchmark Model

In order to validate the calculation procedure in radial loading condition, maximum load that occur on a ball can be checked with the formulation in literature. Maximum load on a ball can be calculated with an equation from [6] [17];

For pure radial loading;

$$Qmax = 4.37 \times Fr/(n \times cos(\propto)) \tag{61}$$

This formulation is derived for angular contact ball bearing. Since radial load is shared by two contact types, Qmax/2 needs to be compared with the output of our analytical solution.

$Qmax/2 = 228.9\ N$ with using (61).

Result is consistent with the output of analytical based MATLAB model;

$Qmax\ (MATLAB) = 222.2\ N$

#### 3.1.2.3. Verification of Pure Moment Loading Results with Benchmark Model

In order to validate the calculation procedure in moment loading condition, maximum load that occur on a ball can be checked with the formulation in literature. Maximum load on a ball can be calculated with an equation from [6] [17];

For pure moment loading;

$$Qmax = 4.37 \times M/(dm \times n \times sin(\propto)) \quad (62)$$

$Qmax = 3366\ N$ with using (62).

Result is consistent with the output of analytical based MATLAB model;

$Qmax\ (MATLAB) = 3500\ N$

Comparison of the analytical results with the results of the formulation in literature is given in Table 3.

**Table 3 - Verification of analytical based MATLAB model results with the results of the benchmark formulation**

| Verification of Results | | | |
|---|---|---|---|
| Force | Benchmark Formulation [N] | Analytically calculated value [N] | Error % |
| *Fa* = 100 kN | Qmax =1046.8 N | Qmax =1014 N | 3% |
| *Fr* = 10 kN | Qmax = 228.9 N | Qmax =222.2 N | 3% |
| *M* = 100 kN.m | Qmax =3366 N | Qmax =3500 N | 4% |

## 3.2 Verifications of Analytical Studies with Numerical FEA Models

In order to pass the design steps, most of the time critical conditions are checked with finite element models. But because of the capabilities of commercial finite element programs, some simplifications and assumptions are made all the time. In this numerical modeling no clearance assumption is needed to done in order to overcome convergence problems. Balls are modeled as non-linear springs in order to eliminate the difficulties of point contact solution of high number of balls. Without any simplification for contacts it would be an over-complex solution for finite element program to overcome for four contacts from each ball it would be about 500 contact for every solution. The proper meshing of such a big structure with 500 point contact would also be an impractical problem to solve.

In the following parts, a simplified finite element method is prepared with using ANSYS, in order to check the solutions of the analytical code. APDL (ANSYS Parametric Design Language) is used for modeling the system of four-point contact bearing. With the help of the parametric design language the steps are minimized with *DO loops. The effort in order to try new cases can be minimized with the design language. Geometry of the bearing is created as parts using *DO command on ANSYS that is also explained in APPENDIX E.

Proper APDL code is used in order to check different load cases. The comparison of the results of analytical model and numerical models are given Table 4 at the end of this part.

### 3.2.1 Raceway Modeling of the Slewing Bearing in FEA Model

Since raceways are assumed as rigid on the analytical model and their stiffness is higher with respect to balls, it is also assumed rigid-like in the FEM model. For rigid-like modeling of raceways, elastic modulus of 210 $x10^3$ GPa is used (1000 times of the original elastic modulus of steel).

The dimensional inputs for the geometry of the bearing for the FEA model are shown in Figure 21 and Figure 22.

Raceways are modeled with SOLID 185 [22] element of ANSYS as shown in Figure 39. This element has orthotropic material properties while it has three degrees of freedom (UX, UY and UZ) and eight nodes. This element is used for modeling solid structures and it has properties such as plasticity and hyper elasticity. The element also has large deflection capabilities.


**Figure 39 - SOLID 185 element of ANSYS [22-23]**

A coarse mesh is applied into raceways in order to have a simplified model. The Rigid-like behavior of the raceways makes that mesh insignificant. Mesh of the raceways is shown in Figure 40.

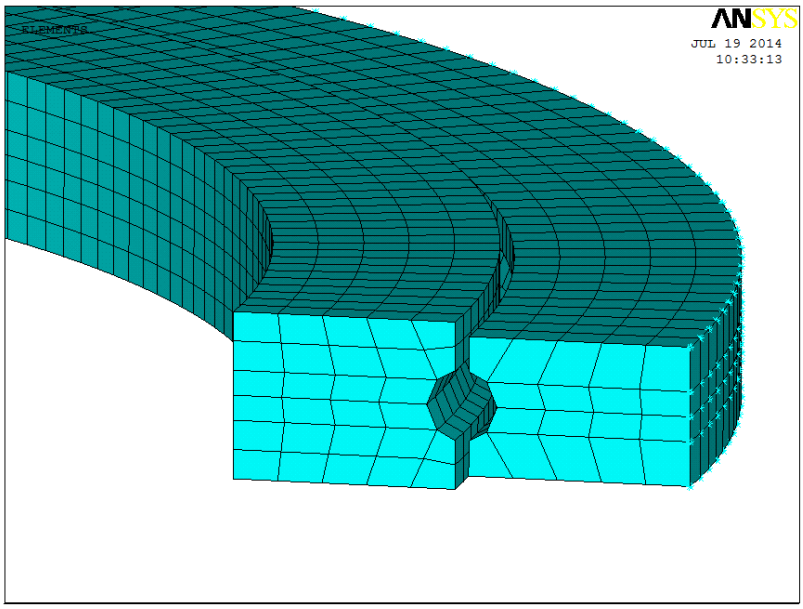


**Figure 40 - Meshing of raceways in FEM**

### 3.2.2 Spring Modeling of the Balls of the Slewing Bearing in FEA Model

While modeling balls as springs, spring element COMBIN 39 [22] is used as spring.

"COMBIN 39 is a unidirectional element with nonlinear generalized force-deflection capability that can be used in any analysis. The element has longitudinal or torsional capability in 1-D, 2-D, or 3-D applications. The longitudinal option is a uniaxial tension-compression element with up to three degrees of freedom at each node: translations in the nodal x, y, and z directions. No bending or torsion is considered. The torsional option is a purely rotational element with three degrees of freedom at each node: rotations about the nodal x, y, and z axes. No bending or axial loads are considered." [22]


**Figure 41 - COMBIN 39 element of ANSYS [22-23]**

Force-deflection constants in Table 1 are used as real constants in ANSYS APDL code. Real constants determine the non-linear stiffness behavior of the spring elements. Relevant part of the APDL code with the real constants, is given in the Appendix E.

### 3.2.3 System Modeling of Raceways and Balls in FEA Model

System is modeled with attaching springs through the nodes that correspond to correct contact angle. The contact angle is given in to APDL code as an input parameter. Locations of the spring nodes are guided by the divisions on the raceway volumes.

In order to be able to select correct nodes for springs to contact in the z-axis, raceways are divided into 2 segments that the division of the segments meets the contact location in desired contact angle. Relevant part of the APDL code is given in the Appendix E.

In order to be able to select correct nodes for springs to contact in the circumferential configuration, raceways are created as equal angled segments that the number of the segments meets the ball number.

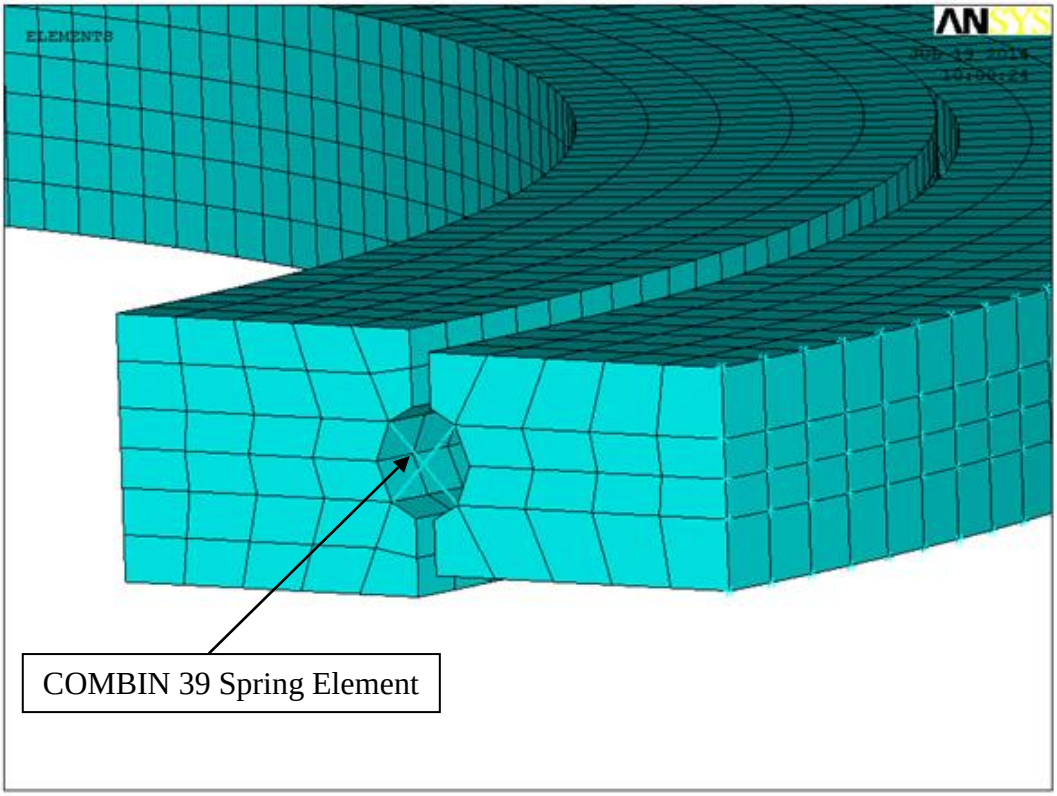


**Figure 42 - Meshing of raceways and balls with solid and spring elements**

Inner face of the inner ring is constrained with zero displacement in 3-DOF's.

For boundary condition applications a master node is created at the center of the bearing. Master node is connected to outer ring with RB2 type rigid links. Moment, axial deflection and radial load are applied through that rigid links.

### 3.2.4 FEM Results of Pure Moment Loading

Finite element analysis for pure moment loading condition is prepared for 100 kN.m moment about y-axis. This loading condition also simulates dominant bending moments that affect slewing bearings. The load is applied as a ramp function and solution is made in 1000 steps. The load is applied to the outer ring via the master node that is created to apply boundary conditions uniformly.

The results of pure moment loading condition are examined as deflection and structural force on spring elements. Displacement in the z-axis for moment loading condition is given in Figure 43.

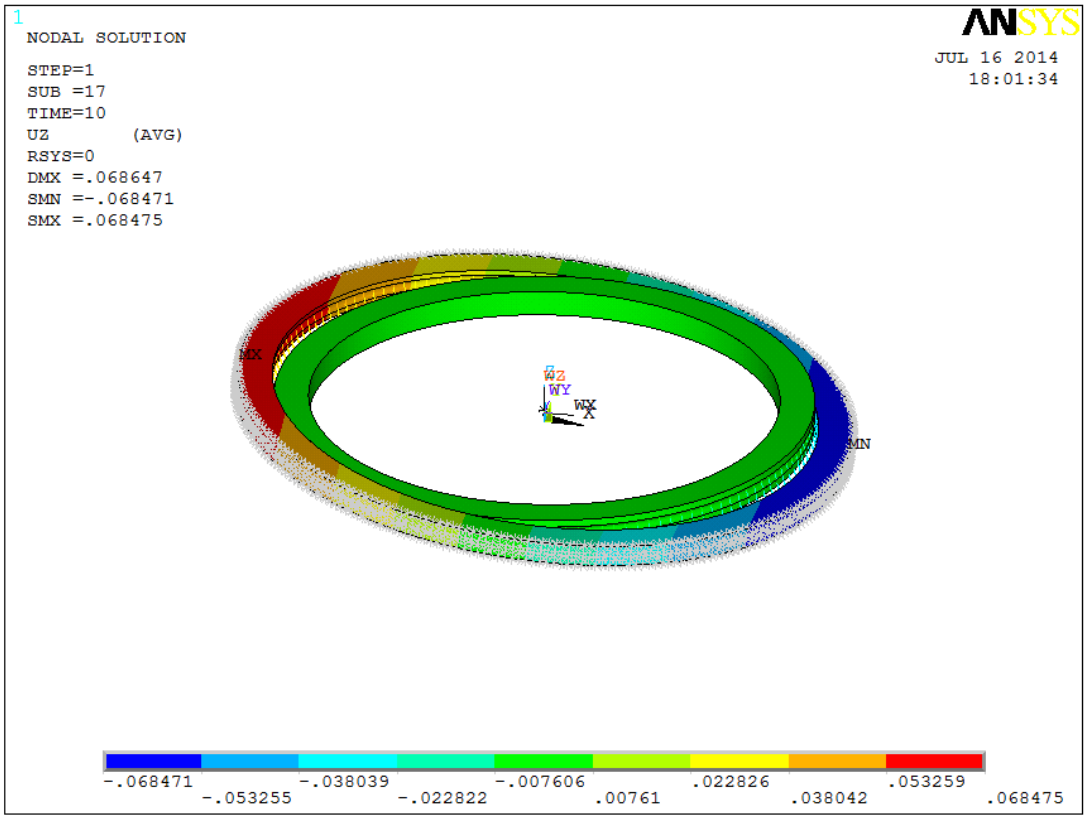


**Figure 43 - Displacement in the z-axis for moment loading condition**

The solution of the numerical solution gives the deflection of 0.068 mm at most in z-axis. When the analytical solution of the MATLAB gives θ = 0.005 degrees of rotation.

When the maximum deflection in z-axis is calculated with analytical based MATLAB model;

$$Zmax = (rout + tout) \times sin\,\theta \tag{63}$$

$$Zmax = (710) \times sin\,0.005 = 0.062\,mm$$

Where;

It can be seen that analytical solution is very consistent with the FEA model.

Load distribution on balls is given as structural force on the springs. Spring forces can be seen on Figure 44. It can be seen that in Figure 44, maximum load on a ball is 3586 N, while the analytic result for same loading condition is given in Figure 38 as 3500 N. The two results are consistent with 2% confidence level.

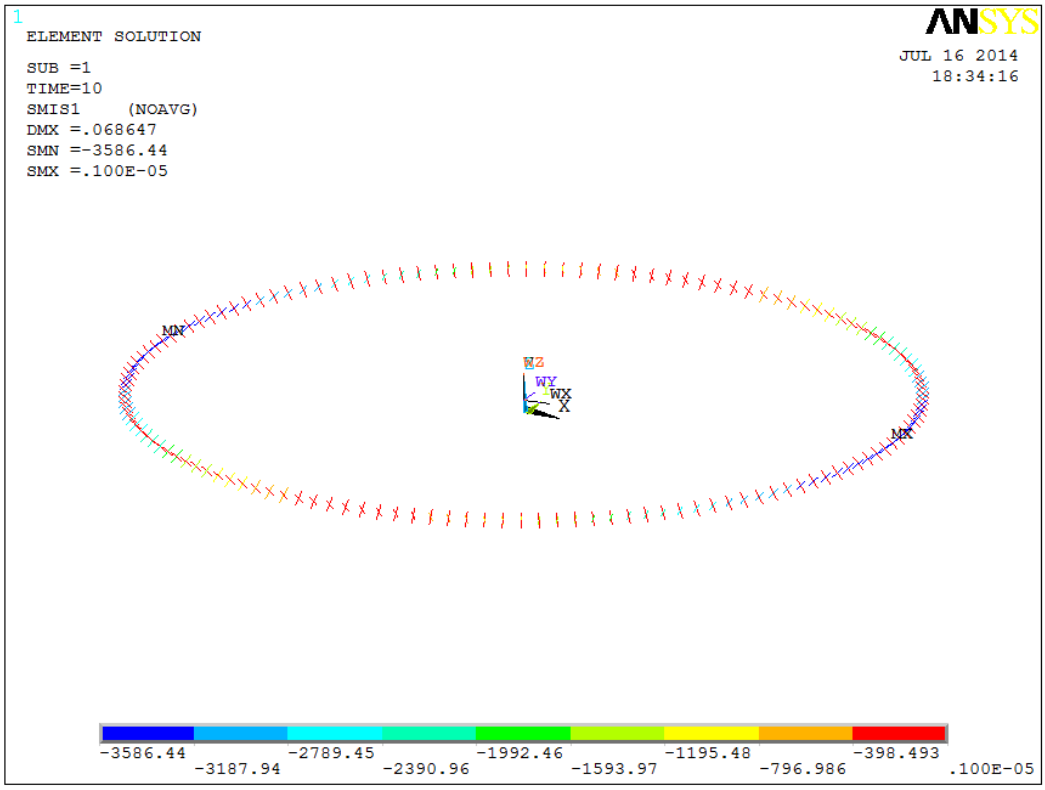


**Figure 44 - Load distribution in Newtons on balls for pure moment loading condition**

### 3.2.5 FEM Results of Pure Axial Displacement

In verification of application of axial load, axial displacement is applied to the outer ring of the slewing bearing. Displacement of the 0.013 mm is applied in the z-axis. Displacement is applied to the outer ring via the master node that is created to apply boundary conditions uniformly. Displacement is applied as a ramp function and solution is made in 1000 steps.

Most of the time, application of displacement is a more convergent method because of the contact background of the FEA programs. Since very little loads can cause large initial displacements in spring elements, the solver may get far away from the correct solution. Applying deflection instead of force can solve the problems of convergence.

In Figure 45 solution for application of 0.013 mm displacement in z-axis is given. From Figure 45 it can be seen that the displacement of 0.013 mm corresponds to 38.5 kN axial force.

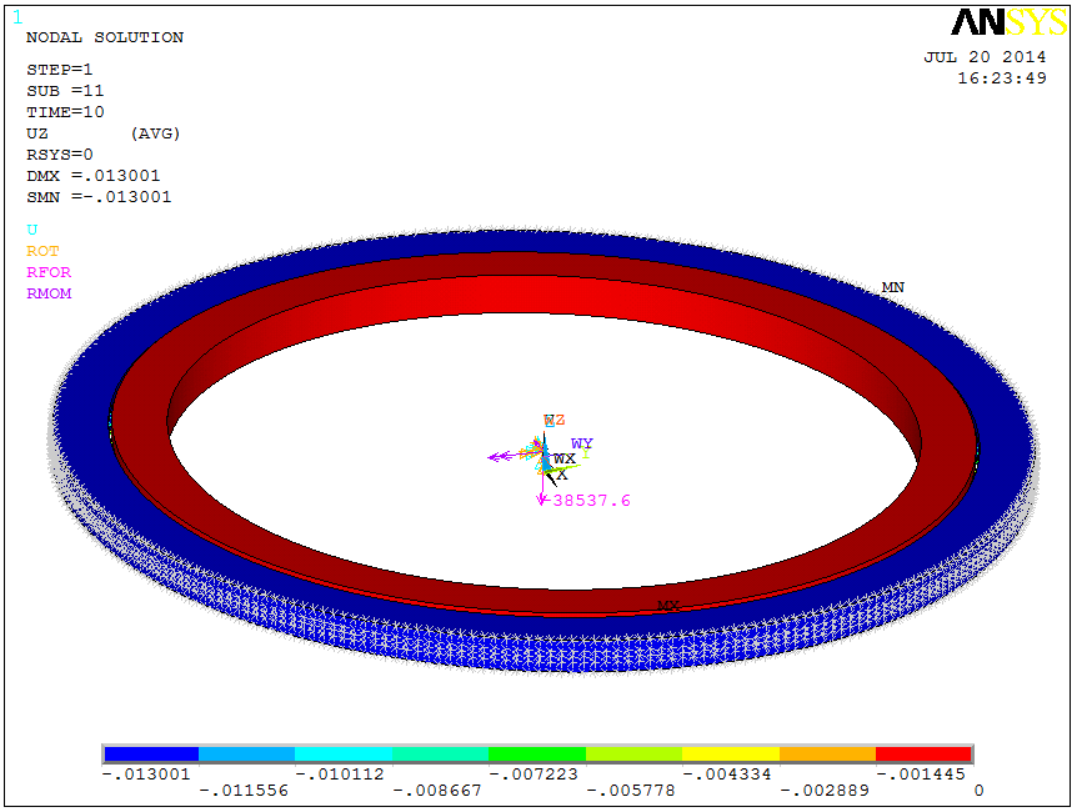


**Figure 45 - Displacement [mm] and reaction force [N] the master node in the z-axis for pure axial displacement condition**

The total load on each ball can be seen in Figure 46. Load on the balls is 395 N in compression for contact type 2.

In order to compare this solution with analytical calculations, the analytic code is run for 38.5 kN axial loading. The displacements are found as follows;

$\delta r = 0.000\, mm$

$\delta z = 0.013\, mm$

$\theta = 0.000\, degrees$

As a result of analytical code, it can be seen that load on each ball is 392.7 N for contact type 2 and zero for contact type 1 as shown in Figure 47.

In Figure 46, it can also be observed that only one type of contact in pure axial loading condition. This result is also consistent with the analytical solution.

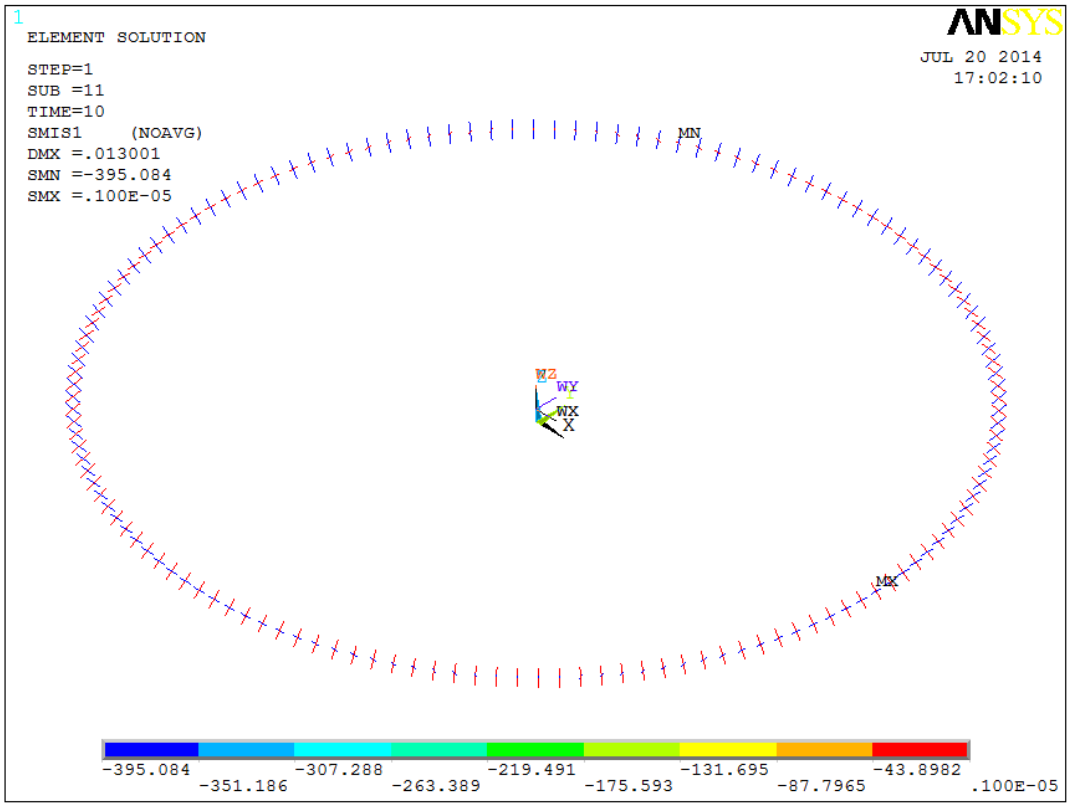


**Figure 46 - Load distribution in Newtons on balls for pure axial displacement condition**

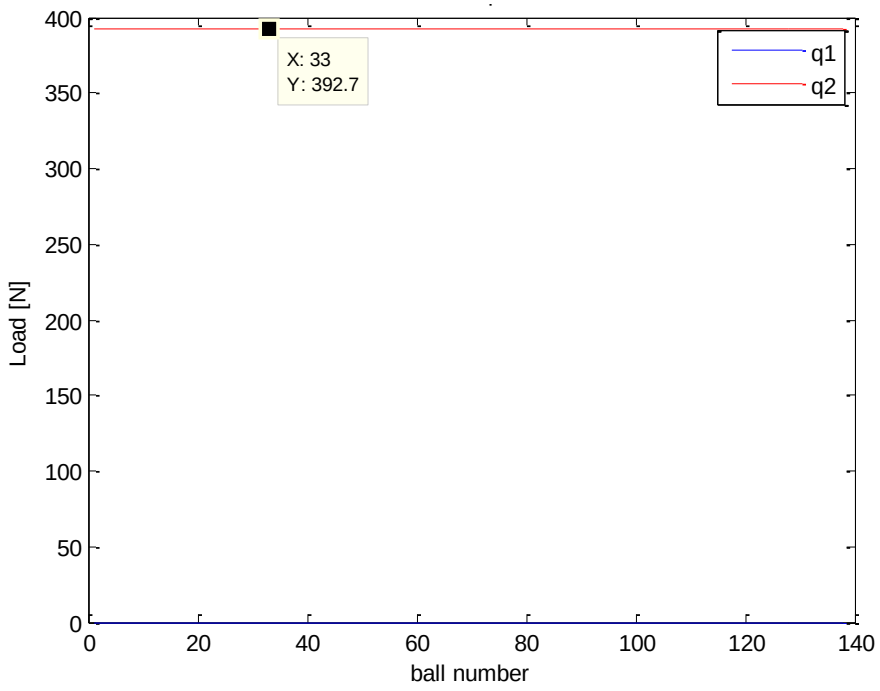


**Figure 47 - Load distribution in on balls for pure axial loading of 38.5 kN**

### 3.2.6 FEM Results of Pure Radial Loading

The finite element analysis for pure radial loading condition is prepared for 10 kN radial load. The load is applied as a ramp function and solution is made in 1000 steps. Load is applied to the outer ring via the master node that is created to apply boundary conditions uniformly.

The results of pure radial loading condition are examined as deflection of outer ring and structural force on spring elements. The displacement in the y-axis for pure radial loading condition is given in Figure 48.

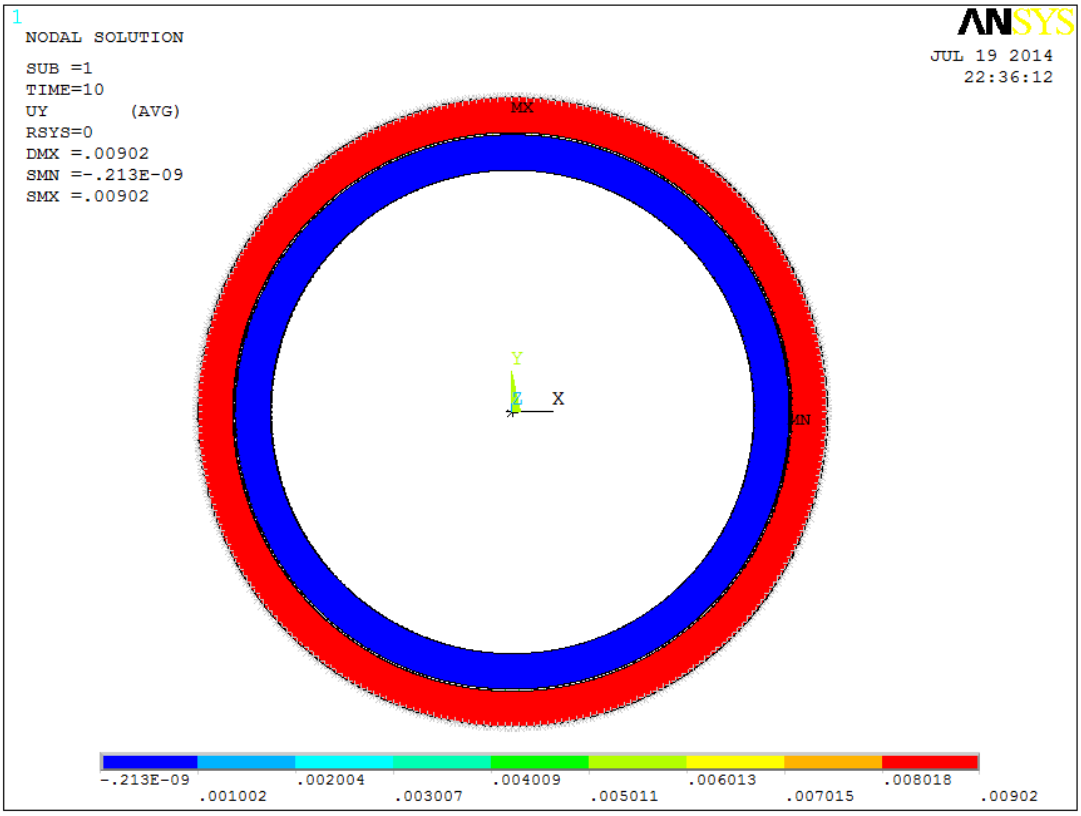


**Figure 48 - Displacement in the y-axis for pure radial loading condition**

The result of numerical solution in Figure 48 is consistent with the analytical solution. As the result of analytical based MATLAB model, deflections were found as follows;

$\delta r = 0.009\, mm$

$\delta z = 0.000\, mm$

$\theta = 0.000\, degrees$

The load distribution in on balls is given as structural force on the springs. Spring forces can be seen on Figure 49. For pure radial loading it can be observed that limited number of balls contribute to the load carrying action.

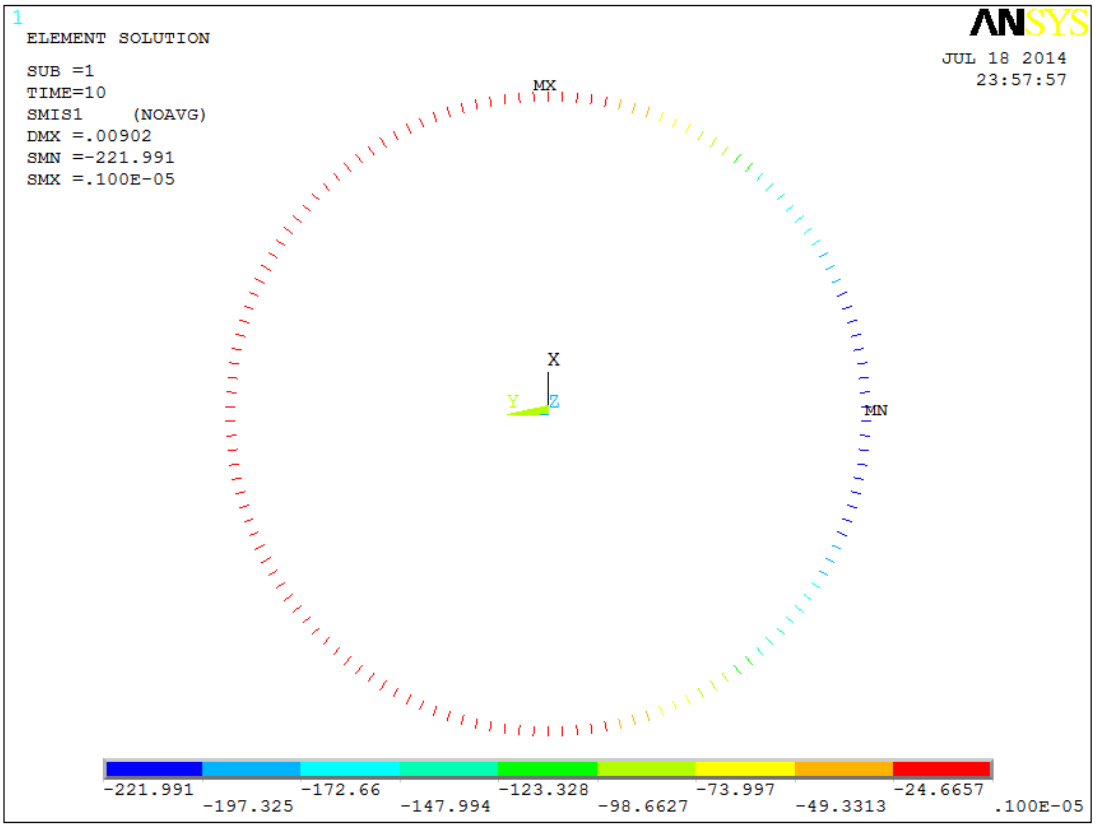


**Figure 49 - Load distribution in Newtons on balls for pure radial loading condition**

The same loading condition is examined for analytical calculation in Figure 32. Maximum radial load of 222.2 N is observed as the result of pure radial load of 10 kN. It is also consistent that the limited number of balls is contributed to carry radial load in analytic result.

The comparison of the results of analytical MATLAB model and numerical FEA models are given in Table 4. It can be said that the results are consistent with respect to each other. It can also be said that the verification of the MATLAB code is done also with the numerical model.

**Table 4 - Comparison of analytical based MATLAB and numerical FEM solution**

| | Analytical MATLAB Solution | Numerical FEM Solution | Error % |
|---|---|---|---|
| Momemt loading<br>M=100 kN.m | δr= 0.071 mm<br>Qmax= 3500 N | 0.062 mm<br>Qmax = 3586 N | 4% |
| Pure radial Loading<br>Fr= 10 kN | δr= 0.0088 mm<br>Qmax =222.2 N | δr= 0.0090 mm<br>Qmax =222 N | 2% |
| Pure axial loading<br>Fa= 38.5 kN | δa=0.0129 mm<br>Qmax =392.7 N | δa= 0.013<br>Qmax =395 N | 0.50% |

# CHAPTER 4

# ANALYTICAL STUDIES FOR FURTHER CASES IN MATLAB

## 4.1 Effect of Clearance (Endplay) on Displacement, Contact Angle and Load Distribution

Because of the production capabilities for any material, perfect sizing is impossible. With the production tolerances every bearing have additional internal clearance or preload in it. In case of no additional preload the clearance is needed to be considered.

Effects of radial and axial clearances lead to divergent solutions in complex FEA models. Modeling high number of balls with defining point contacts on each ball is a very complex model for solving numerically even without a clearance. In order to eliminate the difficulties of the FEA methods, a verified analytical model can be preferred since it is more capable and reliable in complex models.

Clearance in the bearing is a very important parameter since it causes significant changes in the contact angle. Since the change in contact angle cannot be found with finite element methods because of the zero clearance assumption. Even when the clearance is defined, it is also needed to define contact in each ball and proper mesh

should be prepared in the contact areas in order to see the changes in the contact angle. Since there are four contacts for each ball, the solution time would be very long for bearings at about these dimensions. Analytical based MATLAB solution is more reliable in this manner.

The specific slewing bearing that is investigated throughout in this thesis has clearance of 0.1 mm. The effect of 0.1 mm and 0.05 mm clearances are investigated in this part. The studies with zero-clearance are done for the same geometric dimensions in Chapter 2.

### 4.1.1 Effect of Clearance (Endplay) of 0.05 mm for Pure Moment Loading Condition

The moment load is the most dominant loading type in four-point contact bearings. The effect of clearance is firstly investigated for moment load.

Moment of 100 kN.m is applied and the displacement results are found as follows;

$\delta_r$= 0.000 mm
$\delta_z$= 0. 138 mm
$\theta$ = 0. 019 degrees

Load distribution with respect to coordinates of the balls is given in Figure 50. Load vectors in Figure 50 are non-dimensional. The axes of the graph are the coordinates of the balls.

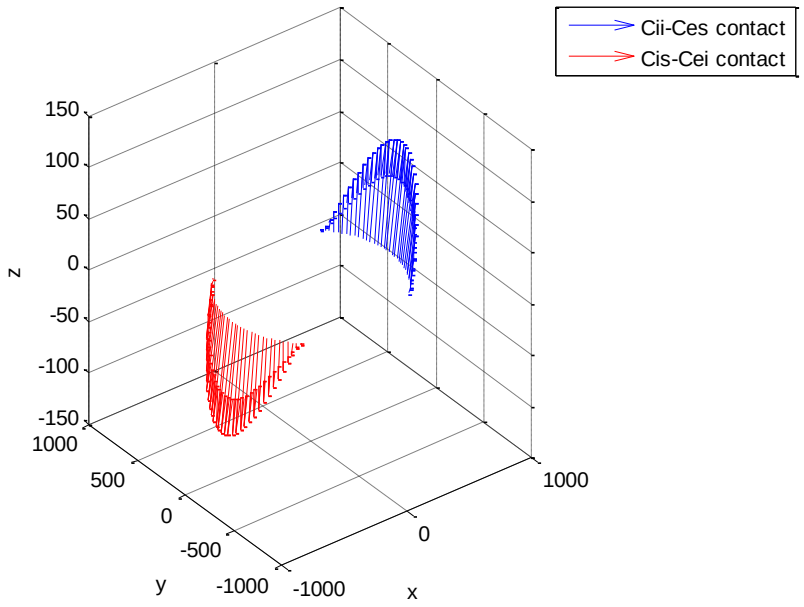


**Figure 50 - Load distribution for 0.05 mm clearance and pure moment loading of 100 kN.m**

The dimensional load distribution on balls are given in Figure 51. It can be realised that there are unloaded balls because of the effect of the clearance. Since there are unloaded balls, the load share of the loaded balls are increased with respect to Figure 38. It can be observed that maximum load on the balls is increased to 5217 N from 3500 N (Figure 38).

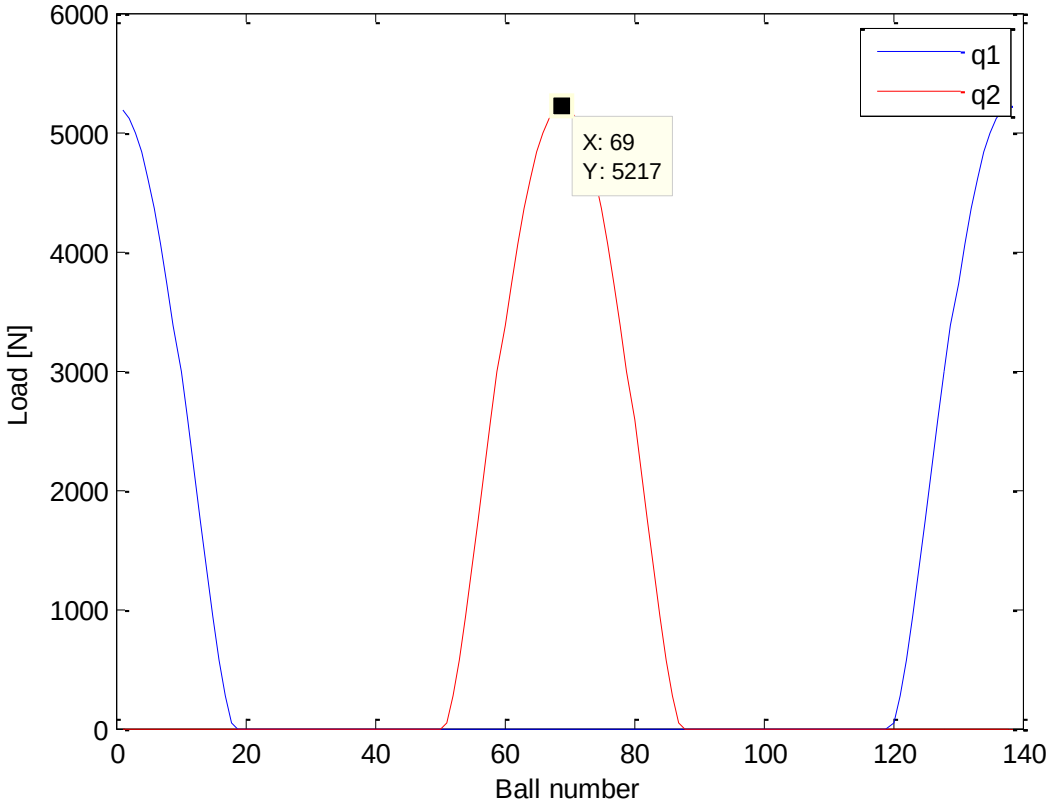


**Figure 51 - Total load distribution on balls for clearance of 0.05 mm due to moment loading of 100 kN.mm**

The contact angle alpha distribution on balls is given in Figure 52. It should be considered that change in the contact angle also affects the total load distribution on balls.

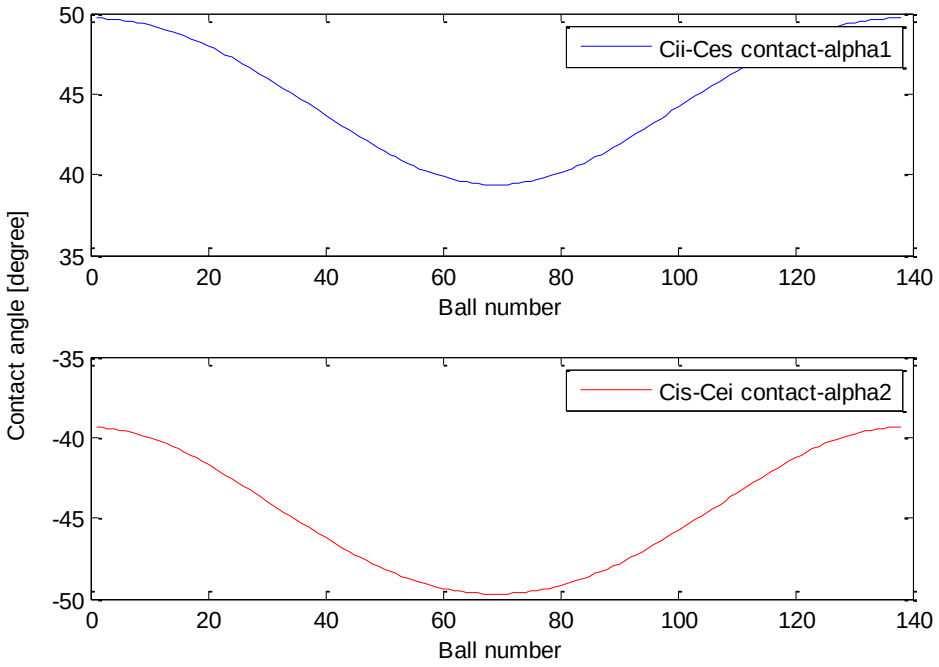


**Figure 52 - Change in the contact angle alpha for clearance of 0.05 mm due to moment loading of 100 kN.m**

Locuses of centers of curvatures are given in Figure 53. This graph gives a demonstration about how the raceway centers of curvature locations are affected.

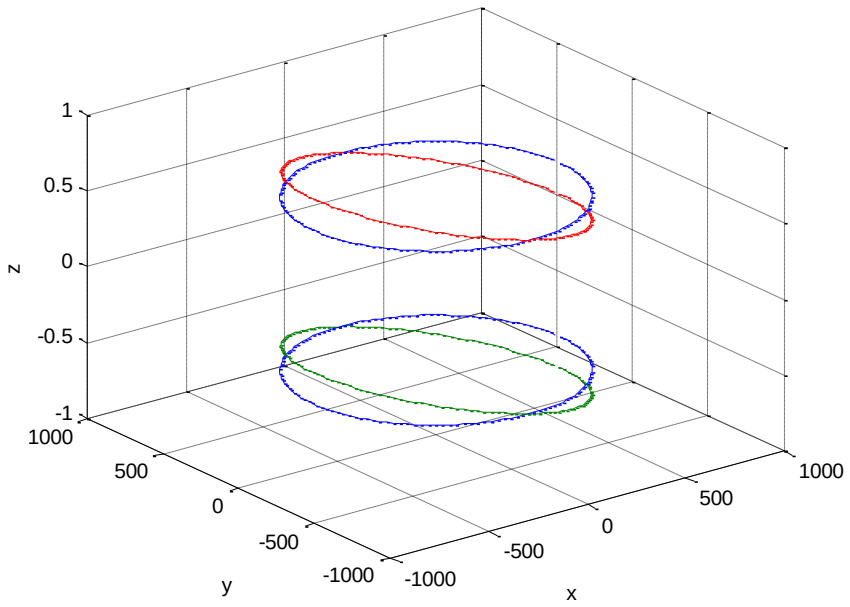


**Figure 53 - Locuses of centers of curvatures**

### 4.1.2 Effect of Clearance (Endplay) of 0.1 mm for Pure Moment Loading Condition

Moment of 100 kN.m is applied for 0.1 mm clearance in this condition and the displacement results are found as follows;

$\delta_r$= 0.000 mm

$\delta_z$= 0.269 mm

$\theta$ = 0.031 degrees

The load distribution with respect to coordinates of the balls is given in Figure 54. Load vectors in Figure 54 are non-dimensional. The axes of the graph are the coordinates of the balls.

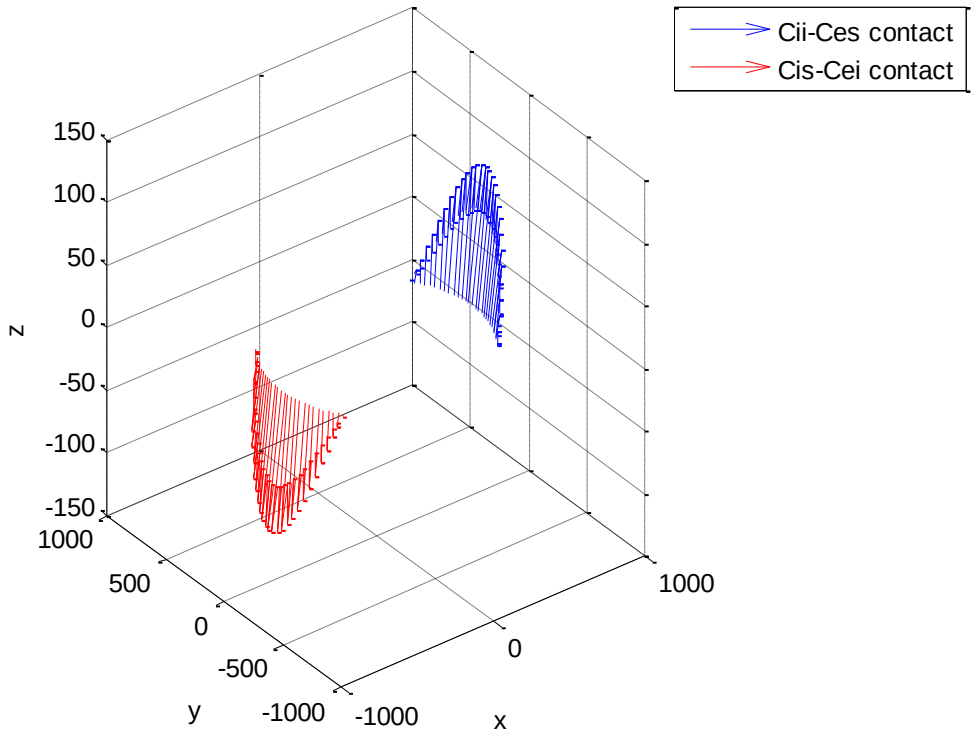


**Figure 54 - Load distribution for 0.05 mm clearance and moment loading**

The dimensional load distribution on balls are given in Figure 55. It can be realised that the number of unloaded balls is increased with respect to Figure 51 because of the increased clearance. It can also be observed that maximum load on the balls is increased to 6.15 kN from 5.22 kN (Figure 51).

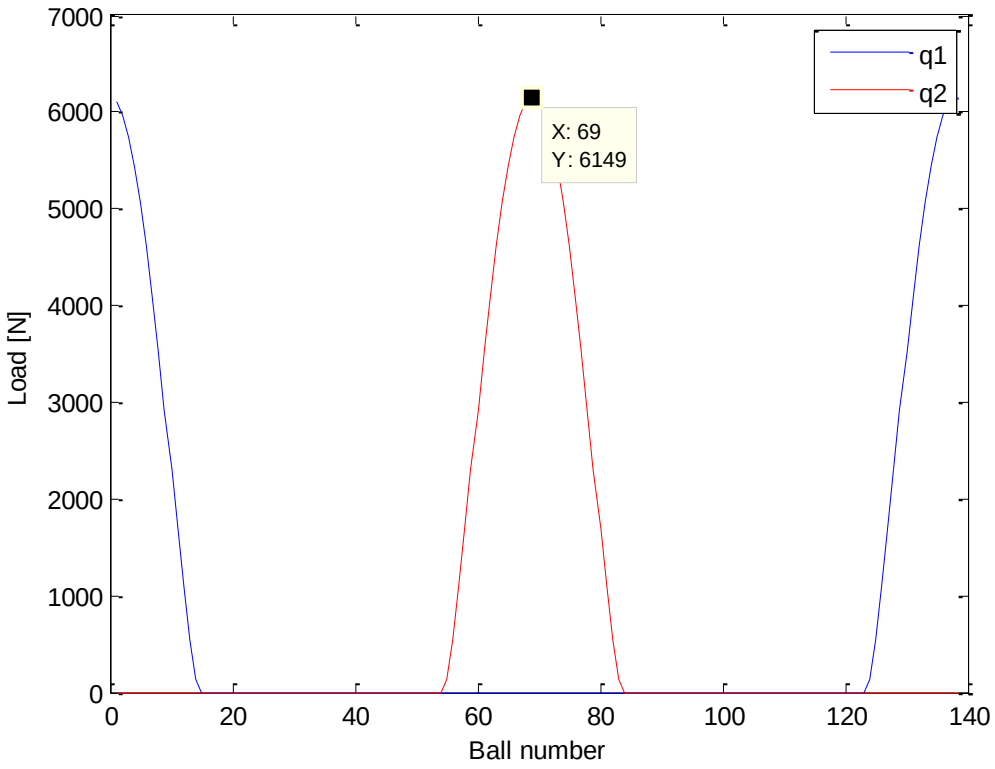


**Figure 55 - Total load distribution on balls for clearance of 0.1 mm due to moment loading**

The contact angle alpha distribution on balls is given in Figure 56. It should not be neglected that the change in the contact angle also affects the total load distribution on balls.

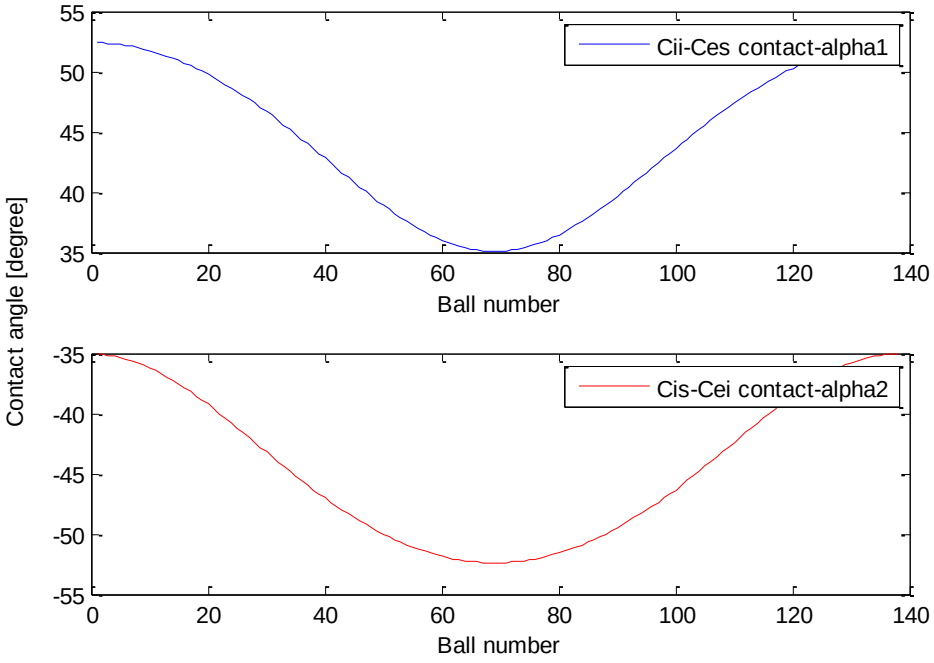


**Figure 56 - Change in the contact angle alpha for clearance of 0.1 mm due to moment loading**

The comparisons of the results for clearance values are given in Table 5.

**Table 5 - Comparison of the results for deflection angle and maximum load with different clearance values due to pure moment loading condition**

| CLEARANCE | Deflection Angle "θ" and Maximum Load "Qmax" for 100 kN.m Moment Loading |
|---|---|
| 0 mm | θ = 0.005 degrees<br>Qmax = 3500 N |
| 0.05 mm | θ = 0. 0188 degrees<br>Qmax =5217 N |
| 0.1 mm | θ =0.0312 degrees<br>Qmax =6149 N |

### 4.1.3 Effect of Clearance of 0.05 mm for Pure Axial Loading Condition

The effect of clearance can also be observed in axial loading condition. Sample calculations are investigated again with clearance values in this part.

In order to make a comparison with the previous samples the axial displacement for 0.05 mm clearance is found as below;

$\delta z = 0.297$ mm

The total loads on the balls are shown in Figure 57 while the contact angles can be examined from Figure 58.

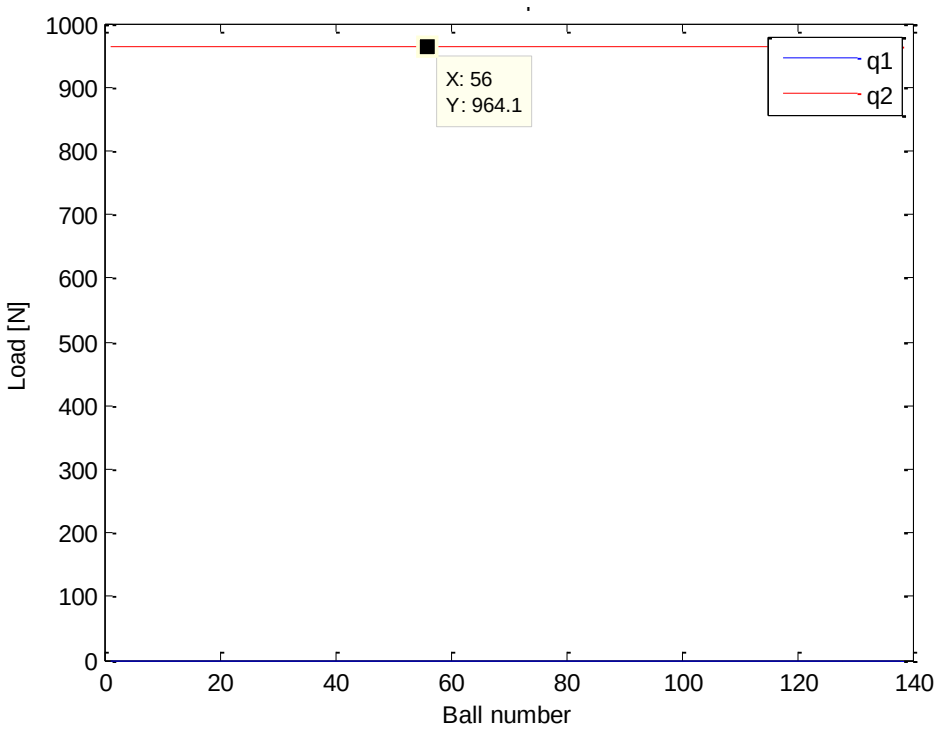


**Figure 57 - Total load distribution on balls for clearance of 0.05 mm due to axial loading of 100 kN**

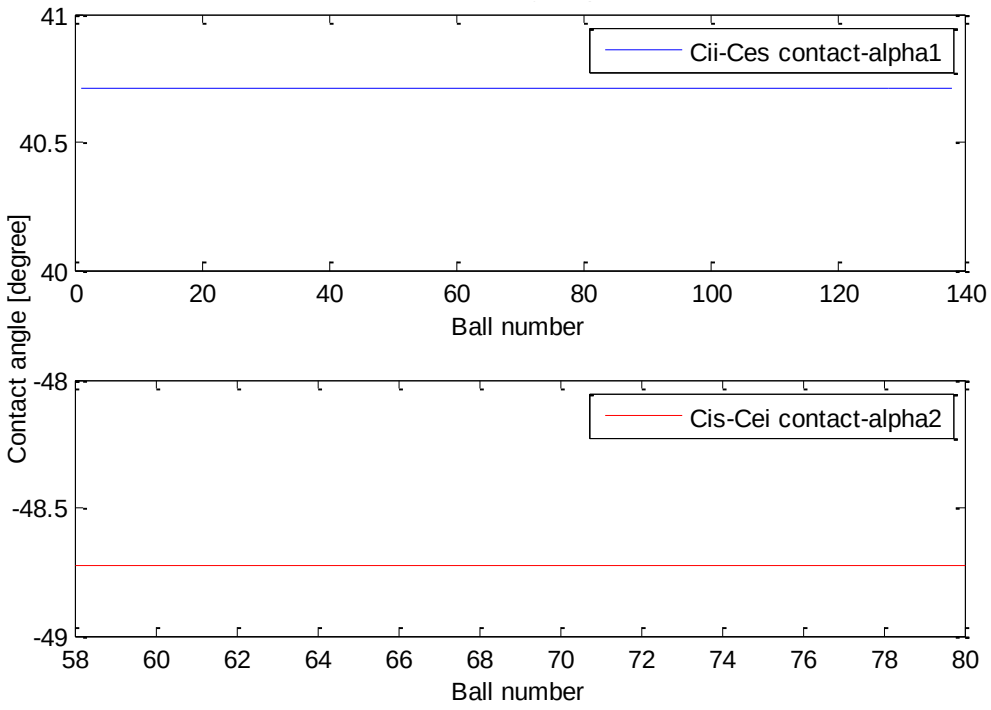


**Figure 58 - Change in the contact angle alpha for clearance of 0.05 mm due to axial loading of 100 kN**

### 4.1.4 Effect of Clearance of 0.1 mm for Pure Axial Loading Condition

The calculations are repeated for 0.1 mm clearance and 100 kN axial load, the axial displacement is found as;

$\delta z = 0.558\, mm$

The total loads on the balls are shown in Figure 59 while the contact angles can be examined from Figure 60.

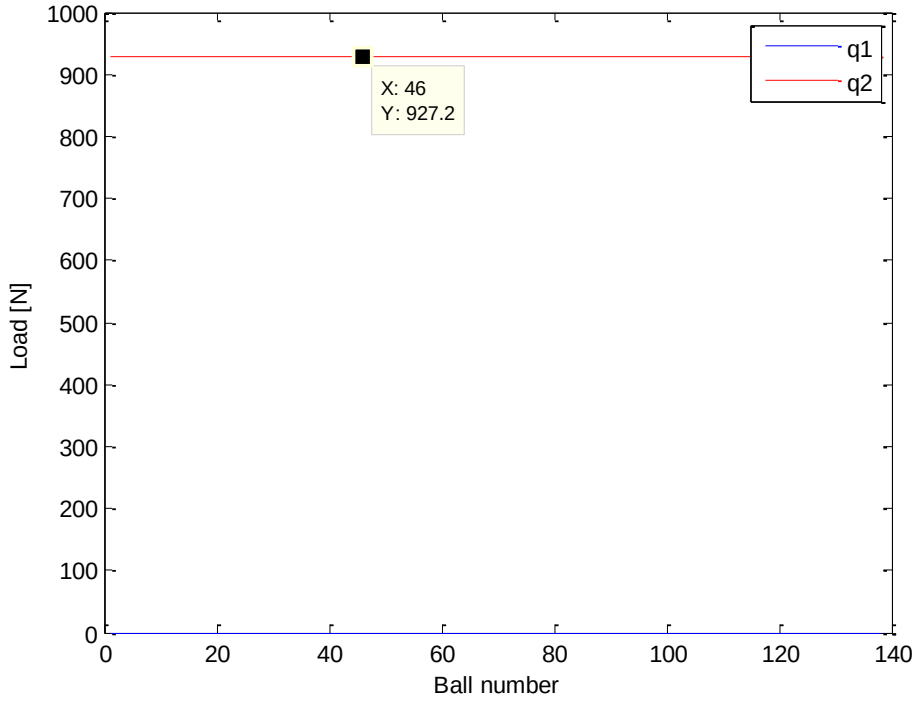


**Figure 59 - Total load distribution on balls for clearance of 0.05 mm due to axial loading of 100 kN**

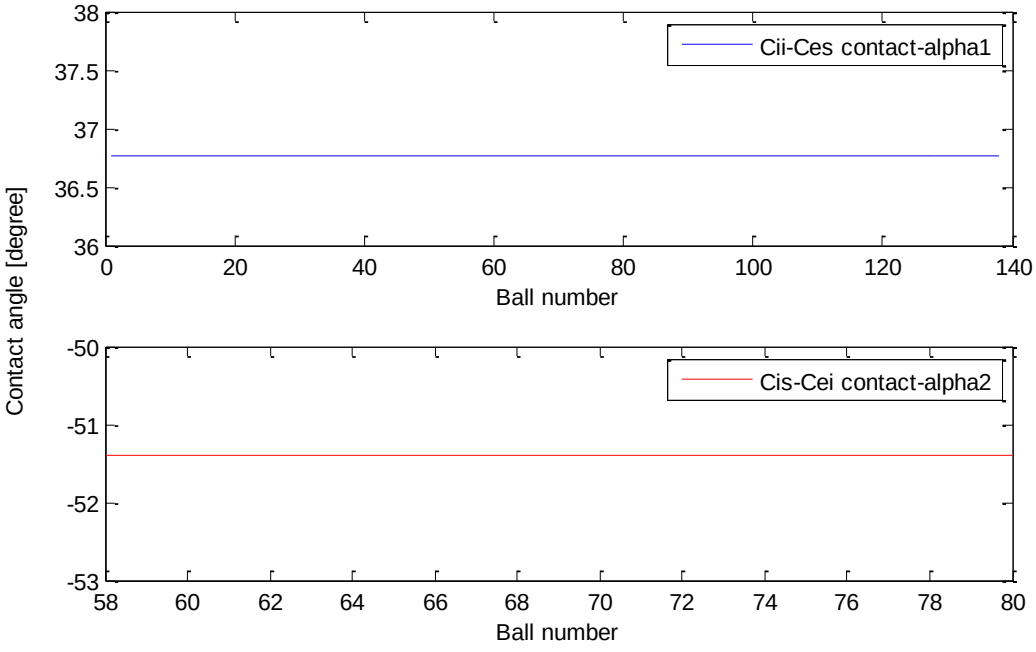


**Figure 60 - Change in the contact angle alpha for clearance of 0.05 mm due to axial loading of 100 kN**

### 4.1.5 Effect of Clearance of 0.05 mm for Pure Radial Loading Condition

The effect of clearance can also be observed in radial loading condition. Sample calculations are investigated again with clearance values in this part. 10 kN of radial force applied as a radial load.

In order to make a comparison with the previous samples the radial displacement for 0.05 mm clearance is found as below;

$\delta r = 0.152\ mm$

The total load on the balls can be seen in Figure 61 while the contact angles can be examined from Figure 62.

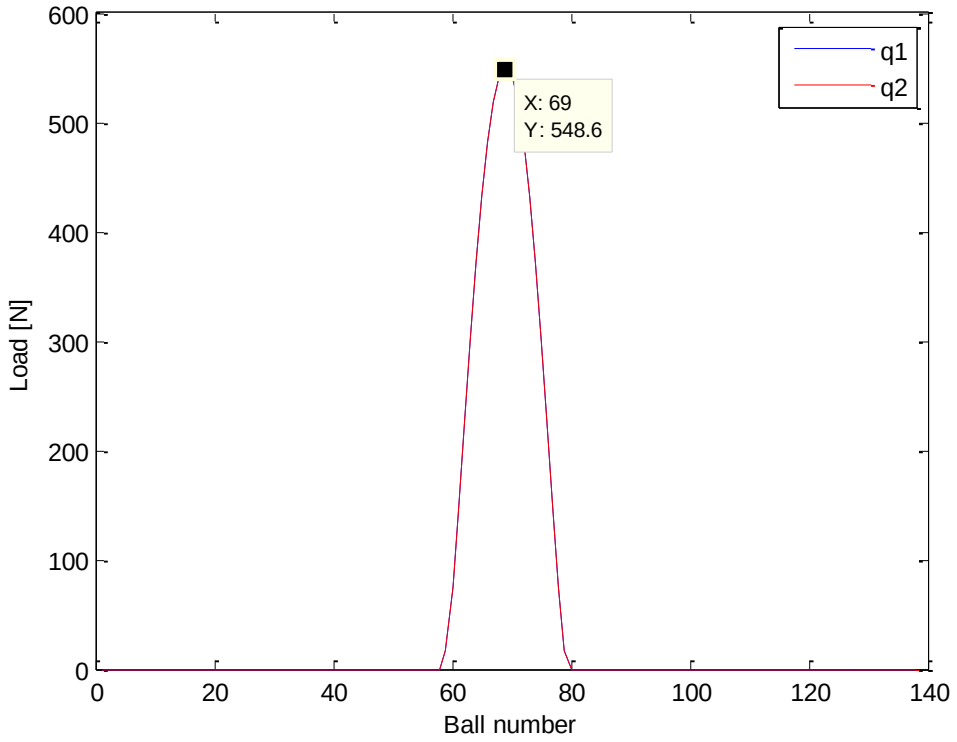


**Figure 61 - Total load distribution on balls for clearance of 0.05 mm due to radial loading of 10 kN**

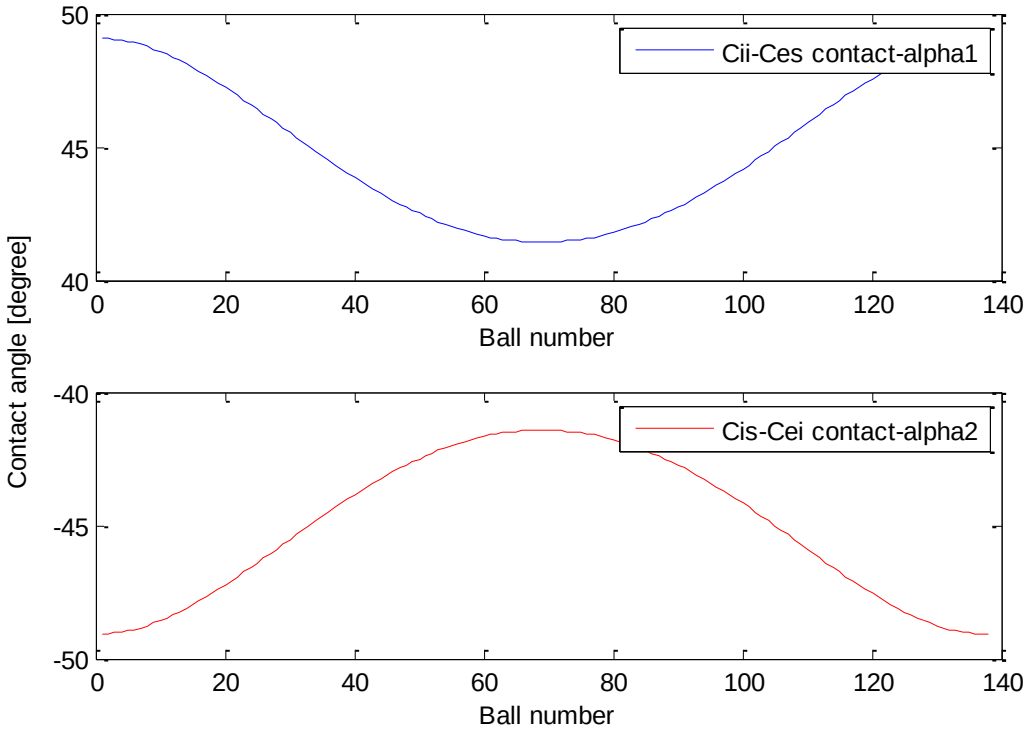


**Figure 62 - Change in the contact angle alpha for clearance of 0.05 mm due to radial loading of 10 kN**

### 4.1.6 Effect of Clearance of 0.1 mm for Pure Radial Loading Condition

The calculations are repeated for 0.1 mm clearance and the radial displacement for 100 kN axial load is found as;

$$\delta r = 0.285\, mm$$

Total load on the balls can be seen in Figure 63 while the contact angles can be examined from Figure 64.

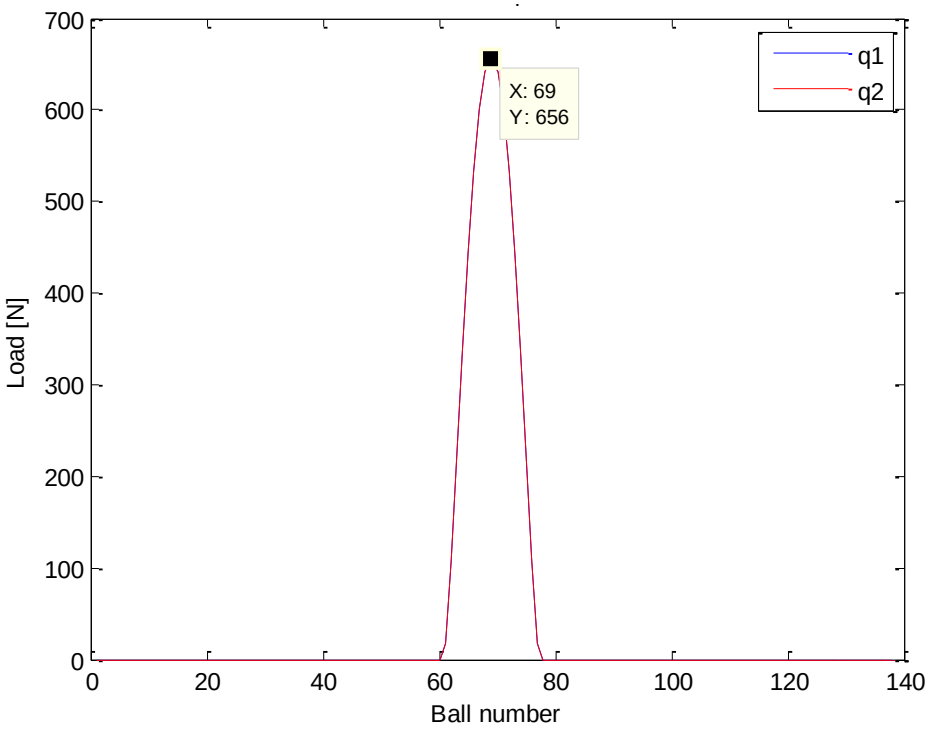


**Figure 63 - Total load distribution on balls for clearance of 0.1 mm due to radial loading of 10 kN**

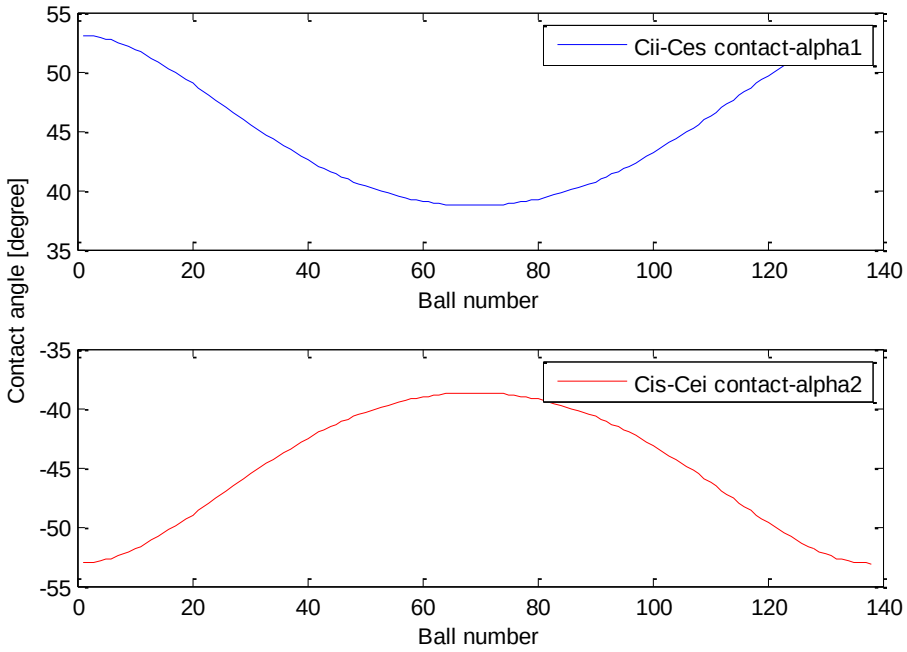


**Figure 64 - Change in the contact angle alpha for clearance of 0.1 mm due to radial loading of 10 kN**

By investigating Figure 57 and Figure 64, it can be concluded that effect of clearance is also dominant in axial and radial loading conditions in addition to moment loading condition.

The results for different clearance studies are summarized in Table 6, while the comparison of Qmax values are given in Figure 65.

**Table 6 - Comparison of deflection angle "θ" and maximum load "Qmax" values for different clearance conditions for different loading types**

| Clearance | Deflection Angle "θ" and Maximum Load "Qmax" | | |
|---|---|---|---|
| | 100 kN.m Moment Loading Condition | 100 kN Axial Loading Condition | 10 kN Radial Loading Condition |
| 0 mm | θ = 0.005 degrees<br>Qmax = 3500 N | δz= 0.024 mm<br>Qmax = 1014 N | δr= 0.009 mm<br>Qmax = 222 N |
| 0.05 mm | θ = 0. 019 degrees<br>Qmax =5217 N | δz = 0.297 mm<br>Qmax =964 N | δr = 0.153 mm<br>Qmax =549 N |
| 0.1 mm | θ =0.031 degrees<br>Qmax =6149N | δz = 0.558 mm<br>Qmax =927 N | δr = 0.285 mm<br>Qmax =656 N |

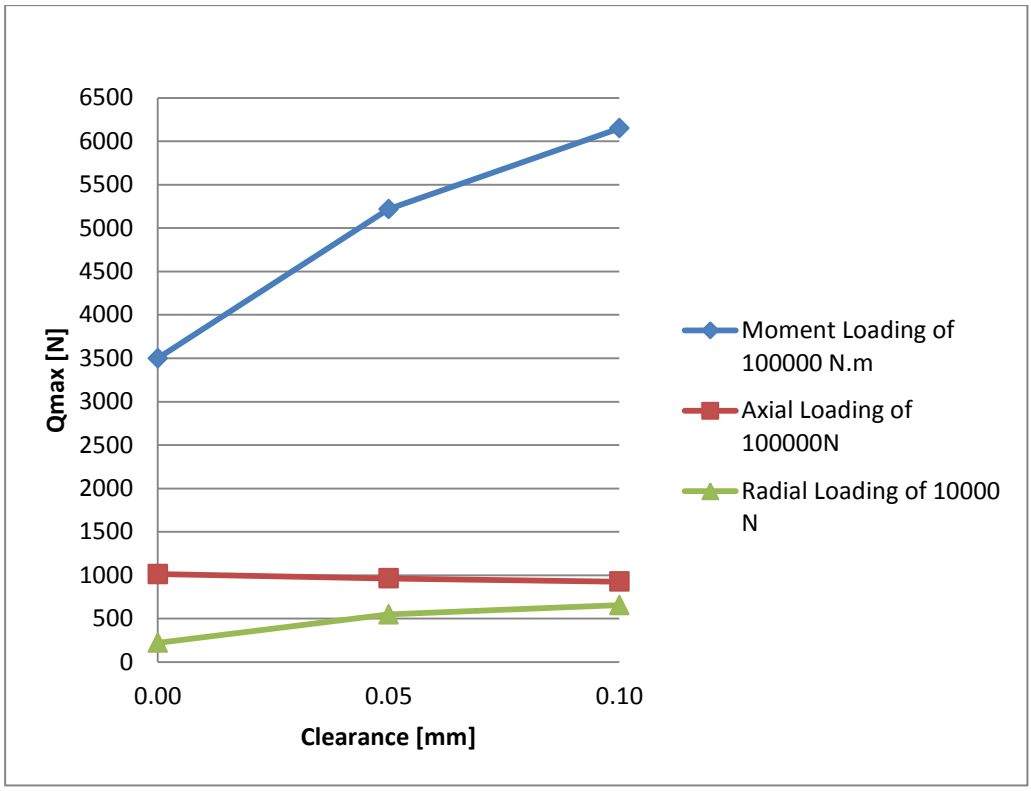


**Figure 65 - Trend of change in the Qmax with respect to clearance**

It can be realised that the effect of clearance is negligible in the load distribution for pure axial loading condition. This result can be explained by the ball number that is contributed to load share. In axial loading condition all the balls are contributing load share independent from the clearance.

## 4.2 Effect of Different Ball Diameter and Radius of Curvature of Raceways on Displacement, Contact Angle and Load Distribution

Using analytical calculations in Chapter 2, a new design for a bearing with a new geometry can be prepared without preparing a new finite element analysis. Coefficient K can be found with using equations (55-58). After obtaining an new coefficient K for new geometry, the analytical code can be used to obtain displacements, contact angle and load distribution.

In this part the effect of the increased raceway radius and decreased ball diameter will be investigated as separate parts in order to observe the independent effects separately.

### 4.2.1 Effect of Increasing Raceway Diameter with Zero-Clearance

In order to see the effect of increasing raceway the raceway radius is increased amout of 20%.

With using (55-58);

$\kappa_j = \kappa_A = \kappa = 0.28$

$K = 271.4$ kN/mm $^{3/2}$

With the decreased coefficient K the same moment condition in Chapter 2 is tested for comparison. In case of increased raceway radius a and h parameters are increased to 2.5 mm.

Analytical deflection result for 100 kN.m moment loading for zero clearance is as follows;

$\theta = 0.007\ degrees$

When it is compared with the result of previous coefficient K (K=450 kN/mm $^{3/2}$) it can be seen that θ is increased to 0.007˚ from 0.005˚. That means, 40% of change in the displacement can be observed for zero-clearance.

The load distribution on balls can be seen in Figure 66. When it is compared to the results of the previous raceway radius in Figure 38, it can be seen that the maximum load on balls is increased in amount of 1%. This change can be commented as an insignificant.

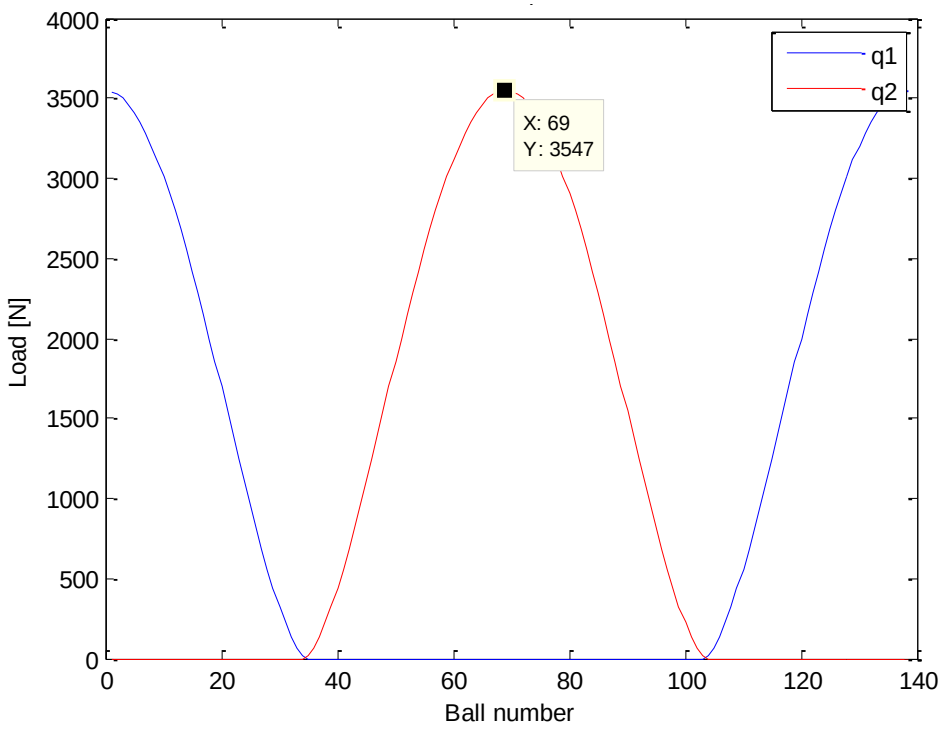


**Figure 66 - Load distribution for K= 271.4 kN/mm$^{3/2}$(1. 2 ×$r_c$), zero clearance and pure moment load of 100 kN.m**

Figure 67 shows that the differences in contact angles is decreased for increased curvature of radius of raceways.

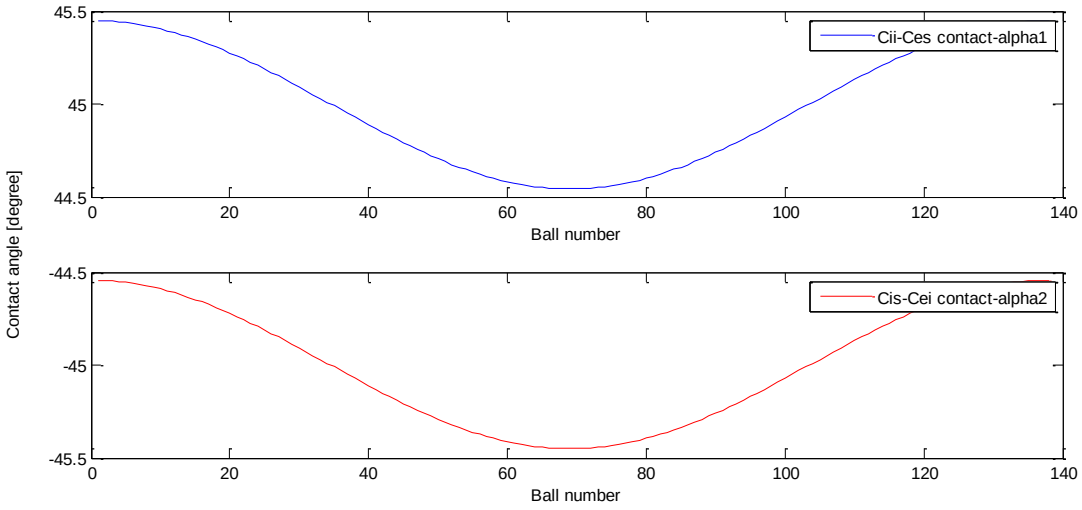


**Figure 67 - Contact angle distribution for K= 271.4 kN/mm$^{3/2}$ (1. 2 ×$r_c$) , zero clearance and pure moment load of 100 kN.m**

### 4.2.2 Effect of Increasing Raceway Diameter with Clearance of 0.05 mm

Analytical deflection result for 100 kN.m moment loading for 0.05 mm clearance is as follows;

$$\theta = 0.022\ degrees$$

When it is compared with the result of previous coefficient K (K=450 kN/mm $^{3/2}$) it can be seen that θ is increased to 0.022˚ from 0.019˚. That means, 15% of change in the displacement can be observed for 0.05 mm clearance.

The load distribution on balls can be seen in Figure 68. When it is compared to the results of the previous raceway radius in Figure 51, it can be seen that the maximum load on balls is decreased in amount of 4%. This change can also be commented as an insignificant.

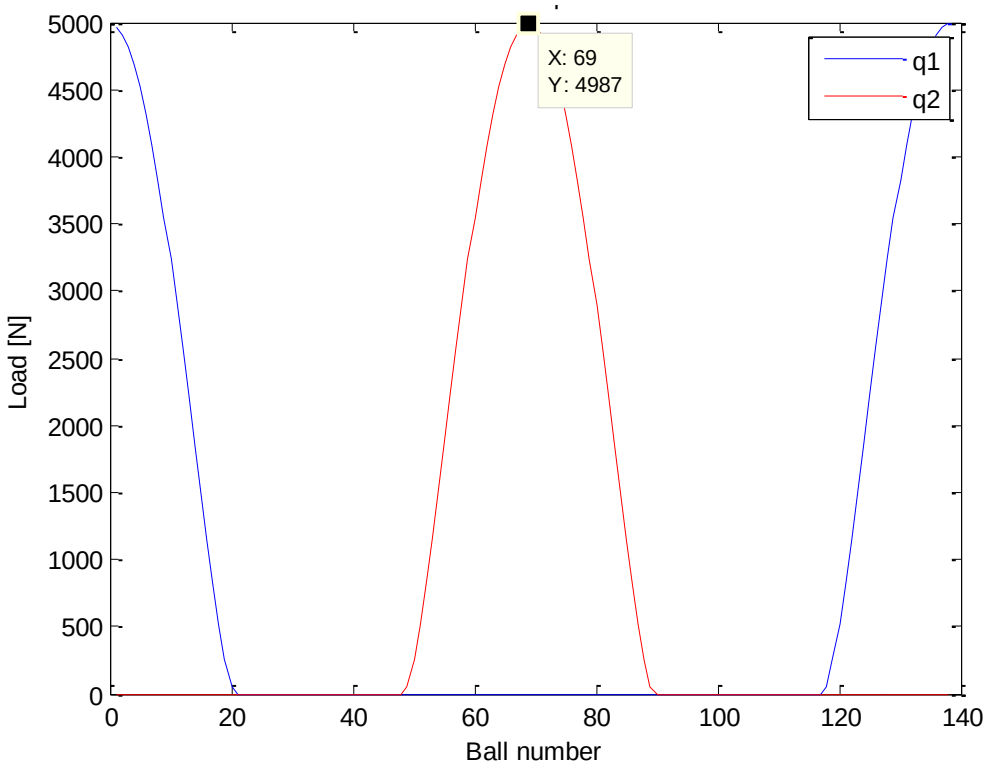


**Figure 68 - Load distribution for K= 271.4 kN/mm$^{3/2}$ (1. 2 ×$r_c$), 0.05 mm clearance and pure moment load of 100 kN.m**

Figure 69 shows that the differences in contact angles is decreased for increased curvature of radius of raceways.

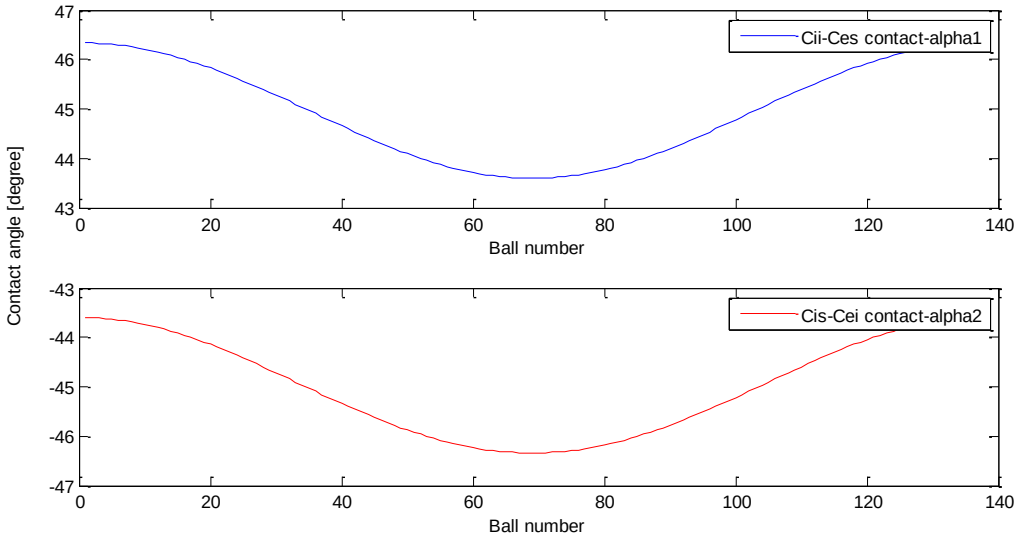


**Figure 69 - Contact angle distribution for K= 271.4 kN/mm$^{3/2}$ (1. 2 $\times r_c$), 0.05 mm clearance and pure moment load of 100 kN.m**

### 4.2.3 Effect of Increasing Raceway Diameter with Clearance of 0.1 mm

Analytical deflection result for 100 kN.m moment loading for 0.1 mm clearance is as follows;

$$\theta = 0.035\, degrees$$

When it is compared with the result of previous coefficient K (K=450 kN/mm $^{3/2}$) it can be seen that θ is increased to 0.035˚ from 0.031˚. That means, 13% of change in the displacement can be observed for 0.1mm clearance.

The load distribution on balls can be seen in Figure 70. When it is compared to the results of the previous raceway radius in Figure 55, it can be seen that the maximum load on balls is decreased in amount of 4%. This change can also be commented as an insignificant.

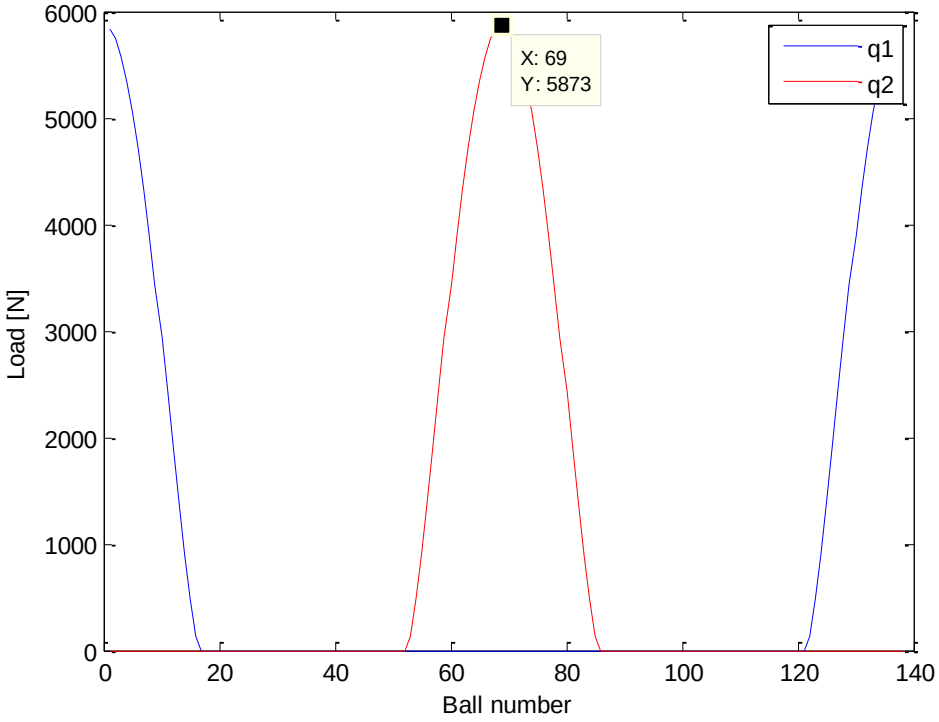


**Figure 70 - Load distribution for K= 271.4 kN/mm$^{3/2}$ (1. 2 $\times r_c$), 0.1 mm clearance and pure moment load of 100 kN.m**

Figure 71 shows that the differences in contact angles is decreased for increased curvature of radius of raceways.

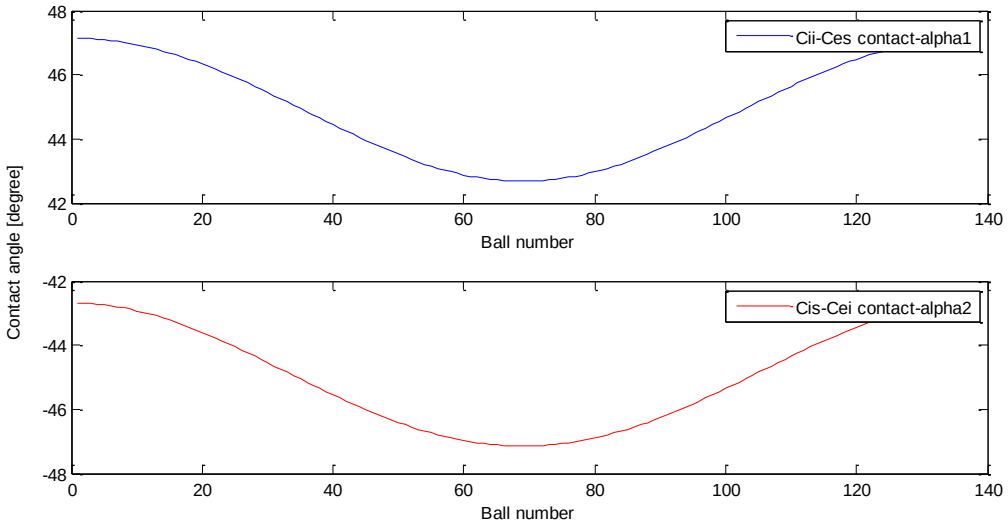


**Figure 71 - Contact angle distribution for K= 271.4 kN/mm$^{3/2}$ (1. 2 $\times r_c$), 0.1 mm clearance and pure moment load of 100 kN.m**

The change in radius of curvature of the raceways is also checked for increased radius of 33%. The effect of the changes in angle θ and maximum load is found consistent. The comparisons of the results are also given in Table 7, Figure 72 and Figure 73.

**Table 7 - Effect of clearance and effect of change in the radius of curvature of the raceways on Qmax and θ**

| Clearance | Radius of curvature of the raceways | | |
|---|---|---|---|
| | $r_c$ | $1.2\times r_c$ | $1.33\times r_c$ |
| 0 mm | θ = 0.005 degrees<br>Qmax = 3500 N | θ = 0.007 degrees<br>Qmax =3530 N | θ = 0.008 degrees<br>Qmax =3553 N |
| 0.05 mm | θ = 0. 019 degrees<br>Qmax =5217 N | θ =0.022 degrees<br>Qmax = 4987 N | θ = 0.023 degrees<br>Qmax = 4905 N |
| 0.1 mm | θ =0.0312 degrees<br>Qmax =6149 N | θ = 0.035 degrees<br>Qmax =5873 N | θ = 0.037 degrees<br>Qmax =5762 N |

It can be said that the effect of geometrical clearance is signnificantly depended on the radius of curvature of the raceways. It can also be validated from equation (17-24) and Figure 25 that the existing radial clearance is dependended on $r_c$ and d as also stated in [24]. Decrease in Fmax can be explained with decreased coefficient K. The contrubituon of the balls that are in contact, is more with respect to the solutions with high contact of rigidity. The contributon of the balls for sample balls is given in Table 8. When there is no additional clearance (0 mm clearance condition) the effect of changing radius of curvature can be observed at about 0.8% therefore the change can be claimed as negligible when there is no additional clearance.

**Table 8 - Sample data region for contribution of balls to load distribution for different $r_c$ values**

| Ball Number | 52 | 53 | 54 | 55 | 56 | 57 | 58 | 59 |
|---|---|---|---|---|---|---|---|---|
| Load on the ball for rc [N] | 0 | 0 | 0 | 1347 | 5523 | 1088 | 1683 | 2304 |
| Load on the ball for 1.2× $r_c$[N] | 0 | 1338 | 4747 | 9068 | 1391 | 1902 | 2422 | 2936 |

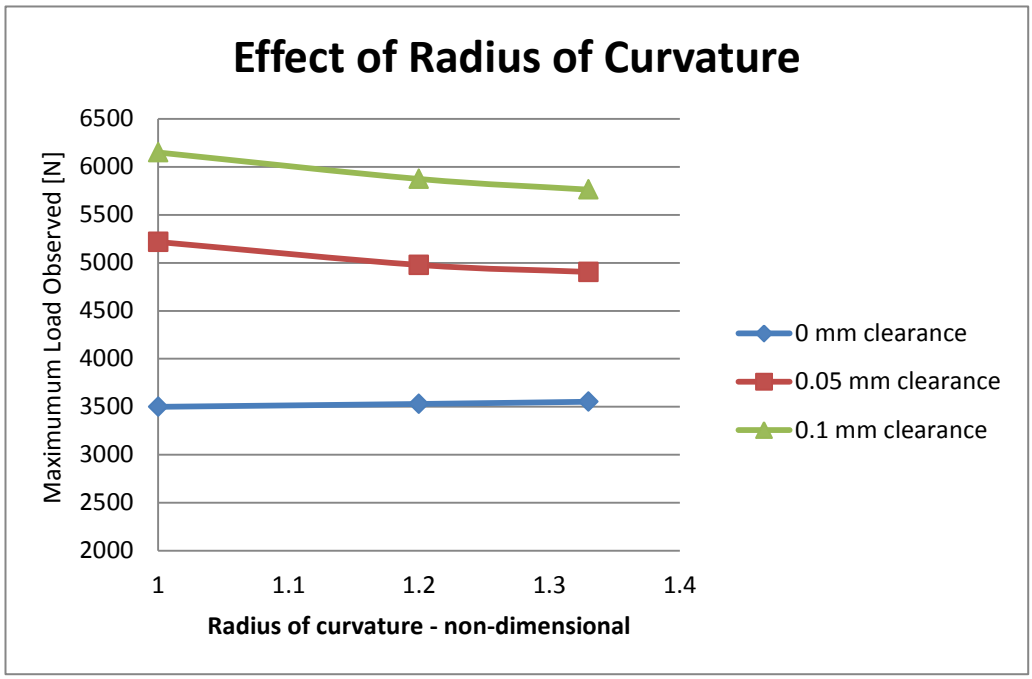


**Figure 72 - Change of maximum load observed on the balls with respect to radius of curvature for pure moment loading**

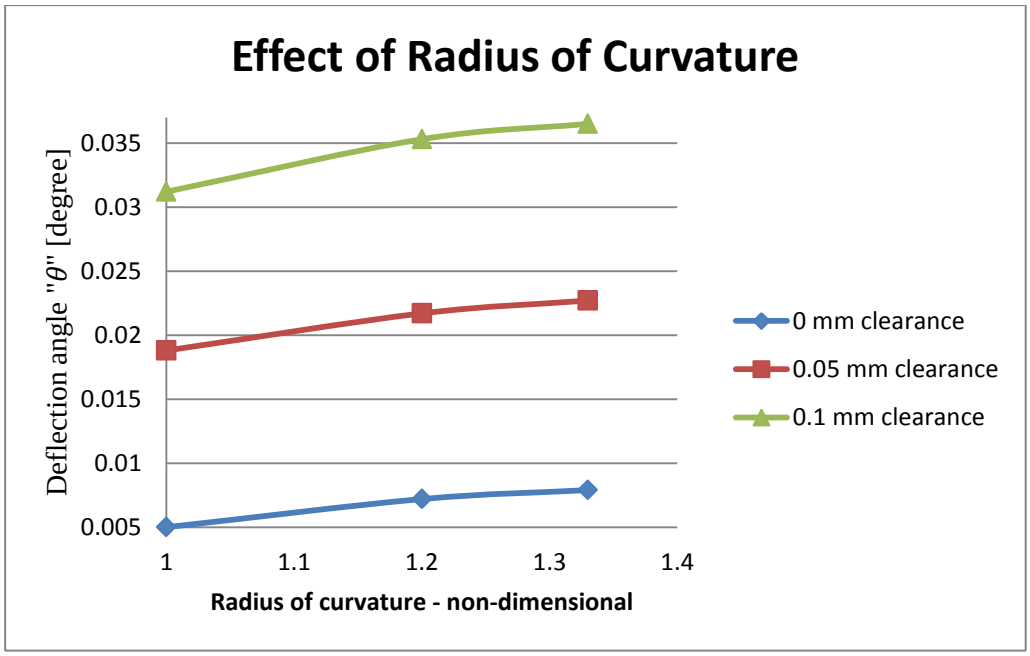


**Figure 73 - Change of deflection angle "θ" with respect to radius of curvature for pure moment loading**

### 4.2.4 Effect of Different Ball Diameter

The ball diameter must be smaller than the diameter of curvature of the raceways. In the specific slewing bearing that is studied in this thesis, radius of ball is too close to the radius of curvature. So the smaller ball diameter of 0.95 times of the diameter is investigated. New a and h parameters are calculated and new coefficient K is obtained.

Decreased ball diameter gave very similar results with increased radius of raceway curvature. The results are given in Table 9.

Figure 74 and Figure 75 are given as a sample graphs for the solution of d = 0.95×d with 0.05 mm and 0.1 mm clearance. When the graphs are compared to Figure 54 and Figure 55 it can be seen that there are decreases in the maximum load.

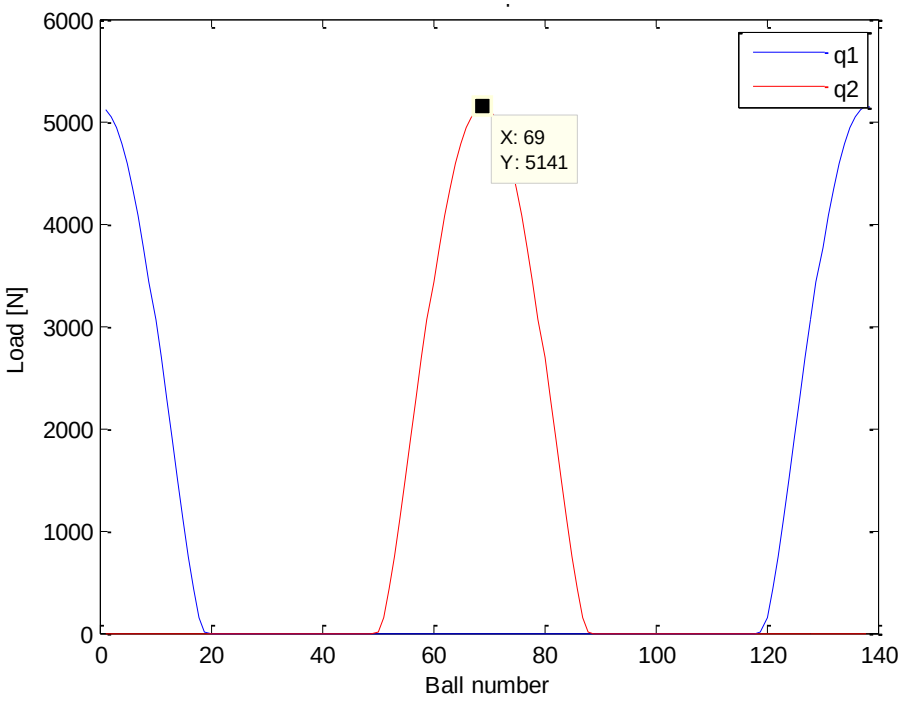


**Figure 74 - Load distribution for K= 387.8 kN/mm$^{3/2}$ (0.95×d) 0.05 mm clearance and pure moment load of 100 kN.m**

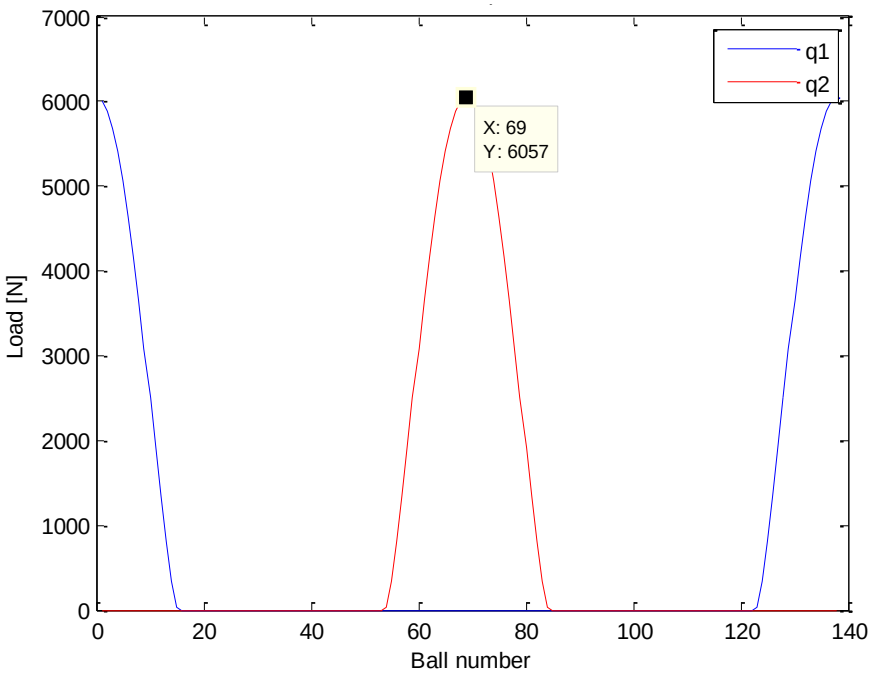


**Figure 75 - Load distribution for K= 387.8 kN/mm$^{3/2}$ (0.95×d) 0.1 mm clearance and pure moment load of 100 kN.m**

Figure 76 shows that the differences in contact angles is decreased for decreased ball diameter.

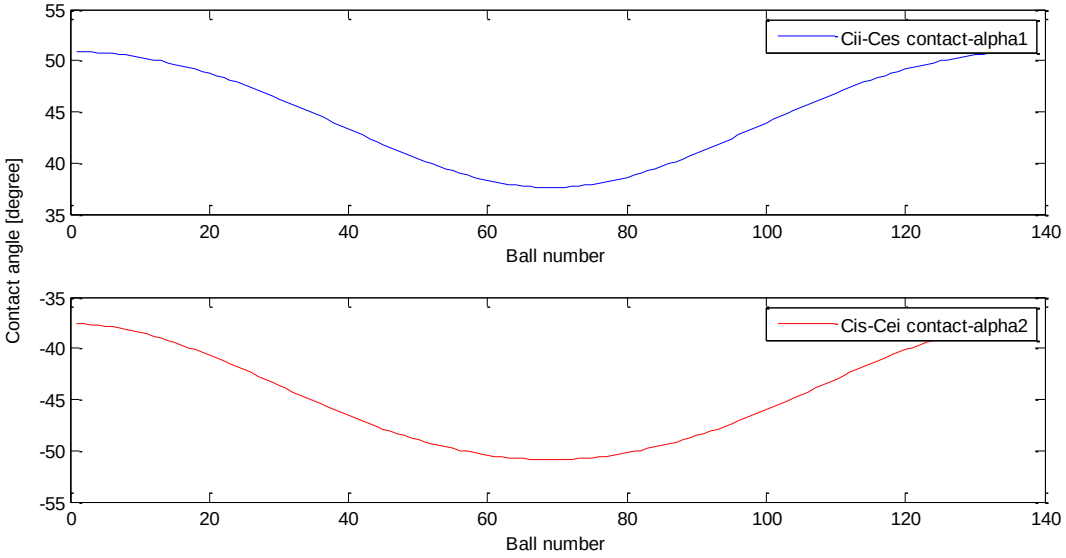


**Figure 76 - Contact angle distribution for K= 387.8 kN/mm$^{3/2}$ (0.95×d) 0.1 mm clearance and pure moment load of 100 kN.m**

It can be realised that the decreasing of ball diameter gives the same load distribution and deflection characteristic properties with increasing radius of curvature of the raceways.The results for decreasing ball diameter are compared in Table 9.

Thedecrease in Fmax can be explained with decreased coefficient K and θ increases because of the existing clearance is a function of $r_c$ and d as also stated in [24].

**Table 9 - Effect of the change in the ball diameter**

| Clearance | Diameter of the ball | |
|---|---|---|
| | d | 0.95×d |
| 0 mm | θ = 0.0050 degrees<br>Qmax = 3500 N | θ = 0.0056 degrees<br>Qmax =3511 N |
| 0.05 mm | θ = 0. 0188 degrees<br>Qmax =5217 N | θ =0.0195 degrees<br>Qmax = 5141 N |
| 0.1 mm | θ =0.0312 degrees<br>Qmax =6149N | θ = 0.0323 degrees<br>Qmax =6057 N |

## 4.3 Effect of Combined Load Case and Clearance on Displacement, Contact Angle and Load Distribution

The effect of combined load case is also investigated with the effect of clearance. A specific load case that is the combination of axial and moment load is investigated for different clearance values.

The investigated sample load case is as follows;

- Moment Loading: 100 kN.m
- Axial Loading: 100 kN

The load distributions for different clearance values of sample load case are given in Figure 77. It can be realized that with the increased clearance the contribution of the balls is decreased as same as in the pure loading conditions.

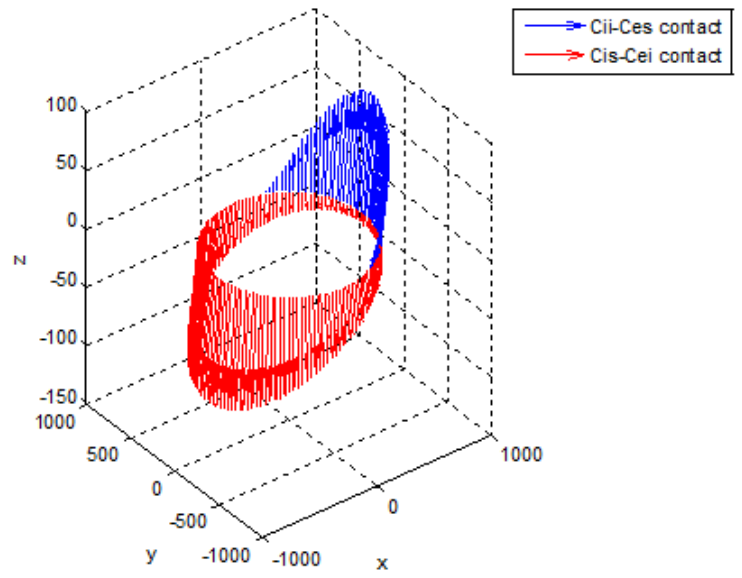


a) 0 mm Clearance

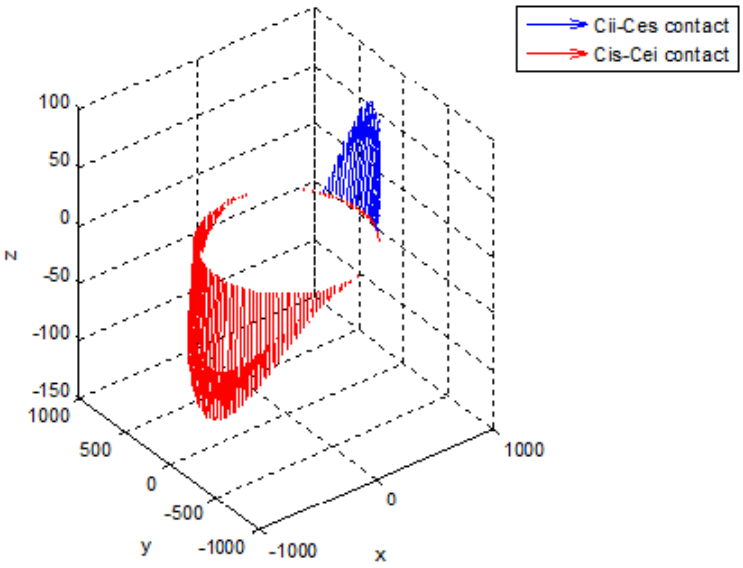


b) 0.1 mm Clearance

**Figure 77 - Load distribution for combined axial and moment loading for a) 0 mm clearance, b) 0.1 mm clearance**

The load distribution for different clearance values are given in Figure 78 and Figure 79. It can also be concluded that the results of different pure loading cases cannot be extrapolated for the combined load cases. It can be realized that the maximum load is affected from the clearance.

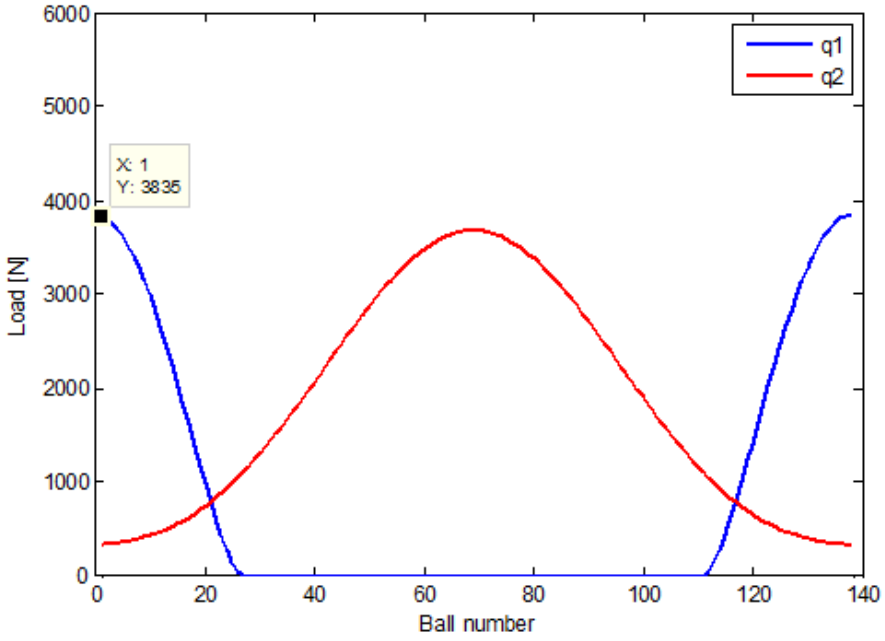


**Figure 78 - Load distribution for combined moment load of 100 kN.m and axial load of 100 kN for clearance of 0 mm**

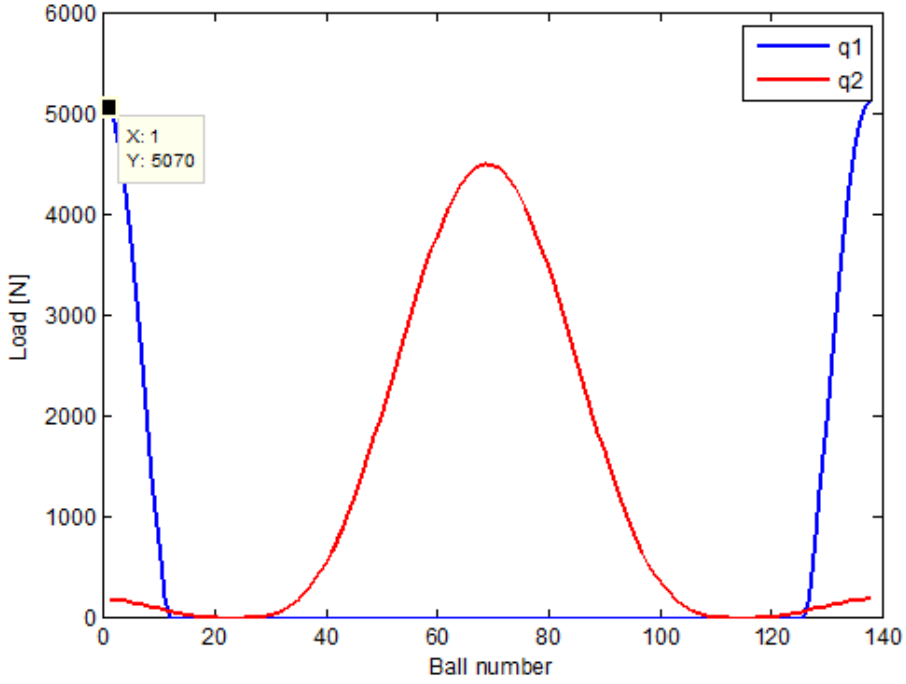


**Figure 79 - Load distribution for combined moment load of 100 kN.m and axial load of 100 kN for clearance of 0.1 mm**

The changes in the contact angles for different clearance values are given in Figure 80 and Figure 81. It can be ralized that the variations in the contact angle can increase up to 30 degrees and it should be noted that this variation plays a big role in the load distribution. It should also be noted that the change in the contact angle can not be determined in FEM without defining contacts on each ball. For the sample bearing examined througout the thesis, defining four contact for each ball means solution of 540 contact which is not feasible because of the solution time consideration.

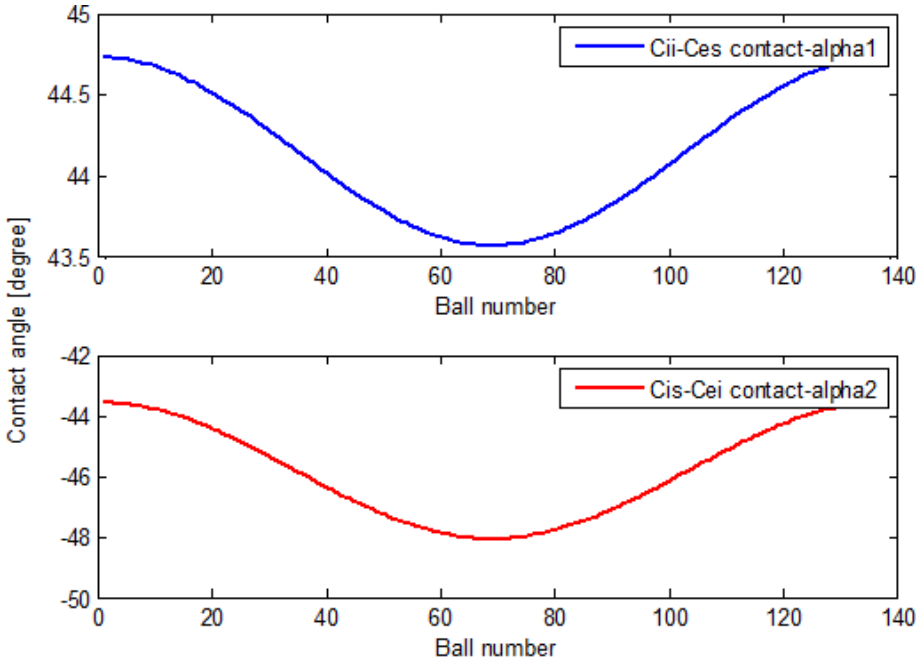


**Figure 80 - Contact angle distribution for combined moment load of 100 kN.m and axial load of 100 kN for clearance of 0 mm**

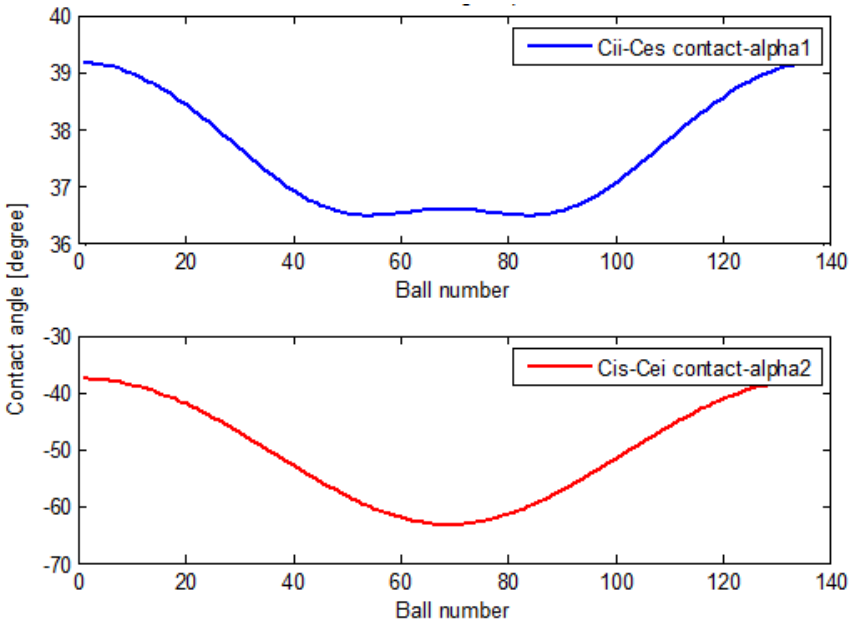


**Figure 81 - Contact angle distribution for combined moment load of 100 kN.m and axial load of 100 kN for clearance of 0.1 mm**

# CHAPTER 5

# DISCUSSION OF THE RESULTS AND CONCLUSIONS

## 5.1 Discussion of the Results

This study is prepared in order to obtain more theoretical knowledge on the loaded behavior of four-point contact bearings. In the first chapter an introduction to four-point contact bearings is represented and background of the thesis is supported with the sample studies from the literature. In addition to slewing bearings, load distribution can also investigated for standard bearings like deep-groove ball bearings and angular contact ball bearings. It is explained in the literature survey that the background of the theory of load distribution in slewing bearings is strongly based on the standard bearing load distribution studies.

In the second chapter, analytical calculation procedure is explained and sample calculations are carried out by using MATLAB. Sample load cases are solved. The samples in second chapter are made for zero-clearance assumption that is what the finite element analysis method and the theoretical calculations are capable to verify.

The results of the samples with zero clearance that are carried out in Chapter 2, give the load distribution characteristics of four-point contact bearings. It is given the

Figure 31 that, the axial force is shared by the balls equally for axial loading condition. Since the load distribution is uniform on the bearings, the maximum load is not observed as a peak value; so the axial loading is not critical for the most of the cases. By investigating Figure 30, it can be concluded that the change in the contact angle is stable for all of the balls and it is insignificant for axial loading condition.

The radial loading condition is also checked in order to observe the load distribution, deflections and contact angles. Since the radial loading is not a dominant loading condition in slewing bearings, respectively lower force value for Fr is applied as a sample. The load distribution on balls is given in Figure 32. The heavily loaded ball is the one that is in the direction of the radial load vector. The two type of contact occurs simultaneously on the same balls only in the radial load case.

The moment loading is the most important case throughout the thesis, because the main purpose is to check the dominant loading in the slewing bearing applications. In the moment loading application, total force value makes a peak on the balls that are on the perpendicular axis to the moment axis. As it is presented in Figure 38, Figure 51, Figure 55, Figure 66, Figure 68, Figure 70, Figure 74 and Figure 75; load distribution makes two peaks for different contact types at the two sides. Results are verified at the third chapter both by theoretical formulation and finite element method.

At the third chapter, both numerical verifications and benchmark formulation verifications are carried out. Since finite element analysis capabilities are limited, assumption of zero-clearance is carried out throughout the finite element analysis method. The results are verified each other so it can be concluded that further studies can be carried out with analytical MATLAB code in order to have more accurate results.

At the fourth chapter, the effects of clearance and inner geometry which are significant parameters for the maximum load and deflection are investigated. It is concluded that the clearance in the bearings is a very important parameter which is needed to be considered. Clearance affects both load distribution and deflection results of all the load cases significantly. Without considering clearances, deviations

in the contact angle cannot be observed. Since the contact angles are determinant for load distribution, a very important parametric change can be ignored without considering clearance. The combination of the effects of contact angle and clearance determines the deflection characteristics and load distribution of the bearings together. By investigating the results given in Table 6, it can be concluded that with the increasing clearance, maximum load on balls increases significantly for moment loading and radial loading conditions while it decreases for axial loading condition. Increasing of maximum load on the balls is because of the fact that decreased number of balls that is in contact while the radial and the moment loading occur. Since the number of balls in contact decreases, it can be concluded that the load share of each ball increases. It can also be observed that the deflection angle θ increases for moment loading condition with the increased clearance. Because of the increased clearance, also the variety of the contact angles increases. This variety around 45˚ can be seen in Figure 56, Figure 69, Figure 71 and Figure 76. Contact angle is another parameter that is effective on the load distribution. The change in this parameter also cannot be seen in FEA methods. The changed trend of load distribution can be investigated from Figure 51, Figure 55, Figure 68, Figure 70, Figure 74 and Figure 75. It can be seen that balls that are close to moment application axis do not share the load while the maximum load occurs on the farthest balls to the moment axis. It can be concluded that during the design steps of the slewing bearings systems with inner clearance, analytical MATLAB model should be considered instead of finite element modeling.

In the second part of the fourth chapter, the effect of increase in radius of curvature of the raceways is studied. The results are given in Table 7 while the load distributions are given in Figure 70, Figure 74 and Figure 75. The trend in the change of load with respect to ball coordinates is similar with the case of original radius of curvature of the raceways. It can be realized that insignificant decrease in the maximum load can be observed with increasing radius of curvature in the bearings with clearance, while the deflection angle θ has an increasing trend. Therefore, it can be suggested that an optimization between deflection angle θ and the maximum load on the balls can be done in the bearings. The decrease in the force on the balls can be

explained with the increase of balls' contribution to load because of the increase in radius of curvature of the raceways which reduced the coefficient K.

In the last part of the fourth chapter, the effect of decreasing ball diameter is investigated. By investigating the results in Table 9, it can be concluded that the decrease of ball diameter gives the same load distribution and deflection characteristic properties with the increasing radius of curvature of the raceways. The same observations for the decreasing radius of raceways can be indicated for the study of decreased ball diameter.

## 5.2 Conclusions

In this thesis, the load distribution and deflection characteristics of four-point contact bearings are studied for different loading conditions, radii of curvatures of the raceways and ball diameters. The results are summarized in the discussion part while they are explained in detail throughout the previous chapters.

In this study, primary goal is to find the bearing performance by a more accurate method. Therefore, both with numerical FEA method and analytical MATLAB model are investigated. The accuracy of the MATLAB model is concluded on the part of the discussion of the results. In addition to MATLAB model's solutions being more accurate it is obvious that modifying the geometry on a finite element model requires more effort than using a prepared MATLAB model. Even when using a prepared APDL code on ANSYS, modeling time of a finite element model on ANSYS can reach up to thirty minutes while MATLAB code takes about only 20 seconds. It also should not be ignored that finite element modeling programs require high capacity computers. Using finite element programs also requires more users' knowledge and the cost is high. In most of the companies, limited number of licenses makes the commercial FEM programs hard to use because of the demand to use that programs, while MATLAB licenses are easier to acquire. Therefore, it can be concluded that the analytical based MATLAB model is more effective in both accuracy, modeling time, solution time, users' knowledge and cost points of view.

As a final conclusion, it can be said that clearance significantly affects the load distribution and deflection characteristics of slewing bearings differently in certain loading conditions. Therefore, it can be concluded that with the procedure verified in this thesis, the design steps can be checked faster and more accurate solutions with fewer assumptions can be made.

## REFERENCES


[1] Naval-technology. (n.d.). Naval-technology. Retrieved August 18, 2014, from http://www.naval-technology.com/projects/sejongthegreatclassd/sejongthegreatclassd/5.html

[2] ROLLIX. (n.d.). *ROLLIX Corporation*. Retrieved July 19, 2014, from http://www.rollix.com/324-4358-6235-6266-6276/Offshore.htm

[3] ROLLIX. (n.d.). *ROLLIX Corporation.* Retrieved July 19, 2014, from http://www.rollix.com/324-4358-6235-6266-6278/Forest-Industries.htm[Accessed 19th July 2014]

[4] Aguirrebeitia, J., Abasolo, M., Aviles R., Bustos, I.F., (2012) General static load-carrying capacity for the design and selection of four contact point slewing bearings: Finite element calculations and theoretical model validation, *Finite Elements in Analysis and Design* 55, 23–30

[5] Göncz, P., Drobne, M., Glodež, S., (2013) Computational model for determination of dynamic load capacity of large three-row roller slewing bearings, *Engineering Failure Analysis* 32, 44–53.

[6] Amasorrain, J. I., Sagartzazu, X., Damian, J., (2003) Load distribution in a four contact-point slewing bearing, *Mechanism and Machine Theory* 38, 479–496.

[7] Glodež, S., Potočnik, R., Flašker, J., (2012) Computational model for calculation of static capacity and lifetime of large slewing bearing's raceway, *Mechanism and Machine Theory* 47, 16–30.

[8] Glodež, S. Potočnik, R., Flašker, J., (2007) A vector approach to the computation of a load distribution in a large slewing bearing, in: Barták, J., Čermak R., (Eds.), *PhD 2007*:

5th International PhD Conference on Mechanical Engineering, 221–224.

[9] Potočnik, R., Flašker, J., Glodež, S., (2012) Computational model for load capacity of large slewing bearin's raceway, *Mechanism and Machine Theory* 47, 16–30

[10] Zupan S., Prebil I., (2001) Carrying angle and carrying capacity of a large single row ball bearing as a function of geometry parameters of the rolling contact and the supporting structure stiffness. *Mechanism and Machine Theory*, 36, 1087–1103.

[11] Glodež S., Potočnik R. , Göncz P., (2013) Static capacity of a large double row slewing ball bearing with predefined irregular geometry. *Mechanism and Machine Theory* 64, 67–79.

[12] Wang Y. S., Yuan Q. Q., (2013) Contact Force Distribution and Static Load-carrying Capacity of Large Size Double Row Four-point Contact Ball Bearing. *Defense Technology* 9, 229-236

[13] Kania L., (2006) Modelling of rollers in calculation of slewing bearing with the use of finite elements. *Mechanism and Machine Theory* 41, 1359–1376.

[14] Pandiyarajan R., Starvin M.S, Ganesh K.C., (2012) Contact Stress Distribution of Large Diameter Ball Bearing Using Hertzian Elliptical Contact Theory, *Procedia Engineering* 38, 264 – 269.

[15] Zhaoping T., Jianping S., (2011) The Contact Analysis for Deep Groove Ball Bearing Based on ANSYS, *Procedia Engineering* 23, 423–428.

[16] Liao N. T., Lin J. F., (2001) A New Method for the Analysis of Deformation and Load in a Ball Bearing With Variable Contact Angle, *Transactions of the ASME* 123, 304-312.

[17] Harris, T. (2006) *Rolling Bearing Analysis*. New York: John Wiley&SonsInc;.

[18] Brandlein J., Eschmann P., Hasbargen L., Weigand K., Ball and Roller Bearings Design and Application. New York: John Wiley&SonsInc; 1999.

[19] ABAQUS (2011) `ABAQUS Documentation', DassaultSystèmes, Providence, RI, USA.

[20] Yetgin, A. (2013). Fracture analysis of welded connections. *Master's Thesis*.

[21] The Math Works, Inc, (2013) *MATLAB Help R2013a*, Massachusetts, USA.

[22] ANSYS, Inc, (2010) ANSYS Mechanical APDL Element Reference, Canonsburg, PA.

[23] ANSYS, Inc, (2011) *ANSYS 14.0 Help Theory Reference*, Canonsburg, PA.

[24] Oswald F. B., Zaretsky E. V., Poplawski J.V., (2012) Effect of Internal Clearance on Load Distribution and Life of Radially Loaded Ball and Roller Bearings, *NASA/TM*, 217115

# APPENDIX A

## SOLUTION PROCEDURE OF MATLAB CODES

The solution procedure through the MATLAB codes is given in Figure 82.

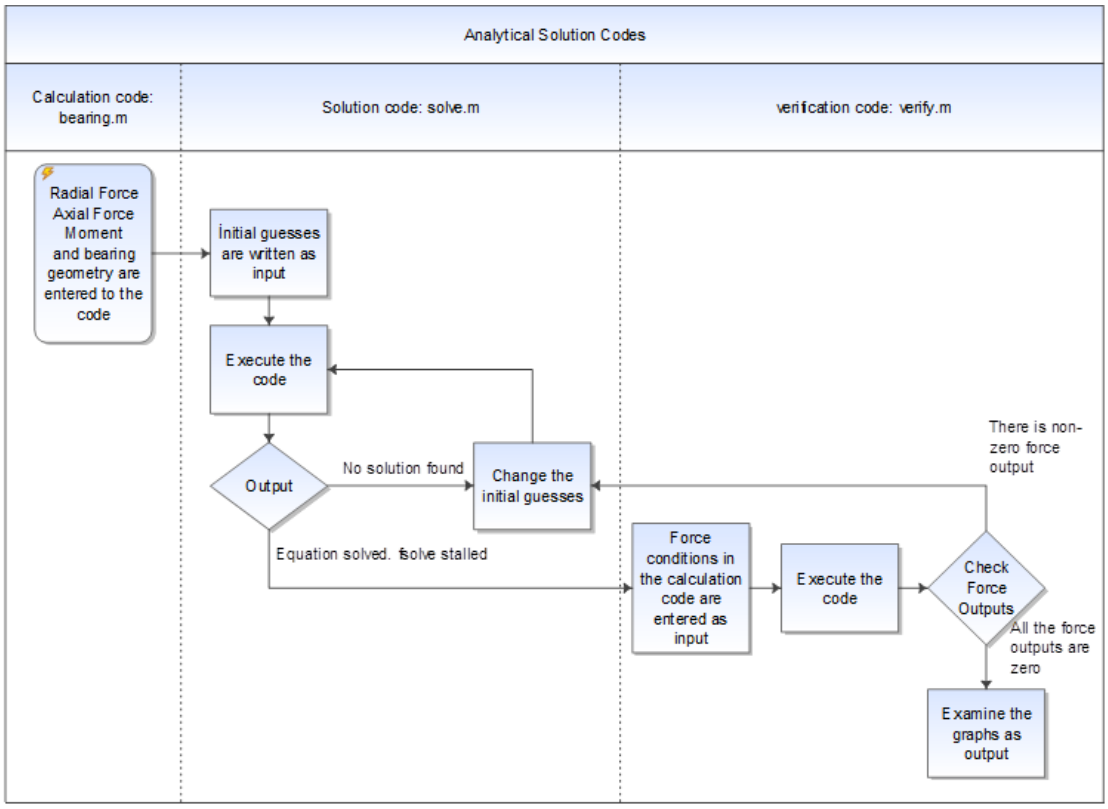


**Figure 82- Working procedure of MATLAB codes that is prepared for analytical calculations**

# APPENDIX B

## MATLAB ANALYTICAL CALCULATION CODES

Important parts of the MATLAB code are given as separate parts.

**Solver Code That Calls the Calcuations (Bearing.m);**

```
clear
clc
close all
x0 = zeros(3,1);
x0(1,1) = 0.00001;     % initial guess  delta_r
x0(2,1) = 0.00001;     % initial guess  delta_z
x0(3,1) = 0.1;         % initial guess  theta
options = optimset('MaxIter',1e4,'MaxFunEvals',1e4,'TolFun',1e-2);
x = fsolve(@bearing_v5,x0,options) % gives the solution of deformations
```

**Sample Calcuation Code That the Net Total Forces are Calculated in During the Iterations(Bearing.m) ;**

The beginning of the calculation code is given below. Analytical calculations are embedded into the code using MATLAB commands.

```
function[14] = bearing_v5(x)
```

```
delta_r = x(1,1);
delta_z = x(2,1);
theta_d = x(3,1);
theta = theta_d*pi/180;
domain = 1;  %number of points (numerical solution parameter)
psi = (1:n)*360/n; % angle of each bearing in degree
K = 45*10^4; % coefficient K
A = 2*sqrt(a^2+h^2); %initial distance between radii of curvature of raceways
Pr = 0.0; %clearance between ball and raceway
ne = 1.5; %exponent of load
%loading parameters
M =100000000; %moment in Nmm
Fz =0; %axial load in N
Fr =0; %radial load in N
phi = ones(1,n)*90; %angle of applied radial load in degree
%Initial coordinates of the center of curvatures of raceways with endplay
j = sqrt((2*Pr+A)^2-(2*h)^2)-2*a; %endplay
XCii1 = ones(domain,1)*(dm/2+h)*cosd(psi);
YCii1 = ones(domain,1)*(dm/2+h)*sind(psi);
ZCii1 = a*ones(domain,n);
XCis1 = ones(domain,1)*(dm/2+h)*cosd(psi);
YCis1 = ones(domain,1)*(dm/2+h)*sind(psi);
ZCis1 = -a*ones(domain,n);
XCei1 = ones(domain,1)*(dm/2-h)*cosd(psi);
YCei1 = ones(domain,1)*(dm/2-h)*sind(psi);
ZCei1 = (a-j)*ones(domain,n);
XCes1 = ones(domain,1)*(dm/2-h)*cosd(psi);
YCes1 = ones(domain,1)*(dm/2-h)*sind(psi);
ZCes1 = (-a-j)*ones(domain,n);
Aprime = A+2*Pr;  %initial distance between radii of curvature of raceways with
endplay
…
```

**VerivicationCode (Bearing.m) ;**

After the iterations are completed, verification code plots the results in accordance with the final displacements. Plotter part of the code is given below;

```
…
%deformation
figure
plot(delta1)
hold on
plot(delta2,'r')
title('delta')
legend('delta1','delta2')
xlabel('Ball number')
figure      %load on each ball
plot(q1,'LineWidth',1)
hold on
plot(q2,'r','LineWidth',1)
title('Total Load on Specific Balls')
legend('q1','q2')
xlabel('Ball number')
ylabel('Load [N]')
figure %angle of each ball
subplot(2,1,1)
plot(alpha1*180/pi)
legend('Cii-Ces contact-alpha1')
title('Contact angle alpha')
xlabel('Ball number')
subplot(2,1,2)
plot(alpha2*180/pi,'r')
xlabel('Ball number')
legend('Cis-Cei contact-alpha2')
ylabel('Contact angle [degree]')
figure              %force on each ball
```

```
quiver3(XCii2,YCii2,ZCii2,q1x,q1y,q1z)
hold on
quiver3(XCis2,YCis2,ZCis2,q2x,q2y,q2z,'r')
xlabel('x')
ylabel('y')
zlabel('z')
title('Load distribution on balls')
legend('Cii-Ces contact','Cis-Cei contact')
figure          %locus of centers of radii of curvature
plot3(XCii2,YCii2,ZCii2,XCes2,YCes2,ZCes2)
hold on
grid on
plot3(XCis2,YCis2,ZCis2,XCei2,YCei2,ZCei2,'r')
title('Locus of centers of radii of curvature')
xlabel('x')
ylabel('y')
zlabel('z')
%sum of reactions
Frt = sqrt(sum(q1x+q2x)^2+sum(q1y+q2y)^2)-sign(delta_r)*Fr
Fzt = sum(q1z')+sum(q2z')+Fz
Mt = sqrt(sum(m1x+m2x)^2+sum(m1y+m2y)^2)-sign(theta_d)*M
F = zeros(3,1);
F(1,1) = Frt;
F(2,1) = Fzt;
F(3,1) = Mt;
…
```

# APPENDIX C

## BACKGROUND OF IMPORTANT MATLAB CODES

**Fsolve definition as given in [21];**

"fsolve solves systems of nonlinear equations of several variables.

fsolve attempts to solve equations of the form:

F(X) = 0 where F and X may be vectors or matrices.

fsolve implements three different algorithms: trust region dogleg, trust region reflective, and Levenberg-Marquardt. The algorithm is chosen one via the option Algorithm: for instance, to choose trust region reflective, it is set;
OPTIONS =optimoptions ('fsolve','Algorithm','trust-region-reflective')
Using this, OPTIONS is passed to fsolve."

**Optimset definition as given in [21];**

"Optimset Create/alter optimization OPTIONS structure.
OPTIONS = optimset('PARAM1',VALUE1,'PARAM2',VALUE2,...) creates an optimization options structure OPTIONS in which the named parameters have the specified values. Any unspecified parameters are set to [] (parameters with value []

indicate to use the default value for that parameter when OPTIONS is passed to the optimization function).

It is sufficient to type only the leading characters that uniquely identify the parameter. Case is ignored for parameter names.

NOTE: For values that are strings, the complete string is required.

OPTIONS = optimset (with no input arguments) creates an options structure OPTIONS where all the fields are set to [].

OPTIONS = optimset(OPTIMFUNCTION) creates an options structure with all the parameter names and default values relevant to the optimization function named in OPTIMFUNCTION.

For example, optimset ('fminbnd') oroptimset(@fminbnd)returns an options structure containing all the parameter names and default values relevant to the function 'fminbnd'."

**Optimset parameters' definition as given in [21];**

" Display - Level of display [ off | iter | notify | final ]

MaxFunEvals - Maximum number of function evaluations allowed

[ positive integer ]

MaxIter - Maximum number of iterations allowed [ positive scalar ]

TolFun - Termination tolerance on the function value [ positive scalar]"

# APPENDIX D

## APDL CODE PREPARED FOR FINITE ELEMENT MODEL

Important parts of the APDL code are given as separate parts.

**Dividing volumes in the z-axis for creating nodes at spring contact locations;**

…

!!!!!! cutting volumes by workplane

wpof,,,bch +rball*cos(contang*pi/180)

VSBW,ALL

wpof,,,-2*rball*cos(contang*pi/180)

VSBW,ALL

…

**Real constants that determine stiffness of the springs as balls;**

…

!Material

MPTEMP,1,0

MPDATA,EX,1,,210000000 %1000 times of original

MPDATA,PRXY,1,,0.3

R,1,-0.1,-14230,-0.0874788,-11643,-0.052859,-6332,

RMORE,-0.0388239,-3442,-0.0258493,-1870,-0.017995,-1015,

RMORE,-0.011433,-550.1141538,-0.00758867,-297.4822209,-0.00502578,-160.3310824,
RMORE,-0.00331719,-85.97417855,-0.00217813,-45.74442878,-0.00141875,-24.04757709,
RMORE,-0.000913,-12.40400188,-0.000575,-6.204607033,-0.00035,-2.946555192,
RMORE,-0.0002,-1.272792206,-0.0001,-0.45,0,0,
RMORE,0.0001,1e-006,0.1,1e-006,
…

# APPENDIX E

## IMPORTANT CODES AND ELEMENT PROPERTIES USED IN ANSYS APDL CODE

***DO command definition as given in [23];**

"*DO command defines the beginning of a do-loop. The command is used as; *DO,Par,IVAL,FVAL,INC

Par: The name of the scalar parameter to be used as the loop index. Any existing parameter of the same name will be redefined. There is no character parameter substitution in the Par field.

IVAL: Initial value of the scalar parameter to be used as the loop index.

FVAL: Final value of the scalar parameter to be used as the loop index.

INC: Increment that is determined for the scalar parameter to be used as the loop index.

All the geometrical volumes created using this command in the circumferential direction. 360 degrees are separated to ball number to obtain the increment value. Springs are attached from those volume intersections."

**COMBIN 39 element type definition as given in [22];**

"COMBIN 39 is a unidirectional element with nonlinear generalized force-deflection capability that can be used in any analysis. The element has longitudinal or torsional capability in 1-D, 2-D, or 3-D applications. The longitudinal option is a uniaxial tension-compression element with up to three degrees of freedom at each node: translations in the nodal x, y, and z directions. No bending or torsion is considered. The torsional option is a purely rotational element with three degrees of freedom at each node: rotations about the nodal x, y, and z axes. No bending or axial loads are considered." [21]

**SOLID 185 element type definition as given in [22];**

"SOLID 185 is used for 3-D modeling of solid structures. It is defined by eight nodes having three degrees of freedom at each node: translations in the nodal x, y, and z directions. The element has plasticity and hyper elasticity, stress stiffening, creep, large deflection, and large strain capabilities. It also has mixed formulation capability for simulating deformations of nearly incompressible elastoplastic materials, and fully incompressible hyperelastic materials." [22]